Transient Wave Imaging

Lili Guadarrama

École Doctorale Polytechnique

Thèse de doctorat

Discipline : Mathématiques Appliquées

présentée par

Lilí Guadarrama Bustos

Imagerie en régime temporel

---

dirigée par Habib Ammari

Soutenue le 4 juin 2010 devant le jury composé de :

M. Vilmos KOMORNIK	Université de Strasbourg	président
M. Yves CAPDEBOSCQ	University of Oxford	rapporteur
M. Knut SØLNA	University of California at Irvine	rapporteur
M. Josselin GARNIER	Universit Paris VII	examinateur
M. Roman NOVIKOV	École Polytechnique	examinateur
M. Habib AMMARI	École Normale Supérieure	directeur

Transient Wave Imaging

Lili Guadarrama Bustos

Centre de Mathématiques Appliquées, Ecole Polytechnique, 91128 Palaiseau, France

E-mail address: lili.guadarrama-bustos@cmap.polytechnique.fr

Contents

Introduction

Extensive work has been carried out in the past decade to image the elastic properties of human soft tissues by inducing motion. This broad field, called elasticity imaging or elastography, is based on the initial idea that shear elasticity can be correlated with the pathology of tissues [**60**].

There are several techniques that can be classified according to the type of mechanical excitation chosen (static compression, monochromatic, or transient vibration) and the way these excitations are generated (externally or internally). Different imaging modalities can be used to estimate the resulting tissue displacements.

A very interesting approach to assessing elasticity is to use the acoustic radiation force of an ultrasonic focused beam to remotely generate mechanical vibrations in organs. The acoustic force is generated by the momentum transfer from the acoustic wave to the medium. The radiation force essentially acts as a dipolar source. A spatio-temporal sequence of the propagation of the induced transient wave can be acquired, leading to a quantitative estimation of the viscoelastic parameters of the studied medium in a source-free region [**33, 34**].

Our aim in this thesis is to provide a solid mathematical foundation for this transient technique and to design accurate methods for anomaly detection using transient measurements. We consider both the acoustic and elastic cases. We develop efficient reconstruction techniques from not only complete measurements but also from limited-view transient data and adapt them in the case of viscous media, where the elastic waves are attenuated and/or dispersed.

We begin with transient imaging in a non-dissipative medium. We develop anomaly reconstruction procedures that are based on rigorously established inner and outer time-domain asymptotic expansions of the perturbations in the transient measurements that are due to the presence of the anomaly. It is worth mentioning that in order to approximate the anomaly as a dipole with certain polarizability, one has to truncate the high-frequency component of the far-field measurements.

Using the outer asymptotic expansion, we design a time-reversal imaging technique for locating the anomaly. Based on such expansions, we propose an optimization problem for recovering geometric properties as well as the physical parameters of the anomaly. We justify both theoretically and numerically that scale separation can be used to obtain local and precise reconstructions. We show the differences between the acoustic and the elastic cases, namely, the anisotropy of the focal spot and the birth of a near fieldlike effect by time reversing the perturbation due to an elastic anomaly. These interesting findings were experimentally observed and first reported in [**43**]. Our asymptotic formalism clearly explains them.

In the case of limited-view transient measurements, we construct Kirchhoff-, back-propagation-, MUSIC-, and arrival time-type algorithms for imaging small

anomalies. Our approach is based on averaging of the limited-view data, using weights constructed by the geometrical control method [**29**]. It is quite robust with respect to perturbations of the non-accessible part of the boundary. Our main finding is that if one can construct accurately the geometric control then one can perform imaging with the same resolution using partial data as using complete data.

We also use our asymptotic formalism to explain how to reconstruct a small anomaly in a viscoelastic medium from wavefield measurements. The visco-elastic medium obeys a frequency power-law. For simplicity, we consider the Voigt model, which corresponds to a quadratic frequency loss. By using the stationary phase theorem, we express the ideal elastic field without any viscous effect in terms of the measured field in a viscous medium. We then generalize the imaging techniques developed for a purely quasi-incompressible elasticity model to recover the viscoelastic and geometric properties of an anomaly from wavefield measurements.

The thesis is organized as follows. In Chapter 1 we provide a mathematical foundation for the acoustic radiation force imaging. From the rigorously established asymptotic expansions of near- and far-field measurements of the transient wave induced by the anomaly, we design asymptotic imaging methods leading to a quantitative estimation of physical and geometrical parameters of the anomaly.

In Chapter 2 we consider a purely quasi-incompressible elasticity model. We rigorously establish asymptotic expansions of near- and far-field measurements of the transient elastic wave induced by a small elastic anomaly. Our proof uses layer potential techniques for the modified Stokes system. Based on these formulas, we design asymptotic imaging methods leading to a quantitative estimation of elastic and geometrical parameters of the anomaly. Using time-reversal, we show how to reconstruct the location and geometric features of the anomaly from the far-field measurements. We put a particular emphasis on the difference between the acoustic and the elastic cases, namely, the anisotropy of the focal spot and the birth of a near fieldlike effect by time reversing the perturbation due to an elastic anomaly.

In Chapter 3 we consider for the wave equation the inverse problem of identifying locations of point sources and dipoles from limited-view data. Using as weights particular background solutions constructed by the geometrical control method, we recover Kirchhoff-, back-propagation-, MUSIC-, and arrival time-type algorithms by appropriately averaging limited-view data. We show both analytically and numerically that if one can construct accurately the geometric control, then one can perform imaging with the same resolution using limited-view as using full-view data.

Chapter 4 is devoted to the problem of reconstructing a small anomaly in a viscoelastic medium from wavefield measurements. Expressing the ideal elastic field without any viscous effect in terms of the measured field in a viscous medium, we generalize the methods described in Chapter 3 to recover the viscoelastic and geometric properties of an anomaly from wavefield measurements.

The four chapters of this thesis are self-contained and can be read independently. Results in this thesis will appear in [**4, 8, 11, 37, 61**].

Introduction en Francais

L'imagerie d'élasticité, ou élastographie consiste á imager les propriétés viscoélastiques des tissus mous du corps humain en observant la réponse en déformation à une excitation mécanique. Cette problématique a donné lieu dans les dix dernières années à de nombreux travaux, motivés par la corrélation entre présence d'une pathologie et observation d'un contrast d'élasticité [**60**]. Différentes techniques peuvent être mises en oeuvre selon le type d'excitation choisie, et la manière d'estimer les déformations résultantes.

Parmi les techniques se trouve une trés intéréssante qui consiste à induire dans le tissu mou une onde de déplacement et à observer la propagation de l'onde pendant sa traversée du milieu d'intérêt. La résolution d'un problème inverse permet de déduire des données de déplacement une estimation de la carte d'élasticité du milieu [**33, 34**].

L'objectif du travail présenté dans ce document est de donner un cadre mathéma tique rigoureux à ce technique, en même temps dessiner des méthodes effectives pour la détection des anomalies à l'aide des mesures en régime temporel. On a consideré le cadre acoustic et le cadre élastique. On a développé des techniques de reconstruction efficaces pour des mesures complètes sur la frontière mais aussi pour des mesures temporelles incomplètes, on a adapté ces techniques au cadre viscoélastique, ca veut dire que les ondes sont atténué ou dispersé ou le deux.

On commence pour considérer une milieu sans dissipation. On a développé des méthodes de reconstruction des anomalies qui sont basé sur des développements asymptotiques de champ proche et de champ lointain, qui sont rigoureusement établis, du perturbation des mesures cause par l'anomalie. Il faut remarquer que pour approximer l'effet de l'anomalie par un dipôle il faut couper les composant de haut fréquence des mesures de champ lointain.

Le développement asymptotique de champ lointain nous permet de développer une technique de type régression temporel pour localiser l'anomalie. On propose en utilisant le développement asymptotique de champ proche une problème de optimisation pour récupérer les propriétés géométriques et les paramètres physiques de l'anomalie. On justifie d'une manière théorique et numérique que la séparation des échelles permet de séparer les différentes informations codées aux différentes échelles. On montre les différences entre le cadre acoustique et l'élastique, principalement la tache focal anisotrope et l'effet de champ proche qu'on obtient en faisant le retournement temporal de la perturbation cause par l'anomalie. Ces observations ont été observé expérimentalement et reporté pour la première fois en [**43**], les quelles sont bien expliques par nos développements asymptotiques.

En ce qui concerne le cadre des mesures partiels, on développe des algorithmes de type Kirchhoff, back-propagation, MUSIC et arrival-time pour localiser l'anomalie. On utilise le méthode du control géométrique [**29**] pour aborder la problématique

des mesures partiels, comme resultat on obtient une méthode qui est robuste en ce qui concerne aux perturbations dans la partie de la frontière qui n'est pas accessible. Si on construit de manier précise le control géométrique, on obtient la même résolution d'imagerie que dans le cadre des mesures complet.

On utilise les développements asymptotiques pour expliquer comment reconstruire une petite anomalie dans un milieu visco-élastique à partir des mesures du champ de déplacement. Dans le milieu visco-élastique la fréquence obéit une loi de puissance, pour simplicité on considère le modèle Voigt qui correspond à une fréquence en puissance deux. On utilise le théorème de la phase stationnaire pour exprimer le champ dans un milieu sans effet de viscosité, que on nommera champ idéal , en termes du champ dans un milieu visco-élastique. Après on généralise les techniques d'imagerie développes pour le modelé purement élastique quasi incompressible pour reconstruire les propriétés visco-élastiques et géométriques d'une anomalie a partir des mesures du champ de déplacement.

Le document s'articule de la facon suivante. Dans le chapitre 1, il est donné un cadre mathématique rigoureux à l'imagerie par force de radiation acoustique. En utilisant les expressions asymptotiques rigoureusement établis pour les mesures du champ proche et lointaine de l'onde temporel cause par l'anomalie, on développe des méthodes asymptotiques d'imagerie qui permet de estimer quantitativement les paramètres physiques et géométriques de l'anomalie.

Dans le chapitre 2 on considère un modèle purement élastique quasi incompressible. Dans le même esprit que le chapitre précèdent des expansions asymptotiques sont rigoureusement établis pour les mesures proche et lointaine de l'onde élastique en régime temporel induit par une petite anomalie élastique. Dans les démonstrations, on utilise des techniques de layer potentiel pour le systéme de Stokes modifie. En utilisant les formules on développe des méthodes asymptotiques d'imagerie qui permet de estimer quantitativement les paramètres physiques et géométriques de l'anomalie. En utilisant une technique de retournement temporel on montre comment reconstruire les propriétés géométriques et localiser l'anomalie a partir des mesures du champ lointaine. On insiste sur les différences entre le cadre acoustique et l'élastique en particulier la tache focal anisotrope et le effet de champ proche qu'on obtient en faisant le retournement temporel de la perturbation cause par l'anomalie élastique.

Dans le chapitre 3 on considère pour l'équation d'onde le problème inverse de localiser point source et dipôles a partir des mesures partiels. En utilisant des solutions particuliers construit par le méthode de control géométrique comme fonctions de poids, on recouvre des algorithmes du type Kirchhoff, back-propagation, MUSIC, arrival-time si on fait une moyen convenable sur les mesures partiels. On montre de manier analytique et numérique que si on arrive à construire précisément le control géométrique alors on peut effectuer l'imagerie avec la même résolution en utilisant mesures partiels ou mesures complet.

Le chapitre 4 est dédié à l'extension des techniques de reconstruction au cadre de la visco-élastique dynamique. A partir d'exprimer le champ idéal en termes des mesures du champ dans une milieu visco-élastique , on généralise les méthodes décrit dans le Chapitre 3 pour récupérer les propriétés visco-élastiques et géométriques de l'anomalie a partir de mesures du champ desplacement.

Les cinq chapitres de cette thèse sont indépendants et peuvent etre lus séparément. Les résultats de cette thèse seront publiés dans [**4, 8, 11, 37, 61**].

Acknowledgments

I would like to express my deep and sincere gratitude to Habib, first for accepting to be my advisor, and then for his patience and his kindness that he had during my thesis. I hope I learned something that will allow me continue in the reseach way. I was very lucky to have such a great person to guide me in my thesis. I want to thank him for everything he did for me. I want to thank Professor Capdeboscq and Professor Sølna for accepting to be my rapporteurs, for their careful reviews of this thesis, their remarks and corrections. I want to thank Professor Kolmornik, Garnier and Novikov for accepting to be my referees.

I am also grateful to the Langevin Institut for opening its door to a theoretical study of transient imaging.

Thanks also to all my colleagues who I worked with, Abdul, Sohuir, Vincent, Eli, it was a pleasure to work with all of you.

I want to thank my dear husband, Arturo, I want to thank him for his faithful support.

Finally I want to tanks to all my friends, for all the good moments we shared.

Financial support was provided by CONACyT.

CHAPTER 1

Transient acoustic imaging

ABSTRACT. This chapter is devoted to provide a solid mathematical foundation for a promising imaging technique based on the acoustic radiation force, which acts as a dipolar source. From the rigorously established asymptotic expansions of near- and far-field measurements of the transient wave induced by the anomaly, we design asymptotic imaging methods leading to a quantitative estimation of physical and geometrical parameters of the anomaly.

1.1. Introduction

An interesting approach to assessing elasticity is to use the acoustic radiation force of an ultrasonic focused beam to remotely generate mechanical vibrations in organs [**60**]. The acoustic force is generated by the momentum transfer from the acoustic wave to the medium. The radiation force essentially acts as a dipolar source. A spatio-temporal sequence of the propagation of the induced transient wave can be acquired, leading to a quantitative estimation of the viscoelastic parameters of the studied medium in a source-free region [**33, 34**].

The aim of this chapter is to provide a solid mathematical foundation for this technique and to design new methods for anomaly detection using the radiation force. These reconstruction procedures are based on rigorously established inner and outer asymptotic expansions of the perturbations of the wavefield that are due to the presence of the anomaly.

To be more precise, suppose that an anomaly D of the form

$$D = \epsilon B + z$$

is present, where ϵ is the (small) diameter of D, B is a reference domain, and z indicates the location of D. A spherical wave

$$U_{\bar{y}}(x,t) := \frac{\delta_{t=|x-\bar{y}|}}{4\pi|x-\bar{y}|}$$

is generated by a point source located at $\bar{y}$ far away from z. When this wave hits the anomaly D, it is perturbed. We will derive asymptotic expansions of this perturbation near and far away from the anomaly as ϵ tends to 0. In fact, we will derive asymptotic expansions of the perturbation $u - U_{\bar{y}}$ after the high frequency component is truncated, where u is the solution to

$$\begin{cases} \partial_t^2 u - \nabla \cdot \big(\chi(\mathbb{R}^3 \setminus \overline{D}) + k\chi(D)\big)\nabla u = \delta_{x=\bar{y}}\delta_{t=0} \quad \text{in} \quad \mathbb{R}^3 \times]0, +\infty[, \\ u(x,t) = 0 \quad \text{for} \quad x \in \mathbb{R}^3 \quad \text{and } t \ll 0. \end{cases}$$

For example, after truncation of the high-frequency component of the solution, the derived asymptotic expansion far away from the anomaly shows that when the spherical wave $U_{\bar{y}}$ reaches the anomaly, it is polarized and emits a new wave. The

threshold of the truncation is determined by the diameter of the anomaly and is of order $O(\epsilon^{-\alpha})$ for $0 \leq \alpha < 1$.

Derivations of asymptotic expansions in this chapter are rigorous. They are based on careful and precise estimates of the dependence with respect to the frequency of the remainders in associated asymptotic formulas for the Helmholtz equation. Using the outer asymptotic expansion, we design a time-reversal imaging technique for locating the anomaly from measurements of the perturbations in the wavefield in the far-field. It turns out that using the far-field measurement we can reconstruct the location and the polarization tensor of the anomaly. However, It is known that it is impossible to separate geometric features such as the volume from the physical parameters using only the polarization tensor. We show that in order to reconstruct the shape and to separate the physical parameters of the anomaly from its volume one should use near-field perturbations of the wavefield. Based on such expansions, we propose an optimization problem for recovering geometric properties as well as the parameters of the anomaly. The connection between our expansions and reconstruction methods for the wave equation in this chapter and those for the Helmholtz equation is discussed in some detail.

In connection with this work, we shall mention on one hand the papers [**103, 15, 62**] for the derivations of asymptotic formula for the Helmholtz equation in the presence of small volume anomalies and on the other hand, the review paper [**26**] and the recent book [**14**] on different algorithms in wave imaging.

The chapter is organized as follows. We rigorously derive in Section 1.2 asymptotic formulas for the Helmholtz equation and estimate the dependence of the remainders in these formulas with respect to the frequency. Based on these estimates, we obtain in Section 1.3 formulas for the transient wave equation that are valid after truncating the high-frequency components of the fields. These formulas describe the effect of the presence of a small anomaly in both the near and far field. In Section 1.4 we propose different methods for detecting the physical and geometric parameters of the anomaly. A time-reversal method is proposed to locate the anomaly and find its polarization tensor from far-field measurements while an optimization problem is formulated for reconstructing geometric parameters of the anomaly and its conductivity.

1.2. Asymptotic expansions for the Helmholtz equation

In this section we rigorously derive asymptotic formulas for the Helmholtz equation and estimate the dependence of the remainders in these formulas with respect to the frequency. For doing so, we rely on a layer-potential technique.

1.2.1. Layer potentials. For $\omega \geq 0$, let

$$\Phi_\omega(x) = -\frac{e^{\sqrt{-1}\omega|x|}}{4\pi|x|}, \quad x \in \mathbb{R}^3, x \neq 0, \tag{1.1}$$

which is the fundamental solution for the Helmholtz operator $\Delta+\omega^2$. For a bounded Lipschitz domain Ω in $\mathbb{R}^3$ and $\omega \geq 0$, let $\mathbf{S}_\Omega^\omega$ be the single-layer potential for $\Delta+\omega^2$, that is,

$$\mathbf{S}_\Omega^\omega[\varphi](x) = \int_{\partial\Omega} \Phi_\omega(x-y)\varphi(y)\, d\sigma(y), \quad x \in \mathbb{R}^3, \tag{1.2}$$

for $\varphi \in L^2(\partial\Omega)$. When $\omega = 0$, $\mathbf{S}_\Omega^0$ is the single layer potential for the Laplacian. Note that $u = \mathbf{S}_\Omega^\omega[\varphi]$ satisfies the Helmholtz equation $(\Delta + \omega^2)u = 0$ in Ω and in $\mathbb{R}^3 \setminus \overline{\Omega}$. Moreover, if $\omega > 0$, it satisfies the radiation condition, namely,

$$\left|\frac{\partial u}{\partial r} - \sqrt{-1}\omega u\right| = O\left(r^{-2}\right) \quad \text{as } r = |x| \to +\infty \quad \text{uniformly in } \frac{x}{|x|}. \tag{1.3}$$

It is well-known that the normal derivative of the single-layer potential on Lipschitz domains obeys the following jump relation

$$\frac{\partial(\mathbf{S}_\Omega^\omega[\varphi])}{\partial\nu}\bigg|_\pm (x) = \left(\pm\frac{1}{2}I + (\mathbf{K}_\Omega^{-\omega})^*\right)[\varphi](x) \quad \text{a.e. } x \in \partial\Omega, \tag{1.4}$$

for $\varphi \in L^2(\partial\Omega)$, where $(\mathbf{K}_\Omega^{-\omega})^*$ is the singular integral operator defined by

$$(\mathbf{K}_\Omega^{-\omega})^*[\varphi](x) = \text{p.v.} \int_{\partial\Omega} \frac{\partial\Phi_\omega(x-y)}{\partial\nu(x)}\varphi(y)d\sigma(y).$$

Here and throughout this chapter the subscripts $\pm$ denote the limit from outside and inside of $\partial\Omega$.

The operator $\mathbf{S}_\Omega^0$ is bounded from $L^2(\partial\Omega)$ into $H^1(\partial\Omega)$ and invertible in three dimensions [**102**]. Moreover, one can easily see that there exists $\omega_0 > 0$ such that for $\omega < \omega_0$

$$\|\mathbf{S}_\Omega^\omega[\varphi] - \mathbf{S}_\Omega^0[\varphi]\|_{H^1(\partial\Omega)} \leq C\omega\|\varphi\|_{L^2(\partial\Omega)} \tag{1.5}$$

for all $\varphi \in L^2(\partial\Omega)$ where C is independent of ω. It is also well-known that the singular integral operator $(\mathbf{K}_\Omega^0)^*$ is bounded on $L^2(\partial\Omega)$ (see [**17**] for example). Similarly to (1.5), one can see that for there exists $\omega_0 > 0$ such that for $\omega < \omega_0$

$$\|(\mathbf{K}_\Omega^{-\omega})^*[\varphi] - (\mathbf{K}_\Omega^0)^*[\varphi]\|_{L^2(\partial\Omega)} \leq C\omega\|\varphi\|_{L^2(\partial\Omega)}$$

for some constant C independent of ω. In view of (1.4), it amounts to

$$\left\|\frac{\partial(\mathbf{S}_\Omega^\omega[\varphi])}{\partial\nu}\bigg|_\pm - \frac{\partial(\mathbf{S}_\Omega^0[\varphi])}{\partial\nu}\bigg|_\pm\right\|_{L^2(\partial\Omega)} \leq C\omega\|\varphi\|_{L^2(\partial\Omega)}. \tag{1.6}$$

1.2.2. Derivations of the asymptotic expansions. Let D be a smooth anomaly with conductivity $0 < k \neq 1 < +\infty$ inside a background medium with conductivity 1. Suppose that $D = \epsilon B + z$, where B is a domain which plays the role of a reference domain, ϵ denotes the small diameter of D, and z indicates the location of D.

Let $\bar{y}$ be a point in $\mathbb{R}^3$ such that $|\bar{y} - z| >> \epsilon$, and let

$$V(x,\omega) := \Phi_\omega(x - \bar{y}) = -\frac{e^{\sqrt{-1}\omega|x-\bar{y}|}}{4\pi|x-\bar{y}|}, \tag{1.7}$$

so that V satisfies

$$\Delta V + \omega^2 V = \delta_{x=\bar{y}}, \tag{1.8}$$

together with the radiation condition (1.3).

Let $v(x,\omega)$ be the solution to

$$\nabla\cdot(\chi(\mathbb{R}^3 \setminus \overline{D}) + k\chi(D))\nabla v + \omega^2 v = \delta_{x=\bar{y}} \tag{1.9}$$

satisfying the radiation condition (1.3). In this section, we derive asymptotic expansion formula for $v - V$ as ϵ tends to 0. An important feature of the asymptotic

formula derived in this section is a careful estimate of the dependency of the remainder term on the frequency.

Put $w = v - V$. Then w is a unique solution to

$$\nabla \cdot (\chi(\mathbb{R}^3 \setminus \overline{D}) + k\chi(D))\nabla w + \omega^2 w = (1-k)\nabla \cdot \chi(D)\nabla V \quad \text{in } \mathbb{R}^3 \tag{1.10}$$

with the radiation condition. In other words, w is the solution to

$$\begin{cases} \Delta w + \dfrac{\omega^2}{k} w = (1 - \dfrac{1}{k})\omega^2 V \quad \text{in } D, \\ \Delta w + \omega^2 w = 0 \quad \text{in } \mathbb{R}^3 \setminus \overline{D}, \\ w|_+ - w|_- = 0 \quad \text{on } \partial D, \\ \left.\dfrac{\partial w}{\partial \nu}\right|_+ - k \left.\dfrac{\partial w}{\partial \nu}\right|_- = (k-1)\dfrac{\partial V}{\partial \nu}, \\ w \text{ satisfies the radiation condition.} \end{cases} \tag{1.11}$$

Therefore, w can be represented as

$$w(x,\omega) = \begin{cases} (\dfrac{1}{k} - 1)\omega^2 \displaystyle\int_D \Phi_{\frac{\omega}{\sqrt{k}}}(x-y)V(y)dy + \mathbf{S}_D^{\frac{\omega}{\sqrt{k}}}[\varphi](x), \quad x \in D, \\ \mathbf{S}_D^{\omega}[\psi](x), \quad x \in \mathbb{R}^3 \setminus \overline{D}, \end{cases} \tag{1.12}$$

where $(\varphi, \psi) \in L^2(\partial D)^2$ is the solution to the integral equation

$$\begin{cases} \mathbf{S}_D^{\frac{\omega}{\sqrt{k}}}[\varphi] - \mathbf{S}_D^{\omega}[\psi] = (1 - \dfrac{1}{k})\omega^2 \displaystyle\int_D \Phi_{\frac{\omega}{\sqrt{k}}}(\cdot - y)V(y)dy, \\ k \left.\dfrac{\partial \mathbf{S}_D^{\frac{\omega}{\sqrt{k}}}[\varphi]}{\partial \nu}\right|_- - \left.\dfrac{\partial \mathbf{S}_D^{\omega}[\psi]}{\partial \nu}\right|_+ = (1-k)\omega^2 \dfrac{\partial}{\partial \nu} \displaystyle\int_D \Phi_{\frac{\omega}{\sqrt{k}}}(\cdot - y)V(y)dy + (1-k)\dfrac{\partial V}{\partial \nu}, \end{cases} \tag{1.13}$$

on ∂D. The unique solvability of (1.13) will be shown in the sequel.

Let

$$\widetilde{\varphi}(\tilde{x}) = \varphi(\epsilon \tilde{x} + z), \quad \tilde{x} \in \partial B,$$

and define $\widetilde{\psi}$ likewise. Then, after changes of variables, (1.13) takes the form

$$\begin{cases} \mathbf{S}_B^{\frac{\epsilon\omega}{\sqrt{k}}}[\widetilde{\varphi}] - \mathbf{S}_B^{\epsilon\omega}[\widetilde{\psi}] = F, \\ k \left.\dfrac{\partial \mathbf{S}_B^{\frac{\epsilon\omega}{\sqrt{k}}}[\widetilde{\varphi}]}{\partial \nu}\right|_- - \left.\dfrac{\partial \mathbf{S}_B^{\epsilon\omega}[\widetilde{\psi}]}{\partial \nu}\right|_+ = G, \end{cases} \quad \text{on } \partial B, \tag{1.14}$$

where

$$F(\tilde{x},\omega) = (1 - \frac{1}{k})\epsilon\omega^2 \int_B \Phi_{\frac{\epsilon\omega}{\sqrt{k}}}(\tilde{x} - \tilde{y})V(\epsilon\tilde{y} + z)d\tilde{y}, \tag{1.15}$$

$$G(\tilde{x},\omega) = (1-k)\epsilon\omega^2 \frac{\partial}{\partial \nu} \int_B \Phi_{\frac{\epsilon\omega}{\sqrt{k}}}(\tilde{x} - \tilde{y})V(\epsilon\tilde{y} + z)d\tilde{y} + (1-k)\frac{\partial V}{\partial \nu}(\epsilon\tilde{x} + z). \tag{1.16}$$

Define an operator $T : L^2(\partial B) \times L^2(\partial B) \to H^1(\partial B) \times L^2(\partial B)$ by

$$T(\widetilde{\varphi}, \widetilde{\psi}) := \left(\mathbf{S}_B^{\frac{\epsilon\omega}{\sqrt{k}}}[\widetilde{\varphi}] - \mathbf{S}_B^{\epsilon\omega}[\widetilde{\psi}], \quad k \left.\frac{\partial \mathbf{S}_B^{\frac{\epsilon\omega}{\sqrt{k}}}[\widetilde{\varphi}]}{\partial \nu}\right|_- - \left.\frac{\partial \mathbf{S}_B^{\epsilon\omega}[\widetilde{\psi}]}{\partial \nu}\right|_+ \right). \tag{1.17}$$

We then decompose T as

$$T = T_0 + T_\epsilon, \tag{1.18}$$

where

$$T_0(\widetilde{\varphi}, \widetilde{\psi}) := \left(\mathbf{S}_B^0[\widetilde{\varphi}] - \mathbf{S}_B^0[\widetilde{\psi}], \quad k\frac{\partial \mathbf{S}_B^0[\widetilde{\varphi}]}{\partial \nu}\Big|_- - \frac{\partial \mathbf{S}_B^0[\widetilde{\psi}]}{\partial \nu}\Big|_+ \right), \tag{1.19}$$

and $T_\epsilon := T - T_0$. In view of (1.5) and (1.6), we have

$$\|T_\epsilon(\widetilde{\varphi}, \widetilde{\psi})\|_{H^1(\partial B)\times L^2(\partial B)} \leq C\epsilon\omega(\|\widetilde{\varphi}\|_{L^2(\partial B)} + \|\widetilde{\psi}\|_{L^2(\partial B)}) \tag{1.20}$$

for some constant C independent of ϵ and ω.

Since $\mathbf{S}_B^0 : L^2(\partial B) \to H^1(\partial B)$ is invertible, we readily see that $T_0 : L^2(\partial B) \times L^2(\partial B) \to H^1(\partial B) \times L^2(\partial B)$ is invertible. In fact, we have the following lemma.

LEMMA 1.1. *For $(f, g) \in H^1(\partial B) \times L^2(\partial B)$ let $(\widetilde{\varphi}, \widetilde{\psi}) = T_0^{-1}(f, g)$. Then*

$$\widetilde{\varphi} = \widetilde{\psi} + (\mathbf{S}_B^0)^{-1}[f],$$
$$\widetilde{\psi} = \left(\frac{k+1}{2(k-1)} I - (\mathbf{K}_B^0)^* \right)^{-1} \left[\frac{k}{k-1}(-\frac{1}{2} I + (\mathbf{K}_B^0)^*)(\mathbf{S}_B^0)^{-1}[f] - \frac{1}{k-1} g \right].$$

Thanks to (1.18) and (1.20), there is $\epsilon_0 > 0$ such that T is invertible if $\epsilon\omega \leq \epsilon_0$ and

$$T^{-1} = T_0^{-1} + E, \tag{1.21}$$

where the operator E satisfies

$$\|E(f, g)\|_{L^2(\partial B)\times L^2(\partial B)} \leq C\epsilon\omega(\|f\|_{H^1(\partial B)} + \|g\|_{L^2(\partial B)})$$

for some constant C independent of ϵ and ω.

Suppose that $\epsilon\omega \leq \epsilon_0 < 1$. Let $(\widetilde{\varphi}_\omega, \widetilde{\psi}_\omega)$ be the solution to (1.14). Then by (1.21) we have

$$(\widetilde{\varphi}_\omega, \widetilde{\psi}_\omega) = T_0^{-1}(F, G) + E(F, G). \tag{1.22}$$

Observe that

$$\|F\|_{H^1(\partial B)} \leq C\epsilon\omega^2. \tag{1.23}$$

On the other hand, G can be written as

$$G(\tilde{x}) = (1-k)\nabla V(z, \omega) \cdot \nu(\tilde{x}) + G_1(\tilde{x}),$$

where G_1 satisfies

$$\|G_1\|_{L^2(\partial B)} \leq C\epsilon\omega^2.$$

Therefore, we have

$$(\widetilde{\varphi}_\omega, \widetilde{\psi}_\omega) = T_0^{-1}\left(0, (1-k)\nabla V(z) \cdot \nu\right) + T_0^{-1}(F, G_1) + E(F, G). \tag{1.24}$$

Note that

$$\|T_0^{-1}(F, G_1) + E(F, G)\|_{L^2(\partial B)\times L^2(\partial B)} \leq C\epsilon\omega^2.$$

We also need asymptotic expansion of $\frac{\partial\widetilde{\varphi}_\omega}{\partial\omega}$ and $\frac{\partial\widetilde{\psi}_\omega}{\partial\omega}$. By differentiating both sides of (1.14) with respect to ω, we obtain

(1.25)
$$\begin{cases} \mathbf{S}_B^{\frac{\epsilon\omega}{\sqrt{k}}}\left[\frac{\partial\widetilde{\varphi}_\omega}{\partial\omega}\right] - \mathbf{S}_B^{\epsilon\omega}\left[\frac{\partial\widetilde{\psi}_\omega}{\partial\omega}\right] = \frac{\partial F}{\partial\omega} \\ \quad -\frac{\epsilon}{4\pi\sqrt{k}}\int_{\partial B} e^{\sqrt{-1}\frac{\epsilon\omega}{\sqrt{k}}|\cdot-\tilde{y}|}\widetilde{\varphi}_\omega(\tilde{y})d\sigma(\tilde{y}) + \frac{\epsilon}{4\pi}\int_{\partial B} e^{\sqrt{-1}\epsilon\omega|\cdot-\tilde{y}|}\widetilde{\psi}_\omega(\tilde{y})d\sigma(\tilde{y}), \\ k\frac{\partial}{\partial\nu}\mathbf{S}_B^{\frac{\epsilon\omega}{\sqrt{k}}}\left[\frac{\partial\widetilde{\varphi}_\omega}{\partial\omega}\right]\Big|_- - \frac{\partial}{\partial\nu}\mathbf{S}_B^{\epsilon\omega}\left[\frac{\partial\widetilde{\psi}_\omega}{\partial\omega}\right]\Big|_+ = \frac{\partial G}{\partial\omega} \\ \quad -\frac{\epsilon}{4\pi\sqrt{k}}\frac{\partial}{\partial\nu}\int_{\partial B} e^{\sqrt{-1}\frac{\epsilon\omega}{\sqrt{k}}|\cdot-\tilde{y}|}\widetilde{\varphi}_\omega(\tilde{y})d\sigma(\tilde{y}) + \frac{\epsilon}{4\pi}\frac{\partial}{\partial\nu}\int_{\partial B} e^{\sqrt{-1}\epsilon\omega|\cdot-\tilde{y}|}\widetilde{\psi}_\omega(\tilde{y})d\sigma(\tilde{y}) \end{cases}$$
on ∂B. One can see from (1.15) and (1.16) that
$$\frac{\partial F}{\partial\omega} = O(\epsilon\omega) \text{ and } \frac{\partial G_1}{\partial\omega} = O(\epsilon\omega).$$
Using the same argument as before, we then obtain

$$(\frac{\partial\widetilde{\varphi}_\omega}{\partial\omega}, \frac{\partial\widetilde{\psi}_\omega}{\partial\omega}) = T_0^{-1}\left(0, (1-k)\nabla\frac{\partial V}{\partial\omega}(z,\omega)\cdot\nu\right) + O(\epsilon\omega), \tag{1.26}$$
where the equality holds in $L^2(\partial B)\times L^2(\partial B)$.

We obtain the following proposition from Lemma 1.1 (with $f=0$), (1.24), and (1.26).

Proposition 1.2. *Let $(\widetilde{\varphi}_\omega, \widetilde{\psi}_\omega)$ be the solution to (1.14). There exists $\epsilon_0 > 0$ such that if $\epsilon\omega < \epsilon_0$, then the following asymptotic expansions hold:*

$$\widetilde{\varphi}_\omega = \left(\frac{k+1}{2(k-1)}I - (\mathbf{K}_B^0)^*\right)^{-1}[\nu]\cdot\nabla V(z,\omega) + O(\epsilon\omega^2), \tag{1.27}$$

$$\widetilde{\psi}_\omega = \left(\frac{k+1}{2(k-1)}I - (\mathbf{K}_B^0)^*\right)^{-1}[\nu]\cdot\nabla V(z,\omega) + O(\epsilon\omega^2), \tag{1.28}$$

and

$$\frac{\partial\widetilde{\varphi}_\omega}{\partial\omega} = \left(\frac{k+1}{2(k-1)}I - (\mathbf{K}_B^0)^*\right)^{-1}[\nu]\cdot\nabla\frac{\partial V}{\partial\omega}(z,\omega) + O(\epsilon\omega), \tag{1.29}$$

$$\frac{\partial\widetilde{\psi}_\omega}{\partial\omega} = \left(\frac{k+1}{2(k-1)}I - (\mathbf{K}_B^0)^*\right)^{-1}[\nu]\cdot\nabla\frac{\partial V}{\partial\omega}(z,\omega) + O(\epsilon\omega), \tag{1.30}$$

where all the equalities hold in $L^2(\partial B)$.

We are now ready to derive the inner expansion of $w = v - V$. Let Ω be a set containing D and let $\widetilde{\Omega} = \frac{1}{\epsilon}\Omega - z$. After changes of variables, (1.12) takes the form

(1.31)
$$w(\epsilon\tilde{x}+z,\omega) = \begin{cases} (\frac{1}{k}-1)\epsilon^2\omega^2\int_B \Phi_{\frac{\epsilon\omega}{\sqrt{k}}}(\tilde{x}-\tilde{y})V(\epsilon\tilde{y}+z)d\tilde{y} + \epsilon\mathbf{S}_B^{\frac{\epsilon\omega}{\sqrt{k}}}[\widetilde{\varphi}_\omega](\tilde{x}), & \tilde{x}\in B, \\ \epsilon\mathbf{S}_B^{\epsilon\omega}[\widetilde{\psi}_\omega](\tilde{x}), & \tilde{x}\in\widetilde{\Omega}\setminus B. \end{cases}$$

Since
$$\left\|\mathbf{S}_B^{\frac{\epsilon\omega}{\sqrt{k}}}[\widetilde{\varphi}_\omega] - \mathbf{S}_B^0[\widetilde{\varphi}_\omega]\right\|_{H^1(\partial B)} \le C\epsilon\omega\|\widetilde{\varphi}_\omega\|_{L^2(\partial B)},$$

we have

$$w(\epsilon\tilde{x}+z,\omega)=\begin{cases}\epsilon\mathbf{S}_B^0[\widetilde{\varphi}_\omega](\tilde{x})+O(\epsilon^2\omega^2), & \widetilde{x}\in B,\\ \epsilon\mathbf{S}_B^0[\widetilde{\psi}_\omega](\tilde{x})+O(\epsilon^2\omega), & \tilde{x}\in\widetilde{\Omega}\setminus B.\end{cases}$$

Here we assumed that $\omega\geq 1$ since the case when $\omega<1$ is much easier to handle. It then follows from (1.27) and (1.28) that

$$w(\epsilon\tilde{x}+z,\omega)=\epsilon\mathbf{S}_B^0\left(\frac{k+1}{2(k-1)}I-(\mathbf{K}_B^0)^*\right)^{-1}[\nu](\tilde{x})\cdot\nabla V(z,\omega)+O(\epsilon^2\omega^2),\quad \widetilde{x}\in\widetilde{\Omega}.$$

On the other hand, we have

$$\frac{\partial w}{\partial\omega}(\epsilon\tilde{x}+z,\omega)=\begin{cases}\epsilon\mathbf{S}_B^{\frac{\epsilon\omega}{\sqrt{k}}}\left[\dfrac{\partial\widetilde{\varphi}_\omega}{\partial\omega}\right](\tilde{x})+O(\epsilon^2\omega), & \widetilde{x}\in B,\\ \epsilon\mathbf{S}_B^{\frac{\epsilon\omega}{\sqrt{k}}}\left[\dfrac{\partial\widetilde{\psi}_\omega}{\partial\omega}\right](\tilde{x})+O(\epsilon^2\omega), & \tilde{x}\in\widetilde{\Omega}\setminus B.\end{cases}$$

Therefore, we have from (1.29) and (1.30)

$$\frac{\partial w}{\partial\omega}(\epsilon\tilde{x}+z,\omega)=\epsilon\mathbf{S}_B^0\left(\frac{k+1}{2(k-1)}I-(\mathbf{K}_B^0)^*\right)^{-1}[\nu](\tilde{x})\cdot\nabla\frac{\partial V}{\partial\omega}(z,\omega)+O(\epsilon^2\omega),\quad \widetilde{x}\in\widetilde{\Omega}.$$

Let

$$\hat{v}_1(\tilde{x}):=\mathbf{S}_B^0\left(\frac{k+1}{2(k-1)}I-(\mathbf{K}_B^0)^*\right)^{-1}[\nu](\tilde{x}).$$

Note that $\hat{v}_1$ is a vector-valued function. It is well-known that $\hat{v}_1$ is the solution to

$$\begin{cases}\Delta\hat{v}_1=0 \quad \text{in } \mathbb{R}^3\setminus\overline{B},\\ \Delta\hat{v}_1=0 \quad \text{in } B,\\ \hat{v}_1|_- -\hat{v}_1|_+=0 \quad \text{on } \partial B,\\ k\dfrac{\partial\hat{v}_1}{\partial\nu}\Big|_- -\dfrac{\partial\hat{v}_1}{\partial\nu}\Big|_+=(k-1)\nu \quad \text{on } \partial B,\\ \hat{v}_1(\tilde{x})=O(|\tilde{x}|^{-2}) \quad \text{as } |\tilde{x}|\to+\infty.\end{cases}\tag{1.32}$$

We finally obtain the following theorem.

THEOREM 1.3. *Let Ω be a bounded domain containing D and let*

$$R(x,\omega)=v(x,\omega)-V(x,\omega)-\epsilon\hat{v}_1\left(\frac{x-z}{\epsilon}\right)\cdot\nabla V(z,\omega).\tag{1.33}$$

There exists $\epsilon_0>0$ such that if $\epsilon\omega<\epsilon_0$, then

$$R(x,\omega)=O(\epsilon^2\omega^2),\quad \nabla_x R(x,\omega)=O(\epsilon\omega^2)\quad x\in\Omega.\tag{1.34}$$

Moreover,

$$\frac{\partial R}{\partial\omega}(x,\omega)=O(\epsilon^2\omega),\quad \nabla_x\left(\frac{\partial R}{\partial\omega}\right)(x,\omega)=O(\epsilon\omega)\quad x\in\Omega.\tag{1.35}$$

Note that the estimates for $\nabla_x R$ in (1.34) and $\nabla_x(\frac{\partial R}{\partial\omega})$ in (1.35) can be derived using (1.31).

Based on Theorem 1.3 we can easily derive an asymptotic expansion of $v(x,\omega)-V(x,\omega)$ for $|x-z|\geq C>0$ for some constant C. For doing so, we first define the polarization tensor $M=M(k,B)$ associated with the domain B and the conductivity contrast k, $0<k\neq 1<+\infty$, as follows (see [**17**]):

$$M(k,B):=(k-1)\int_B \nabla(\hat{v}_1(\tilde{x})+\tilde{x})\,d\tilde{x}. \tag{1.36}$$

It should be noticed that the polarization tensor M can be explicitly computed for balls and ellipsoids in three-dimensional space. We also list important properties of M [**17**]:

(i) M is symmetric.
(ii) If $k>1$, then M is positive definite, and it is negative definite if $0<k<1$.
(iii) The following Hashin-Shtrikman bounds

$$\begin{cases} \dfrac{1}{k-1}\,\mathrm{trace}(M)\leq(2+\dfrac{1}{k})|B|, \\ (k-1)\,\mathrm{trace}(M^{-1})\leq\dfrac{2+k}{|B|}, \end{cases} \tag{1.37}$$

hold [**80, 39**], where trace denotes the trace of a matrix.

It is worth mentioning that the equality in the second inequality in (1.37) holds if and only if B is an ellipsoid [**72**].

Note that $u:=v-V$ satisfies

$$(\Delta+\omega^2)u=(k-1)\nabla\cdot\chi(D)\nabla v,$$

with the radiation condition. Therefore, using the Lipmann-Schwinger integral representation

$$v(x,\omega)-V(x,\omega)=(1-k)\int_D \nabla v(y,\omega)\cdot\nabla\Phi_\omega(x-y)\,dy,$$

together with the asymptotic expansion of v in D in Theorem 1.3, we obtain that for x away from z, there exists $\epsilon_0>0$ such that if $\epsilon\omega<\epsilon_0$, then

$$\begin{aligned} v(x,\omega)-V(x,\omega) &= (1-k)\int_D\left(\nabla V(y,\omega)+\nabla\hat{v}_1(\frac{y-z}{\epsilon})\cdot\nabla V(z,\omega)\right)\cdot\nabla\Phi_\omega(x-y)\,dy \\ &+ O(\epsilon^4\omega^3). \end{aligned}$$

Now if we approximate $\nabla V(y,\omega)$ and $\nabla\Phi_\omega(x-y)$ for $y\in D$ by $\nabla V(z,\omega)$ and $\nabla\Phi_\omega(x-z)$, respectively, we obtain the following theorem.

THEOREM 1.4. *Let Ω' be a compact region away from D ($dist(\Omega',D)\geq C>0$ for some constant C) and let*

$$R(x,\omega)=v(x,\omega)-V(x,\omega)+\epsilon^3\nabla V(z,\omega)M(k,B)\nabla\Phi_\omega(x-z). \tag{1.38}$$

There exists $\epsilon_0>0$ such that if $\epsilon\omega<\epsilon_0$, then

$$R(x,\omega)=O(\epsilon^4\omega^3),\quad x\in\Omega'. \tag{1.39}$$

Moreover,

$$\frac{\partial R}{\partial\omega}(x,\omega)=O(\epsilon^4\omega^2),\quad x\in\Omega'. \tag{1.40}$$

Note that, in view of the asymptotic formulae derived in [**63**] for the case of a circular anomaly, the range of frequencies for which formula (1.39) is valid is optimal.

1.3. Far- and near-field asymptotic formulas for the transient wave equation

Let D be a smooth anomaly with conductivity $0 < k \neq 1 < +\infty$ inside a background medium with conductivity 1. Suppose that $D = \epsilon B + z$ as before.

Let $\bar{y}$ be a point in $\mathbb{R}^3$ such that $|\bar{y} - z| \geq C > 0$ for some constant C. Define

$$U_{\bar{y}}(x,t) := \frac{\delta_{t=|x-\bar{y}|}}{4\pi|x-\bar{y}|}, \tag{1.41}$$

where δ is the Dirac mass.

$U_{\bar{y}}$ is the Green function associated with the retarded layer potentials and satisfies [**53, 58**]

$$\begin{cases} (\partial_t^2 - \Delta)U_{\bar{y}}(x,t) = \delta_{x=\bar{y}}\delta_{t=0} \quad \text{in } \mathbb{R}^3 \times \mathbb{R}, \\ U_{\bar{y}}(x,t) = 0 \quad \text{for} \quad x \in \mathbb{R}^3 \quad \text{and } t \ll 0. \end{cases}$$

For $\rho > 0$, we define the operator P_ρ on tempered distributions by

$$P_\rho[\psi](t) = \int_{|\omega|\leq\rho} e^{-\sqrt{-1}\omega t}\hat{\psi}(\omega)\, d\omega, \tag{1.42}$$

where $\hat{\psi}$ denotes the Fourier transform of ψ. The operator P_ρ truncates the high-frequency component of ψ. Since

$$\hat{U}_{\bar{y}}(x,\omega) = V(x,\omega) := \frac{e^{\sqrt{-1}\omega|x-\bar{y}|}}{4\pi|x-\bar{y}|}$$

using the notation in (1.7), we have

$$P_\rho[U_{\bar{y}}](x,t) = \int_{|\omega|\leq\rho} e^{-\sqrt{-1}\omega t}V(x,\omega)d\omega = \frac{\psi_\rho(t-|x-\bar{y}|)}{4\pi|x-\bar{y}|} \quad \text{for } x \neq \bar{y}, \tag{1.43}$$

where

$$\psi_\rho(t) := \frac{2\sin\rho t}{t} = \int_{|\omega|\leq\rho} e^{-\sqrt{-1}\omega t}d\omega. \tag{1.44}$$

One can easily show that $P_\rho[U_{\bar{y}}]$ satisfies

$$(\partial_t^2 - \Delta)P_\rho[U_{\bar{y}}](x,t) = \delta_{x=\bar{y}}\psi_\rho(t) \quad \text{in } \mathbb{R}^3 \times \mathbb{R}. \tag{1.45}$$

We consider the wave equation in the whole three-dimensional space with appropriate initial conditions:

$$\begin{cases} \partial_t^2 u - \nabla \cdot \big(\chi(\mathbb{R}^3 \setminus \overline{D}) + k\chi(D)\big)\nabla u = \delta_{x=\bar{y}}\delta_{t=0} \quad \text{in} \quad \mathbb{R}^3 \times]0,+\infty[, \\ u(x,t) = 0 \quad \text{for} \quad x \in \mathbb{R}^3 \quad \text{and } t \ll 0. \end{cases} \tag{1.46}$$

The purpose of this section is to derive asymptotic expansions for $P_\rho[u - U_{\bar{y}}](x,t)$. For that purpose, we observe that

$$P_\rho[u](x,t) = \int_{|\omega|\leq\rho} e^{-\sqrt{-1}\omega t}v(x,\omega)d\omega, \tag{1.47}$$

where v is the solution to (1.9). Therefore, according to Theorem 1.3, we have

$$P_\rho[u-U_{\bar{y}}](x,t)-\epsilon\hat{v}_1\left(\frac{x-z}{\epsilon}\right)\cdot\nabla P_\rho[U_{\bar{y}}](x,t)=\int_{|\omega|\le\rho}e^{-\sqrt{-1}\omega t}R(x,\omega)d\omega.$$

Suppose that $|t|\ge c_0$ for some positive number c_0 (c_0 is of order the distance between $\bar{y}$ and z). Then, we have by an integration by parts

$$\begin{aligned}\left|\int_{|\omega|\le\rho}e^{-\sqrt{-1}\omega t}R(x,\omega)d\omega\right| &= \left|\frac{1}{t}\int_{|\omega|\le\rho}\frac{d}{d\omega}e^{-\sqrt{-1}\omega t}R(x,\omega)d\omega\right| \\ &\le \frac{1}{|t|}\left(|R(x,\rho)|+|R(x,-\rho)|\right)+\int_{|\omega|\le\rho}\left|\frac{\partial}{\partial\omega}R(x,\omega)\right|d\omega \\ &\le C\epsilon^2\rho^2.\end{aligned}$$

Since $\epsilon\hat{v}_1\left(\frac{x-z}{\epsilon}\right)\cdot\nabla P_\rho[U_{\bar{y}}]=O(\epsilon\rho)$, we arrive at the following theorem.

THEOREM 1.5. *Suppose that $\rho=O(\epsilon^{-\alpha})$ for some $\alpha<1$. Then*

$$P_\rho[u-U_{\bar{y}}](x,t)=\epsilon\hat{v}_1\left(\frac{x-z}{\epsilon}\right)\cdot\nabla P_\rho[U_{\bar{y}}](x,t)+O(\epsilon^{2(1-\alpha)}).$$

We now derive a far-field asymptotic expansion for $P_\rho[u-U_{\bar{y}}]$. Define

$$U_z(x,t):=\frac{\delta_{t=|x-z|}}{4\pi|x-z|}. \tag{1.48}$$

We have

$$P_\rho[U_z](x,t)=\int_{|\omega|\le\rho}e^{-\sqrt{-1}\omega t}\Phi_\omega(x-z)\,d\omega.$$

From Theorem 1.4, we compute

$$\begin{aligned}&\int_{|\omega|\le\rho}e^{-\sqrt{-1}\omega t}(v(x,\omega)-V(x,\omega))\,d\omega \\ &\quad=-\epsilon^3\int_{|\omega|\le\rho}e^{-\sqrt{-1}\omega t}\nabla V(z,\omega)M(k,B)\nabla\Phi_\omega(x-z)\,d\omega \\ &\quad+\int_{|\omega|\le\rho}e^{-\sqrt{-1}\omega t}R(x,\omega)\,d\omega,\end{aligned}$$

where the remainder is estimated by

$$\int_{|\omega|\le\rho}e^{-\sqrt{-1}\omega t}R(x,\omega)\,d\omega=O(\epsilon^{4(1-\frac{3}{4}\alpha)}).$$

Since

$$\begin{aligned}&\int_{|\omega|\le\rho}e^{-\sqrt{-1}\omega t}\nabla V(z,\omega)M(k,B)\nabla\Phi_\omega(x-z)\,d\omega \\ &\quad=\int_{\mathbb{R}}\nabla\left(\frac{\psi_\rho(t-\tau-|x-z|)}{4\pi|x-z|}\right)M(k,B)\nabla\left(\frac{\psi_\rho(\tau-|z-\bar{y}|)}{4\pi|z-\bar{y}|}\right)d\tau,\end{aligned}$$

and

$$\epsilon^3\int_{\mathbb{R}}\nabla P_\rho[U_z](x,t-\tau)\cdot M(k,B)\nabla P_\rho[U_{\bar{y}}](z,\tau)\,d\tau=O(\epsilon^3\rho^2),$$

the following theorem holds.

THEOREM 1.6. *Suppose that $\rho = O(\epsilon^{-\alpha})$ for some $\alpha < 1$. Then for $|x - z| \geq C > 0$, the following far-field expansion holds*

$$P_\rho[u - U_{\bar{y}}](x,t) = -\epsilon^3 \int_{\mathbb{R}} \nabla P_\rho[U_z](x, t-\tau) \cdot M(k,B) \nabla P_\rho[U_{\bar{y}}](z,\tau)\, d\tau + O(\epsilon^{4(1-\frac{3}{4}\alpha)})$$

for x away from z.

It should be noted that Theorem 1.6 says that the perturbation due to the anomaly is (approximately) a wave emitted from the point z at $t = T := |z - \bar{y}|$. The anomaly behaves then like a dipolar source. This is the key point of our approach for designing time-reversal imaging procedure in the next section. We also emphasize that the approximation holds after truncation of the frequencies higher than $\epsilon^{-\alpha}$ ($\alpha < 1$). This has an important meaning in relation to the resolution limit in imaging as explained in the next section. Moreover, from the optimality of the range of frequencies for which formula (1.38) is valid, it follows that $\alpha < 1$ is indeed the optimal exponent.

1.4. Reconstruction methods

A model problem for the acoustic radiation force imaging is (1.46), where $\bar{y}$ is the location of the pushing ultrasonic beam. The transient wave $u(x,t)$ is the induced wave. The inverse problem is to reconstruct the shape and the conductivity of the small anomaly D from either far-field or near-field measurements of u.

1.4.1. Time-reversal. Let $w(x,t) := u(x,t) - U_{\bar{y}}(x,t)$. We present a method for detecting the location z of the anomaly from measurements of w for x away from z. To detect the anomaly one can use a time-reversal technique. The main idea of time-reversal is to take advantage of the reversibility of the wave equation in a non-dissipative unknown medium in order to back-propagate signals to the sources that emitted them. See [**54, 41, 89, 55**]. Some interesting mathematical works started to investigate different aspects of time-reversal phenomena: see, for instance, [**28**] for time-reversal in the time-domain, [**51, 84, 64, 44, 45**] for time-reversal in the frequency domain, and [**57, 36**] for time-reversal in random media.

In the context of anomaly detection, one measures the perturbation of the wave on a closed surface surrounding the anomaly, and retransmits it through the background medium in a time-reversed chronology. Then the perturbation will travel back to the location of the anomaly.

Suppose that we are able to measure the perturbation w and its normal derivative at any point x on a sphere S englobing the anomaly D. The time-reversal operation is described by the transform $t \mapsto t_0 - t$. Both the perturbation w and its normal derivative on S are time-reversed and emitted from S. Then a time-reversed perturbation, denoted by $w_{\rm tr}$, propagates inside the volume Ω surrounded by S. Taking into account the definition (1.48) of the outgoing fundamental solution, spatial reciprocity and time reversal invariance of the wave equation, the time-reversed perturbation $w_{\rm tr}$ due to the anomaly D in Ω should be defined as follows.

DEFINITION 1.7. *The time-reversed perturbation is given by*

$$w_{tr}(x,t) = \int_{\mathbb{R}} \int_S \left[U_x(x', t-s) \frac{\partial w}{\partial \nu}(x', t_0 - s) - \frac{\partial U_x}{\partial \nu}(x', t-s) w(x', t_0 - s) \right] d\sigma(x')\, ds,$$

where

$$U_x(x',t-s)=\frac{\delta_{t=s+|x-x'|}}{4\pi|x-x'|}.$$

However, with the high frequency component of w truncated, we take the following definition:

$$\begin{aligned} w_{\rm tr}(x,t) &= \int_{\mathbb{R}}\int_S \Big[U_x(x',t-s)\frac{\partial P_\rho[u-U_{\bar y}]}{\partial\nu}(x',t_0-s) \\ &\quad -\frac{\partial U_x}{\partial\nu}(x',t-s)P_\rho[u-U_{\bar y}](x',t_0-s)\Big]\,d\sigma(x')\,ds\,. \end{aligned} \tag{1.49}$$

According to Theorem 1.6, we have

$$P_\rho[u-U_{\bar y}](x,t)\approx -\epsilon^3\int_{\mathbb{R}}\nabla P_\rho[U_z](x,t-\tau)\cdot p(z,\tau)\,d\tau$$

where

$$p(z,\tau)=M(k,B)\nabla P_\rho[U_{\bar y}](z,\tau). \tag{1.50}$$

Therefore it follows that

$$\begin{aligned} w_{\rm tr}(x,t) &\approx -\epsilon^3\int_{\mathbb{R}}p(z,\tau)\cdot\int_{\mathbb{R}}\int_S\Big[U_x(x',t-s)\frac{\partial\nabla_z P_\rho[U_z]}{\partial\nu}(x',t_0-s-\tau) \\ &\quad -\frac{\partial U_x}{\partial\nu}(x',t-s)\nabla_z P_\rho[U_z](x',t_0-s-\tau)\Big]\,d\sigma(x')\,ds\,d\tau, \\ &\approx -\epsilon^3\int_{\mathbb{R}}p(z,\tau)\cdot\nabla_z\int_{\mathbb{R}}\int_S\Big[U_x(x',t-s)\frac{\partial P_\rho[U_z]}{\partial\nu}(x',t_0-s-\tau) \\ &\quad -\frac{\partial U_x}{\partial\nu}(x',t-s)P_\rho[U_z](x',t_0-s-\tau)\Big]\,d\sigma(x')\,ds\,d\tau. \end{aligned}$$

Multiplying the equation

$$\Big(\partial_s^2-\Delta_{x'}\Big)U_x(x',t-s)=\delta_{s=t}\delta_{x'=x}$$

by $P_\rho[U_z](x',t_0-\tau-s)$, integrating by parts, and using the equation

$$\Big(\partial_s^2-\Delta_{x'}\Big)P_\rho[U_z](x',t_0-\tau-s)=\psi_\rho(s-t_0+\tau)\delta_{x'=z}\quad\text{in }\mathbb{R}^3\times\mathbb{R},$$

we have

$$\begin{aligned} &\int_{\mathbb{R}}\int_S\Big[U_x(x',t-s)\frac{\partial P_\rho[U_z]}{\partial\nu}(x',t_0-s-\tau) \\ &\qquad -\frac{\partial U_x}{\partial\nu}(x',t-s)P_\rho[U_z](x',t_0-s-\tau)\Big]\,d\sigma(x')\,ds \\ &= P_\rho[U_z](x,t_0-\tau-t)-P_\rho[U_z](x,t-t_0+\tau). \end{aligned} \tag{1.51}$$

It then follows that

$$w_{\rm tr}(x,t)\approx -\epsilon^3\int_{\mathbb{R}}p(z,\tau)\cdot\nabla_z\big[P_\rho[U_z](x,t_0-\tau-t)-P_\rho[U_z](x,t-t_0+\tau)\big]d\tau. \tag{1.52}$$

The formula (1.52) can be interpreted as the superposition of incoming and outgoing waves, centered on the location z of the anomaly. To see it more clearly, let us assume that $p(z,\tau)$ is concentrated at $\tau=T:=|z-\bar y|$, which is reasonable

since $p(z,\tau) = M(k,B)\nabla P_\rho[U_{\bar{y}}](z,\tau)$ peaks at $\tau = T$. Under this assumption, the formula (1.52) takes the form

$$w_{\rm tr}(x,t) \approx -\epsilon^3 p\cdot\nabla_z\big[P_\rho[U_z](x,t_0-T-t) - P_\rho[U_z](x,t-t_0+T)\big], \tag{1.53}$$

where $p = p(z,T)$. It is clearly sum of incoming and outgoing spherical waves.

Formula (1.53) has an important physical interpretation. By changing the origin of time, T can be set to 0 without loss of generality. By taking Fourier transform of (1.52) over the time variable t, we obtain that

$$\hat{w}_{\rm tr}(x,\omega) \propto \epsilon^3 p\cdot\nabla\left(\frac{\sin(\omega|x-z|)}{|x-z|}\right), \tag{1.54}$$

where ω is the wavenumber. This shows that the anti-derivative of time-reversal perturbation $w_{\rm tr}$ focuses on the location z of the anomaly with a focal spot size limited to one-half the wavelength which is in agreement with the Rayleigh resolution limit. It should be pointed out that in the frequency domain, (1.54) is valid only for $\lambda = 2\pi/\omega \gg \epsilon$, ϵ being the characteristic size of the anomaly. In fact, according to Theorem 1.6, it is valid for frequencies less than $O(\epsilon^{-\alpha})$ for $\alpha < 1$.

In the frequency domain, suppose that one measures the perturbation $v - V$ and its normal derivative on a sphere S englobing the anomaly D. To detect the anomaly D one computes

$$\hat{w}(x,\omega) := \int_S \left[\Phi_\omega(x-x')\overline{\frac{\partial(v-V)}{\partial\nu}(x',\omega)} - \overline{(v-V)(x',\omega)}\frac{\partial\Phi_\omega}{\partial\nu}(x-x')\right]d\sigma(x'),$$

in the domain Ω surrounded by S. Observe that $\hat{w}(x,\omega)$ is a solution to the Helmholtz equation: $(\Delta+\omega^2)\hat{w} = 0$ in Ω.

An identity parallel to (1.51) can be derived in the frequency domain. Indeed, it plays a key role in achieving the resolution limit. Applying Green's theorem to $\Phi_\omega(x-x')$ and $\overline{\Phi_\omega(z-x')}$, we have

$$\begin{aligned}\int_S \left[\Phi_\omega(x-x')\overline{\frac{\partial\Phi_\omega}{\partial\nu}(z-x')} - \overline{\Phi_\omega}(z-x')\frac{\partial\Phi_\omega}{\partial\nu}(x-x')\right]d\sigma(x')\\ = 2\sqrt{-1}\Im m\,\Phi_\omega(z-x).\end{aligned} \tag{1.55}$$

In view of (1.55), we immediately find from the asymptotic expansion in Theorem 1.4 that

$$(v-V)(x,\omega) \propto \epsilon^3\hat{p}\cdot\nabla\left(\frac{\sin(\omega|x-z|)}{|x-z|}\right), \tag{1.56}$$

where $\hat{p} = M(k,B)\nabla V(z,\omega)$. The above approximation shows that the anti-derivative of $\hat{w}(x,\omega)$ has a peak at the location z of the anomaly and also proves the Rayleigh resolution limit. Note that (1.54) is in a good agreement with (1.56) even though the high-frequency component has been truncated.

It is also worth noticing that a formula similar to (1.56) can be derived in an inhomogeneous medium Ω surrounded by S. We have

$$\begin{aligned}\int_S \left[\mathcal{G}(x-x',\omega)\overline{\frac{\partial\mathcal{G}}{\partial\nu}(x'-z,\omega)} - \overline{\mathcal{G}(x'-z,\omega)}\frac{\partial\mathcal{G}}{\partial\nu}(x-x',\omega)\right]d\sigma(x')\\ = 2\sqrt{-1}\Im m\,\mathcal{G}(x-z,\omega),\end{aligned} \tag{1.57}$$

where $\mathcal{G}$ is the Green function in the inhomogeneous medium Ω. Identity (1.57) shows that the sharper the behavior of $\Im m\,\mathcal{G}$ at z is, the higher is the resolution.

It would be quite interesting to see how the behavior of $\Im m\, \mathcal{G}$ depends on the heterogeneity of the medium.

Once the location z of the anomaly is found, the polarization tensor associated with the anomaly D can be found using the formula in Theorem 1.6. Since $M(k, D) = \epsilon^3 M(k, B)$, we minimize over symmetric positive matrices $M(k, D)$ the quantity

$$\sum_{l=1}^{L} \left| P_\rho[u - U_{\bar{y}}](x_l, t) + \int_{\mathbb{R}} \nabla P_\rho[U_z](x_l, t-\tau) M(k, D) \cdot \nabla P_\rho[U_{\bar{y}}](z, \tau)\, d\tau \right|,$$

for L measurement points $x_1, \ldots, x_L$. It is worth emphasizing that the polarization tensor $M(k, D)$ contains the mixed information of volume $|D|$ and the conductivity k of the anomaly and it is not possible to separate these two information from M.

However, from the near-field measurements, the shape and the conductivity of the anomaly D can be approximately reconstructed.

1.4.2. Kirchhoff imaging. Suppose that $|z - \bar{y}| \gg 1$ and $|x - z| \gg 1$. Then

$$v(x, \omega) - V(x, \omega) \approx -\frac{\omega^2 \epsilon^3}{16\pi^2} \frac{(z - \bar{y}) M(k, B)(z - x)}{|z - \bar{y}|^2 |z - x|^2} e^{-\sqrt{-1}\omega z \cdot (\frac{\bar{y}}{|\bar{y}|} + \frac{x}{|x|})}, \tag{1.58}$$

which holds for a broadband of frequencies. Then, for a given search point z^S, the Kirchhoff imaging functional can be written as

$$\mathcal{I}_{\mathrm{KI}}(z^S, \frac{x}{|x|}) := \frac{1}{L} \sum_{\omega_l, l=1,\ldots,L} \frac{1}{\omega_l^2} e^{\sqrt{-1}\omega_l z^S \cdot (\frac{\bar{y}}{|\bar{y}|} + \frac{x}{|x|})} (v(x, \omega_l) - V(x, \omega_l)),$$

where L is the number of frequencies (ω_l). See [**52**] and the references therein.

In view of (1.58), we have

$$\mathcal{I}_{\mathrm{KI}}(z^S, \frac{x}{|x|}) \approx C_d \int_\omega e^{\sqrt{-1}\omega_l (z^S - z) \cdot (\frac{\bar{y}}{|\bar{y}|} + \frac{x}{|x|})}\, d\omega,$$

for some constant C_d independent of ω and z^S and therefore,

$$\mathcal{I}_{\mathrm{KI}}(z^S, \frac{x}{|x|}) \approx C_d \delta_{(z^S - z) \cdot (\frac{\bar{y}}{|\bar{y}|} + \frac{x}{|x|}) = 0}.$$

Hence, to determine the location z of the anomaly, one needs three different measurement directions $x/|x|$.

1.4.3. Back-propagation imaging. From single frequency measurements, one can detect the anomaly using a back-propagation-type algorithm. Let $\theta_l = x_l/|x_l|$ for $l = 1, \ldots, L$, be L measurement directions. For a given search point z^S, the back-propagation imaging functional is given by

$$\mathcal{I}_{\mathrm{BP}}(z^S) := \frac{1}{L} \sum_{\theta_l, l=1,\ldots,L} e^{\sqrt{-1}\omega z^S \cdot (\frac{\bar{y}}{|\bar{y}|} + \theta_l)} (v(r\theta_l, \omega) - V(r\theta_l, \omega)), \quad r \gg 1.$$

Since for sufficiently large L, since

$$\frac{1}{L} \sum_{l=1}^{L} e^{\sqrt{-1}\omega \theta_l \cdot x} \approx \begin{cases} j_0(\omega|x|) & \text{for } d = 3, \\ J_0(\omega|x|) & \text{for } d = 2, \end{cases}$$

where j_0 is the spherical Bessel function of order zero and J_0 is the Bessel function of the first kind and of order zero, it follows from (1.58) that

$$\mathcal{I}_{\rm BP}(z^S) \approx C_d \begin{cases} j_0(\omega|z-z^S|) & \text{for } d=3, \\ J_0(\omega|z-z^S|) & \text{for } d=2. \end{cases}$$

for some constant C_d independent of z^S.

Note that $\mathcal{I}_{\rm BP}$ uses a single frequency which can be selected as the highest one among those that maximize the signal-to-noise ratio.

1.4.4. Near-field imaging. In view of Theorem 1.5, to reconstruct the shape and the conductivity of the anomaly D we solve analogously to [**10**] the following minimization problem. Suppose that the location z of the anomaly $D = z + \epsilon B$ and its characteristic size ϵ are known. Let W be a domain containing D and define the functional

$$L(f,k) = \frac{1}{2\Delta T}\int_{T-\frac{\Delta T}{2}}^{T+\frac{\Delta T}{2}} \left\| P_\rho[u-U_{\bar y}](x,t) - \epsilon \hat v_1\left(\frac{x-z}{\epsilon}\right)\cdot \nabla P_\rho[U_{\bar y}](x,t)\right\|^2_{L^2(W)} dt$$
$$+ \beta \int_W |\nabla f(x)|\, dx,$$

where k is the conductivity of D, β is a regularization parameter, f is the binary representation of D, *i.e.*,

$$f(x) = \begin{cases} 1 & \text{if } x \in D, \\ -1 & \text{if } x \notin D, \end{cases}$$

and $\hat v_1$ is the function corresponding to B as defined in (1.32). Here it suffices to take ΔT to be of order $O(\frac{\epsilon}{\sqrt{k}})$. We then minimize over binary functions f and constants $0 < k < +\infty$

$$\min_{k,f} L(f,k) \tag{1.59}$$

subject to (1.32). We may relax the minimization problem (1.59) to function of bounded variation. We refer to [**10**] for the details.

Note that we have to choose a window W that is not so small to preserve some stability and not so big so that we can gain some accuracy. We refer to [**9**] for a discussion on the critical size of the window W that switches between far-field and near-field reconstructions.

1.5. Numerical illustrations

To illustrate our main findings in this chapter, we first tested the accuracy of the derived asymptotic expansions. Then we implemented the imaging algorithms for anomaly detection.

The configuration is the following: a spherical anomaly of radius 0.05 and physical parameter $k = 3$ is placed at $z = (-0.1, 0, 0)$. The source is at $\bar y = (3, 0, 0)$. To truncate the high frequencies, we took $\rho = 2.15$ or equivalently $\alpha = 1/3$.

Figure 1.1 shows comparisons between the fields computed by the asymptotic formulas and by the direct Freefem++ code. The Freefem++ code is based on a finite element discretization in space and a finite difference scheme in time. We have chosen a Crank-Nicolson scheme with step $\Delta t = 0.01$. The near fields were computed at $x = (-0.3, 0, 0)$ and the far-fields were computed at $x = (-8, 0, 0)$.

The fields obtained from the asymptotic formulas are in good agreement with those computed by the Freefem++ code.

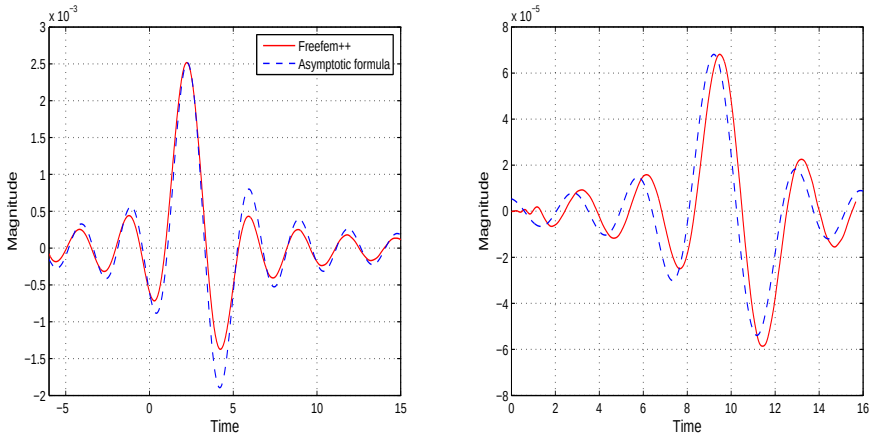

FIGURE 1.1. Comparisons between the near fields (on the left) and between the far-fields (on the right).

Now we turn to imaging. Figure 1.2 shows the performance of the time-reversal for detecting the anomaly.

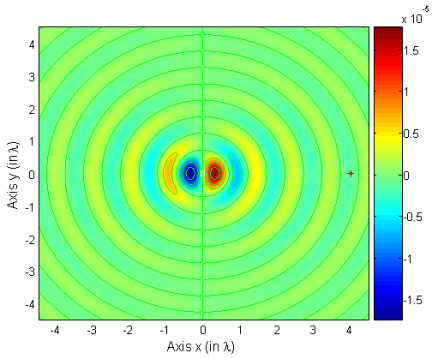

FIGURE 1.2. Detection result using the time-reversal technique. Here '*' shows the transceiver location.

Consider a linear array of 58 receivers placed parallel to the y-axis and spaced by half a wavelength. Figure 1.3 shows the detection result by back-propagation.

Now, consider receivers located at

$$[4\lambda\cos(\pi/4), 4\lambda\sin(\pi/4), 0], [4\lambda\cos(\pi/4), -4\lambda\sin(\pi/4), 0], [4\lambda\cos(\pi/4), 0, 4\lambda\sin(\pi/4)].$$

Figures 1.4, 1.5, and 1.6 show the results of the Kirchhoff imaging functionals for these three different receiver locations. The position of the anomaly is obtained as the intersection of the three planes where each of the Kirchhoff functional attains its maximum. See Figure 1.8.

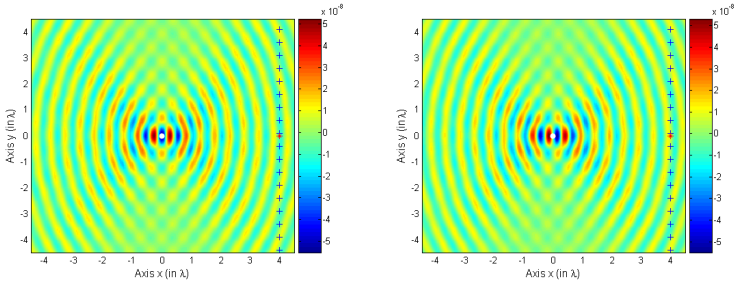

FIGURE 1.3. Real and imaginary parts of the Back-propagation functional. Here '*' and '+' respectively show the transceiver and receiver locations.

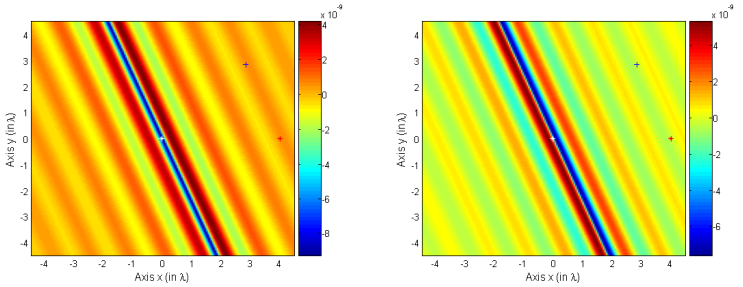

FIGURE 1.4. Real and imaginary part of the Kirchhoff functional when the receiver is at $[4\lambda\cos(\pi/4), 4\lambda\sin(\pi/4), 0]$, '*' indicates the transceiver location and '+' the receiver location.

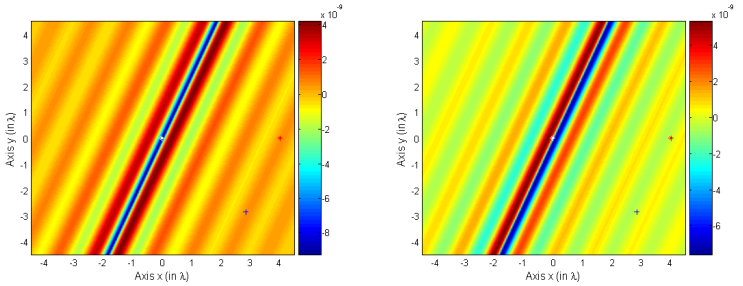

FIGURE 1.5. Real and imaginary part of the Kirchhoff functional when the receiver is at $[4\lambda\cos(\pi/4), -4\lambda\sin(\pi/4), 0]$.

1.6. Concluding remarks

In this chapter, based on careful estimates of the dependence with respect to the frequency of the remainders in asymptotic formulas for the Helmholtz equation, we have rigorously derived the effect of a small conductivity anomaly on transient wave. We have provided near- and far-field asymptotic expansions of the perturbation in the wavefield after truncating its high-frequency component. The threshold of the frequency truncation is of order $\epsilon^{-\alpha}$ $(\alpha < 1)$ where ϵ is the diameter of the

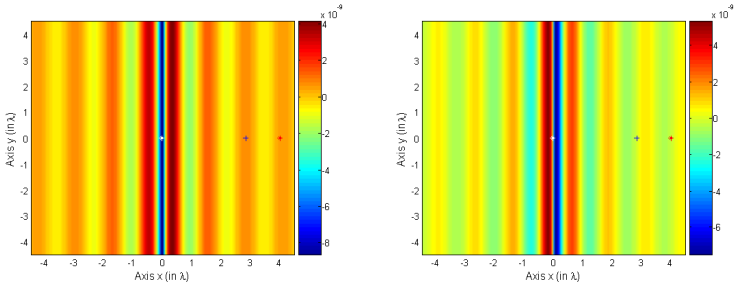

FIGURE 1.6. Real and imaginary part of the Kirchhoff functional when the receiver is at the position $[4\lambda\cos(\pi/4), 0, 4\lambda\sin(\pi/4)]$.

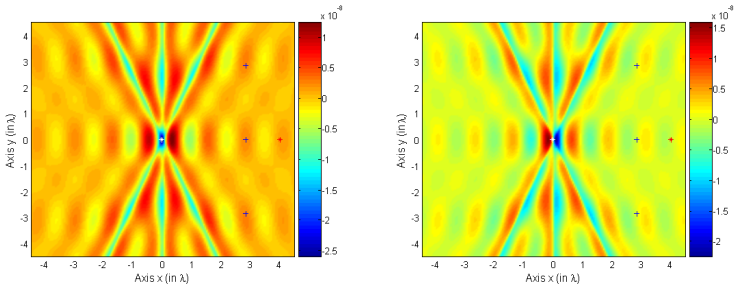

FIGURE 1.7. Sum of the Real and the imaginary parts of the Kirchhoff functional.

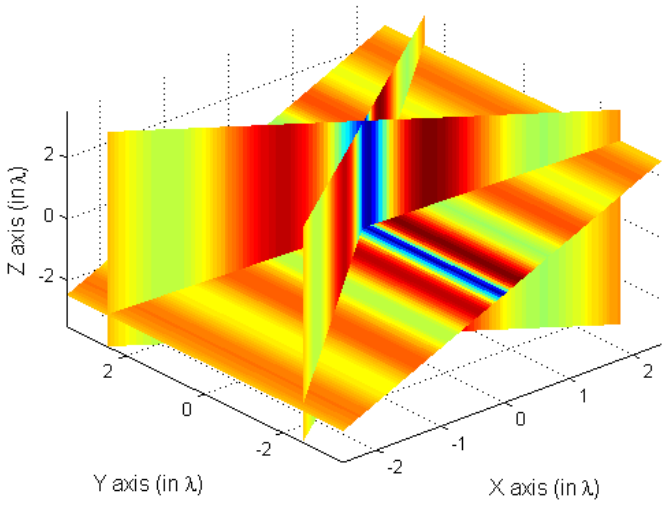

FIGURE 1.8. Intersection of the three planes where the real parts of the Kirchhoff functionals attain their maximum for three different receivers.

anomaly. We have also designed a time-reversal imaging technique for locating the anomaly from far-field measurements of the perturbations in the wavefield and reconstructing its polarization tensor. Using a near-field asymptotic formula, we have proposed an optimization problem to reconstruct the shape and to separate the physical parameters of the anomaly from its volume. The connection between our expansions and reconstruction methods for the wave equation in this chapter and those for the Helmholtz equation has been discussed.

The method and the results of this chapter will be generalized in Chapter 2 to dynamic elastic imaging which has important applications in medical imaging [**34**] as well as in seismology [**1**].

CHAPTER 2

Transient elasticity imaging and time reversal

ABSTRACT. In this chapter we consider a purely quasi-incompressible elasticity model. We rigorously establish asymptotic expansions of near- and far-field measurements of the transient elastic wave induced by a small elastic anomaly. Our proof uses layer potential techniques for the modified Stokes system. Based on these formulas, we design asymptotic imaging methods leading to a quantitative estimation of elastic and geometrical parameters of the anomaly.

2.1. Introduction

In this chapter, we neglect the viscosity effect of tissues and only consider a purely quasi-incompressible elasticity model. We derive asymptotic expansions of the perturbations of the elastic wavefield that are due to the presence of a small anomaly in both the near- and far-field regions as the size of the anomaly goes to zero. Then we design an asymptotic imaging method leading to a quantitative estimation of the shear modulus and shape of the anomaly from near-field measurements. Using time-reversal, we show how to reconstruct the location and geometric features of the anomaly from the far-field measurements. We put a particular emphasis on the difference between the acoustic and the elastic cases, namely, the anisotropy of the focal spot and the birth of a near-field like effect by time reversing the perturbation due to an elastic anomaly.

The results of this chapter extend those in Chapter 1 to transient wave propagation in elastic media.

The chapter is organized as follows. In Section 2.2 we rigorously derive asymptotic formulas for quasi-incompressible elasticity and estimate the dependence of the remainders in these formulas with respect to the frequency. Based on these estimates, we obtain in Section 2.3 formulas for the transient wave equation that are valid after truncating the high-frequency components of the elastic fields. These formulas describe the effect of the presence of a small elastic anomaly in both the near- and far-field. We then investigate in Section 2.4 the use of time-reversal for locating the anomaly and detecting its overall geometric and material parameters via the viscous moment tensor. An optimization problem is also formulated for reconstructing geometric parameters of the anomaly and its shear modulus from near-field measurements.

2.2. Asymptotic expansions

We suppose that an elastic medium occupies the whole space $\mathbb{R}^3$. Let the constants λ and μ denote the Lamé coefficients of the medium, that are the elastic parameters in absence of any anomaly. With these constants, $\mathcal{L}_{\lambda,\mu}$ denotes the

linear elasticity system, namely

$$\mathcal{L}_{\lambda,\mu}\mathbf{u} := \mu\Delta\mathbf{u} + (\lambda+\mu)\nabla\nabla\cdot\mathbf{u}. \tag{2.1}$$

The traction on a smooth boundary $\partial\Omega$ is given by the conormal derivative $\partial\mathbf{u}/\partial\nu$ associated with $\mathcal{L}_{\lambda,\mu}$,

$$\frac{\partial\mathbf{u}}{\partial\nu} := \lambda(\nabla\cdot\mathbf{u})\mathbf{N} + \mu\widehat{\nabla}\mathbf{u}\mathbf{N}, \tag{2.2}$$

where $\mathbf{N}$ denotes the outward unit normal to $\partial\Omega$. Here $\widehat{\nabla}$ denotes the symmetric gradient, *i.e.*,

$$\widehat{\nabla}\mathbf{u} := \nabla\mathbf{u} + \nabla\mathbf{u}^T, \tag{2.3}$$

where the superscript T denotes the transpose.

The time-dependent linear elasticity system is given by

$$\partial_t^2\mathbf{u} - \mathcal{L}_{\lambda,\mu}\mathbf{u} = 0. \tag{2.4}$$

The fundamental solution or the Green function for the system (2.4) is given by $\mathbf{G} = (G_{ij})$ where

$$G_{ij} = \frac{1}{4\pi}\frac{3\gamma_i\gamma_j-\delta_{ij}}{r^3}H^{\sqrt{\mu}}_{\sqrt{\lambda+2\mu}}(x,t) + \frac{1}{4\pi(\lambda+2\mu)}\frac{\gamma_i\gamma_j}{r}\delta_{t=\frac{r}{\sqrt{\lambda+2\mu}}} - \frac{1}{4\pi\mu}\frac{\gamma_i\gamma_j-\delta_{ij}}{r}\delta_{t=\frac{r}{\sqrt{\mu}}}. \tag{2.5}$$

Here $r = |x|, \gamma_i = x_i/r$, δ_{ij} denotes the Kronecker symbol, δ denotes the Dirac delta function, and $H^{\sqrt{\mu}}_{\sqrt{\lambda+2\mu}}(x,t)$ is defined by

$$H^{\sqrt{\mu}}_{\sqrt{\lambda+2\mu}}(x,t) := \begin{cases} t & \text{if } \dfrac{r}{\sqrt{\lambda+2\mu}} < t < \dfrac{r}{\sqrt{\mu}}, \\ 0 & \text{otherwise.} \end{cases} \tag{2.6}$$

Note that $(1/r^3)\,H^{\sqrt{\mu}}_{\sqrt{\lambda+2\mu}}(x,t)$ behaves like $1/r^2$ for times $(r/\sqrt{\lambda+2\mu}) < t < (r/\sqrt{\mu})$. See [**1**].

Suppose that there is an elastic anomaly D, given by $D = \epsilon B + z$, which has the elastic parameters $(\widetilde{\lambda},\tilde{\mu})$. Here B is a $\mathcal{C}^2$-bounded domain containing the origin, z the location of the anomaly, and ϵ a small positive parameter representing the order of magnitude of the anomaly size.

For a given point source $\bar{y}$ away from the anomaly D and a constant vector $\mathbf{a}$, we consider the following transient elastic wave problem in the presence of an anomaly:

$$\begin{cases} \partial_t^2\mathbf{u} - \mathcal{L}_{\lambda,\mu}\mathbf{u} = \delta_{t=0}\delta_{x=\bar{y}}\mathbf{a} \quad \text{in} \quad (\mathbb{R}^3\setminus\overline{D})\times\mathbb{R}, \\ \partial_t^2\mathbf{u} - \mathcal{L}_{\tilde{\lambda},\tilde{\mu}}\mathbf{u} = 0 \quad \text{in} \quad D\times\mathbb{R}, \\ \mathbf{u}\big|_+ - \mathbf{u}\big|_- = 0 \quad \text{on } \partial D\times\mathbb{R}, \\ \dfrac{\partial\mathbf{u}}{\partial\nu}\big|_+ - \dfrac{\partial\mathbf{u}}{\partial\tilde{\nu}}\big|_- = 0 \quad \text{on} \quad \partial D\times\mathbb{R}, \\ \mathbf{u}(x,t) = 0 \quad \text{for } x\in\mathbb{R}^3 \quad \text{and } t\ll 0, \end{cases} \tag{2.7}$$

where $\partial\mathbf{u}/\partial\nu$ and $\partial\mathbf{u}/\partial\tilde{\nu}$ denote the conormal derivatives on ∂D associated respectively with $\mathcal{L}_{\lambda,\mu}$ and $\mathcal{L}_{\tilde{\lambda},\tilde{\mu}}$. Here and throughout this chapter the subscripts $\pm$ denote the limit from outside and inside D, respectively.

As was observed in [**60, 82**], the Poisson ratio of human tissues is very close to 1/2, which amounts to λ/μ and $\tilde{\lambda}/\tilde{\mu}$ being very large. So we seek for a good approximation of the problem (2.7) as λ and $\widetilde{\lambda}$ go to $+\infty$. To this end, let

$$p := \begin{cases} \lambda \nabla \cdot \mathbf{u} & \text{in} \quad (\mathbb{R}^3 \setminus \overline{D}) \times \mathbb{R}, \\ \widetilde{\lambda} \nabla \cdot \mathbf{u} & \text{in} \quad D \times \mathbb{R}. \end{cases}$$

One can show by modifying a little the argument in [**10**] that as λ and $\widetilde{\lambda}$ go to $+\infty$ with $\widetilde{\lambda}/\lambda$ of order one, the displacement field $\mathbf{u}$ can be represented in the form of the following series:

$$\begin{aligned} \mathbf{u}(x,t) &= \mathbf{u}_0(x,t) + \Big(\frac{1}{\lambda}\chi(\mathbb{R}^3 \setminus \overline{D}) + \frac{1}{\widetilde{\lambda}}\chi(D)\Big)\, \mathbf{u}_1(x,t) \\ &\qquad + \Big(\frac{1}{\lambda^2}\chi(\mathbb{R}^3 \setminus \overline{D}) + \frac{1}{\widetilde{\lambda}^2}\chi(D)\Big)\, \mathbf{u}_2(x,t) + \dots\,, \\ p &= p_0 + \Big(\frac{1}{\lambda}\chi(\mathbb{R}^3 \setminus \overline{D}) + \frac{1}{\widetilde{\lambda}}\chi(D)\Big)\, p_1 + \Big(\frac{1}{\lambda^2}\chi(\mathbb{R}^3 \setminus \overline{D}) + \frac{1}{\widetilde{\lambda}^2}\chi(D)\Big)\, p_2 + \dots\,, \end{aligned}$$

where the leading-order term $(\mathbf{u}_0(x,t), p_0(x))$ is solution to the following homogeneous time-dependent Stokes system

$$\begin{cases} \partial_t^2 \mathbf{u}_0 - \nabla \cdot (\tilde{\mu}\chi(D) + \mu\chi(\mathbb{R}^3 \setminus \overline{D}))\nabla \mathbf{u}_0 - \nabla p_0 = \delta_{t=0}\delta_{x=y}\mathbf{a} \quad \text{in } \mathbb{R}^3 \times \mathbb{R}, \\ \nabla \cdot \mathbf{u}_0 = 0 \quad \text{in } \mathbb{R}^3 \times \mathbb{R}, \\ \mathbf{u}_0(x,t) = 0 \quad \text{for } x \in \mathbb{R}^3 \quad \text{and } t \ll 0. \end{cases} \tag{2.8}$$

The inverse problem considered in this chapter is to image an anomaly D with shear modulus $\tilde{\mu}$ inside a background medium of shear modulus $\mu \neq \tilde{\mu}$ from near-field or far-field measurements of the transient elastic wave $\mathbf{u}(x,t)$ (approximated by $\mathbf{u}_0(x,t)$) that is the solution to (2.7) (approximated by (2.8)).

In order to design an accurate and robust algorithm to detect the anomaly D incorporating the fact that D is of small size of order ϵ, we will derive an asymptotic expansion of $\mathbf{u}_0$ as $\epsilon \to 0$. As shown in [**3**], this scale separation methodology yields to accurate imaging algorithms.

2.2.1. Layer potentials for the Stokes system. We begin by reviewing some basic facts on layer potentials for the Stokes system, which we shall use in the next subsection. Relevant derivations or proofs of these facts can be found in [**77**] and [**10**].

We consider the following modified Stokes system:

$$\begin{cases} (\Delta + \kappa^2)\mathbf{v} - \nabla q = 0, \\ \nabla \cdot \mathbf{v} = 0. \end{cases} \tag{2.9}$$

Here $\mathbf{v}$ is the displacement field and q is the pressure. Let $\partial_i = \frac{\partial}{\partial x_i}$. The fundamental tensor $\mathbf{\Gamma}^\kappa = (\Gamma^\kappa_{ij})_{i,j=1}^3$ and $\mathbf{F} = (F_1, F_2, F_3)$ to (2.9) in three dimensions are given by

$$\begin{cases} \Gamma^\kappa_{ij}(x) = -\dfrac{\delta_{ij}}{4\pi}\dfrac{e^{\sqrt{-1}\kappa|x|}}{|x|} - \dfrac{1}{4\pi\kappa^2}\partial_i\partial_j\dfrac{e^{\sqrt{-1}\kappa|x|} - 1}{|x|}, \\ \\ F_i(x) = -\dfrac{1}{4\pi}\dfrac{x_i}{|x|^3}. \end{cases} \tag{2.10}$$

If $\kappa = 0$, let

$$\Gamma^0_{ij}(x) = -\frac{1}{8\pi}\Big(\frac{\delta_{ij}}{|x|} + \frac{x_i x_j}{|x|^3}\Big). \tag{2.11}$$

Then $\mathbf{\Gamma}^0 = (\Gamma^0_{ij})$ together with $\mathbf{F}$ is the fundamental tensor for the standard Stokes system given by

$$\begin{cases} \Delta \mathbf{v} - \nabla q = 0, \\ \nabla \cdot \mathbf{v} = 0. \end{cases}$$

One can easily see that

$$\Gamma^\kappa_{ij}(x) = \Gamma^0_{ij}(x) - \frac{\delta_{ij}\kappa\sqrt{-1}}{6\pi} + O(\kappa^2) \tag{2.12}$$

uniformly in x as long as $|x|$ is bounded.

For a bounded $\mathcal{C}^2$-domain D and $\kappa \geq 0$, let

$$\begin{cases} \mathbf{S}^\kappa_D[\varphi](x) := \displaystyle\int_{\partial D} \mathbf{\Gamma}^\kappa(x-y)\varphi(y)d\sigma(y), \\ \mathcal{Q}_D[\varphi](x) := \displaystyle\int_{\partial D} \mathbf{F}(x-y)\cdot\varphi(y)\,d\sigma(y), \end{cases} \qquad x \in \mathbb{R}^3 \tag{2.13}$$

for $\varphi = (\varphi_1, \varphi_2, \varphi_3) \in L^2(\partial D)^3$. When $\kappa = 0$, $\mathbf{S}^0_D$ is the single layer potential for the Stokes system. It is worth emphasizing that $\mathbf{S}^\kappa_D[\varphi](x)$ is a vector while $\mathcal{Q}_D[\varphi](x)$ is a scalar, and the pair $(\mathbf{S}^\kappa_D[\varphi], \mathcal{Q}_D[\varphi])$ is a solution to (2.9).

By abuse of notation, let

$$\frac{\partial \mathbf{u}}{\partial \mathbf{N}} = (\widehat{\nabla}\mathbf{u})\mathbf{N} \quad \text{on } \partial D.$$

We define the conormal derivative $\partial/\partial n$ (for the Stokes system) on ∂D by

$$\frac{\partial \mathbf{v}}{\partial n}\Big|_\pm = \frac{\partial \mathbf{v}}{\partial \mathbf{N}}\Big|_\pm - q\big|_\pm \mathbf{N}$$

for a pair of solutions $(\mathbf{v}, q)$ to (2.9). It is well-known that

$$\frac{\partial \mathbf{S}^\kappa_D[\varphi]}{\partial n}\Big|_\pm = (\pm\frac{1}{2}I + (\mathbf{K}^\kappa_D)^*)[\varphi] \quad \text{a.e. on } \partial D, \tag{2.14}$$

where $\mathbf{K}^\kappa_D$ is the boundary integral operator defined by

$$\mathbf{K}^\kappa_D[\varphi](x) := \text{p.v.} \int_{\partial D} \left[\frac{\partial}{\partial \mathbf{N}(y)}(\mathbf{\Gamma}^\kappa(x-y)\varphi(y)) + \mathbf{F}(x-y)\mathbf{N}(y)\cdot\varphi(y)\right] d\sigma(y) \tag{2.15}$$

for almost all $x \in \partial D$ and $(\mathbf{K}^\kappa_D)^*$ is the L^2-adjoint operator of $\mathbf{K}^{-\kappa}_D$:

$$(\mathbf{K}^\kappa_D)^*[\varphi](x) := \text{p.v.} \int_{\partial D} \left[\frac{\partial}{\partial \mathbf{N}(x)}(\mathbf{\Gamma}^\kappa(x-y)\varphi(y)) + \mathbf{F}(x-y)\cdot\varphi(y)\mathbf{N}(x)\right] d\sigma(y). \tag{2.16}$$

Here p.v. denotes the Cauchy principal value.

Let $H^1(\partial D) := \{\varphi \in L^2(\partial D), \partial\varphi/\partial\tau \in L^2(\partial D)\}$, $\partial/\partial\tau$ being the tangential derivative. The operator $\mathbf{S}^0_D$ is bounded from $L^2(\partial D)^3$ into $H^1(\partial D)^3$ and invertible in three dimensions. Moreover, one can see that for κ small

$$\|\mathbf{S}^\kappa_D[\varphi] - \mathbf{S}^0_D[\varphi]\|_{H^1(\partial D)} \leq C\kappa\|\varphi\|_{L^2(\partial D)} \tag{2.17}$$

for all $\varphi \in L^2(\partial D)^3$, where C is independent of κ. It is also well-known that the singular integral operator $(\mathbf{K}_D^0)^*$ is bounded on $L^2(\partial D)^3$. Similarly to (2.17), one can see that for κ small

$$\|(\mathbf{K}_D^{-\kappa})^*[\varphi] - (\mathbf{K}_D^0)^*[\varphi]\|_{L^2(\partial D)} \leq C\kappa\|\varphi\|_{L^2(\partial D)}$$

for some constant C independent of κ, which in view of (2.14) yields

$$\left\| \frac{\partial(\mathbf{S}_D^{\kappa}[\varphi])}{\partial n}\Big|_{\pm} - \frac{\partial(\mathbf{S}_D^{0}[\varphi])}{\partial n}\Big|_{\pm} \right\|_{L^2(\partial D)} \leq C\kappa\|\varphi\|_{L^2(\partial D)}. \tag{2.18}$$

2.2.2. Derivation of asymptotic expansions. Recall that $\bar{y}$ is a point source in $\mathbb{R}^3$ such that $|\bar{y} - z| \gg \epsilon$. Taking the Fourier transform of (2.8) in the t-variable yields

$$\begin{cases} (\Delta + \dfrac{\omega^2}{\mu})\hat{\mathbf{u}}_0 - \dfrac{1}{\mu}\nabla\hat{p}_0 = \dfrac{1}{\mu}\delta_{x=\bar{y}}\,\mathbf{a} & \text{in } \mathbb{R}^3 \setminus \overline{D}, \\ (\Delta + \dfrac{\omega^2}{\tilde{\mu}})\hat{\mathbf{u}}_0 - \dfrac{1}{\tilde{\mu}}\nabla\hat{p}_0 = 0 & \text{in } D, \\ \hat{\mathbf{u}}_0|_+ - \hat{\mathbf{u}}_0|_- = 0 & \text{on } \partial D, \\ (\hat{p}_0|_- - \hat{p}_0|_+)\mathbf{N} + \mu\dfrac{\partial\hat{\mathbf{u}}_0}{\partial\mathbf{N}}\Big|_+ - \tilde{\mu}\dfrac{\partial\hat{\mathbf{u}}_0}{\partial\mathbf{N}}\Big|_- = 0 & \text{on } \partial D, \\ \nabla\cdot\hat{\mathbf{u}}_0 = 0 & \text{in } \mathbb{R}^3, \end{cases} \tag{2.19}$$

subject to the radiation condition:

$$\begin{cases} \hat{p}_0(x) \to 0 \quad \text{as } r = |x| \to +\infty, \\ \partial_r\nabla\times\hat{\mathbf{u}}_0 - \sqrt{-1}\dfrac{\omega}{\sqrt{\mu}}\nabla\times\hat{\mathbf{u}}_0 = o(\dfrac{1}{r}) \quad \text{as } r = |x| \to +\infty \text{ uniformly in } \dfrac{x}{|x|}, \end{cases} \tag{2.20}$$

where $\hat{\mathbf{u}}_0$ and $\hat{p}_0$ denote the Fourier transforms of $\mathbf{u}_0$ and of p_0, respectively. We say that $(\hat{\mathbf{u}}_0, \hat{p}_0)$ satisfies the radiation condition if (2.20) holds.

Let

$$\hat{\mathbf{U}}_0(x,\omega) := \frac{1}{\mu}\mathbf{\Gamma}^{\frac{\omega}{\sqrt{\mu}}}(x - \bar{y})\mathbf{a}, \tag{2.21}$$

$$\hat{q}_0(x) := \mathbf{F}(x - \bar{y})\cdot\mathbf{a}. \tag{2.22}$$

Then the pair $(\hat{\mathbf{U}}_0(x,\omega), \hat{q}_0(x))$ satisfies

$$\begin{cases} (\Delta + \dfrac{\omega^2}{\mu})\hat{\mathbf{U}}_0 - \dfrac{1}{\mu}\nabla\hat{q}_0 = \dfrac{1}{\mu}\delta_{x=\bar{y}}\,\mathbf{a} \quad \text{in } \mathbb{R}^3, \\ \nabla\cdot\hat{\mathbf{U}}_0 = 0 \quad \text{in } \mathbb{R}^3. \end{cases} \tag{2.23}$$

In view of (2.19) and (2.23), it is natural to expect that $\hat{\mathbf{u}}_0$ converges to $\hat{\mathbf{U}}_0$ as ϵ tends to 0. We shall derive an asymptotic expansion for $\hat{\mathbf{u}}_0 - \hat{\mathbf{U}}_0$ as ϵ tends to zero and carefully estimate the dependence of the remainder on the frequency ω.

Let $\mathbf{w} = \hat{\mathbf{u}}_0 - \hat{\mathbf{U}}_0$ and introduce

$$p := \begin{cases} \dfrac{1}{\mu}(\hat{p}_0 - \hat{q}_0) & \text{in } \mathbb{R}^3 \setminus \overline{D}, \\ \dfrac{1}{\tilde{\mu}}(\hat{p}_0 - \hat{q}_0) & \text{in } D. \end{cases}$$

Then the pair $(\mathbf{w}, p)$ satisfies

$$
\begin{cases}
(\Delta + \dfrac{\omega^2}{\mu})\mathbf{w} - \nabla p = 0 & \text{in } \mathbb{R}^3 \setminus \overline{D}, \\
(\Delta + \dfrac{\omega^2}{\tilde{\mu}})\mathbf{w} - \nabla p = (\dfrac{1}{\mu} - \dfrac{1}{\tilde{\mu}})(\omega^2 \hat{\mathbf{U}}_0 - \nabla \hat{q}_0) & \text{in } D, \\
\mathbf{w}|_+ - \mathbf{w}|_- = 0 & \text{on } \partial D, \\
\mu(\dfrac{\partial \mathbf{w}}{\partial \mathbf{N}}\Big|_+ - p|_+ \mathbf{N}) - \tilde{\mu}(\dfrac{\partial \mathbf{w}}{\partial \mathbf{N}}\Big|_- - p|_- \mathbf{N}) = (\tilde{\mu} - \mu)\dfrac{\partial \hat{\mathbf{U}}_0}{\partial \mathbf{N}} & \text{on } \partial D, \\
\nabla \cdot \mathbf{w} = 0, & \\
(\mathbf{w}, p) \text{ satisfies the radiation condition.} &
\end{cases} \tag{2.24}
$$

Therefore, we can represent $(\mathbf{w}, p)$ as

$$
\mathbf{w}(x) = \begin{cases}
(\dfrac{1}{\mu} - \dfrac{1}{\tilde{\mu}}) \displaystyle\int_D \mathbf{\Gamma}^{\frac{\omega}{\sqrt{\tilde{\mu}}}}(x - y)(\omega^2 \hat{\mathbf{U}}_0(y) - \nabla \hat{q}_0(y))\, dy + \mathbf{S}_D^{\frac{\omega}{\sqrt{\tilde{\mu}}}}[\varphi](x) & \text{in } D, \\
\mathbf{S}_D^{\frac{\omega}{\sqrt{\tilde{\mu}}}}[\psi](x) & \text{in } \mathbb{R}^3 \setminus \overline{D},
\end{cases} \tag{2.25}
$$

and

$$
p(x) = \begin{cases}
(\dfrac{1}{\mu} - \dfrac{1}{\tilde{\mu}}) \displaystyle\int_D \mathbf{F}(x - y) \cdot (\omega^2 \hat{\mathbf{U}}_0(y) - \nabla \hat{q}_0(y))\, dy + \mathcal{Q}_D[\varphi](x) & \text{in } D, \\
\mathcal{Q}_D[\psi](x) & \text{in } \mathbb{R}^3 \setminus \overline{D},
\end{cases} \tag{2.26}
$$

where (φ, ψ) is the solution to the following system of integral equations

$$
\begin{cases}
\mathbf{S}_D^{\frac{\omega}{\sqrt{\tilde{\mu}}}}[\varphi](x) - \mathbf{S}_D^{\frac{\omega}{\sqrt{\tilde{\mu}}}}[\psi](x) = (\dfrac{1}{\mu} - \dfrac{1}{\tilde{\mu}}) \displaystyle\int_D \mathbf{\Gamma}^{\frac{\omega}{\sqrt{\tilde{\mu}}}}(x - y)(\omega^2 \hat{\mathbf{U}}_0(y) - \nabla \hat{q}_0(y))\, dy, \\
\mu \dfrac{\partial \mathbf{S}_D^{\frac{\omega}{\sqrt{\tilde{\mu}}}}[\varphi]}{\partial n}\Big|_+(x) - \tilde{\mu} \dfrac{\partial \mathbf{S}_D^{\frac{\omega}{\sqrt{\tilde{\mu}}}}[\psi]}{\partial n}\Big|_-(x) = (\tilde{\mu} - \mu)\dfrac{\partial \hat{\mathbf{U}}_0}{\partial \mathbf{N}} \\
\qquad + (\dfrac{\tilde{\mu}}{\mu} - 1)\dfrac{\partial}{\partial \mathbf{N}} \displaystyle\int_D \mathbf{\Gamma}^{\frac{\omega}{\sqrt{\tilde{\mu}}}}(x - y)(\omega^2 \hat{\mathbf{U}}_0(y) - \nabla \hat{q}_0(y))\, dy \\
\qquad - (\dfrac{\tilde{\mu}}{\mu} - 1) \displaystyle\int_D \mathbf{F}(x - y) \cdot (\omega^2 \hat{\mathbf{U}}_0(y) - \nabla \hat{q}_0(y))\, dy\, \mathbf{N}.
\end{cases} \tag{2.27}
$$

In order to prove the unique solvability of (2.27), let us make a change of variables: Recalling that D is of the form $D = \epsilon B + z$, we put

$$
\tilde{\varphi}(\tilde{x}) = \varphi(\epsilon \tilde{x} + z), \quad \tilde{x} \in \partial B, \tag{2.28}
$$

and define similarly $\tilde{\psi}$. Then after scaling, (2.27) takes the form

$$
\begin{cases}
\mathbf{S}_B^{\frac{\epsilon\omega}{\sqrt{\tilde{\mu}}}}[\tilde{\varphi}](\tilde{x}) - \mathbf{S}_B^{\frac{\epsilon\omega}{\sqrt{\tilde{\mu}}}}[\tilde{\psi}](\tilde{x}) = \mathbf{A}(\tilde{x}), \\
\tilde{\mu} \dfrac{\partial \mathbf{S}_B^{\frac{\epsilon\omega}{\sqrt{\tilde{\mu}}}}[\tilde{\varphi}]}{\partial n}\Big|_-(\tilde{x}) - \mu \dfrac{\partial \mathbf{S}_D^{\frac{\epsilon\omega}{\sqrt{\tilde{\mu}}}}[\tilde{\psi}]}{\partial n}\Big|_+(\tilde{x}) = \mathbf{B}(\tilde{x}),
\end{cases} \qquad \tilde{x} \in \partial B \tag{2.29}
$$

where $\mathbf{A} = (A_1, A_2, A_3)$ and $\mathbf{B} = (B_1, B_2, B_3)$ are defined in an obvious way, namely

$$\mathbf{A}(\tilde{x}) = \epsilon(\frac{1}{\mu} - \frac{1}{\tilde{\mu}}) \int_B \mathbf{\Gamma}^{\frac{\epsilon\omega}{\sqrt{\mu}}}(\tilde{x} - \tilde{y})(\omega^2 \hat{\mathbf{U}}_0(\epsilon\tilde{y} + z) - \nabla \hat{q}_0(\epsilon\tilde{y} + z))\, d\tilde{y}, \tag{2.30}$$

and

$$\begin{aligned} \mathbf{B}(\tilde{x}) &= (\tilde{\mu} - \mu)\frac{\partial \hat{\mathbf{U}}_0}{\partial \mathbf{N}}(\epsilon\tilde{x} + z) \\ &+ \epsilon(\frac{\tilde{\mu}}{\mu} - 1)\frac{\partial}{\partial \mathbf{N}} \int_B \mathbf{\Gamma}^{\frac{\epsilon\omega}{\sqrt{\mu}}}(\tilde{x} - \tilde{y})(\omega^2 \hat{\mathbf{U}}_0(\epsilon\tilde{y} + z) - \nabla \hat{q}_0(\epsilon\tilde{y} + z))\, d\tilde{y} \\ &- \epsilon(\frac{\tilde{\mu}}{\mu} - 1) \int_D \mathbf{F}(\tilde{x} - \tilde{y}) \cdot (\omega^2 \hat{\mathbf{U}}_0(\epsilon\tilde{y} + z) - \nabla \hat{q}_0(\epsilon\tilde{y} + z))\, dy\, \mathbf{N}(\tilde{x}). \end{aligned} \tag{2.31}$$

We emphasize that the normal vector $\mathbf{N}$ above is that on ∂B.

We may rewrite (2.29) as

$$\mathcal{T}(\tilde{\varphi}, \tilde{\psi}) = (\mathbf{A}, \mathbf{B}), \tag{2.32}$$

where $\mathcal{T}$ is an operator from $L^2(\partial B)^3 \times L^2(\partial B)^3$ into $H^1(\partial B)^3 \times L^2(\partial B)^3$ defined by

$$\mathcal{T}(\tilde{\varphi}, \tilde{\psi}) = \begin{pmatrix} \mathbf{S}_B^{\frac{\epsilon\omega}{\sqrt{\mu}}} & -\mathbf{S}_B^{\frac{\epsilon\omega}{\sqrt{\mu}}} \\ \tilde{\mu}\frac{\partial}{\partial n}\mathbf{S}_B^{\frac{\epsilon\omega}{\sqrt{\mu}}}|_- & -\mu\frac{\partial}{\partial n}\mathbf{S}_B^{\frac{\epsilon\omega}{\sqrt{\mu}}}|_+ \end{pmatrix} \begin{pmatrix} \tilde{\varphi} \\ \tilde{\psi} \end{pmatrix}.$$

We then decompose the operator $\mathcal{T}$ as

$$\mathcal{T} = \mathcal{T}_0 + \mathcal{T}_\epsilon, \tag{2.33}$$

where

$$\mathcal{T}_0(\tilde{\varphi}, \tilde{\psi}) := \begin{pmatrix} \mathbf{S}_B^0 & -\mathbf{S}_B^0 \\ \tilde{\mu}\frac{\partial}{\partial n}\mathbf{S}_B^0|_- & -\mu\frac{\partial}{\partial n}\mathbf{S}_B^0|_+ \end{pmatrix} \begin{pmatrix} \tilde{\varphi} \\ \tilde{\psi} \end{pmatrix},$$

and $\mathcal{T}_\epsilon = \mathcal{T} - \mathcal{T}_0$. Then by (2.17) and (2.18), it follows that

$$||\mathcal{T}_\epsilon(\tilde{\varphi}, \tilde{\psi})||_{H^1(\partial B)\times L^2(\partial B)} \leq C\epsilon\omega(||\tilde{\varphi}||_{L^2(\partial B)} + ||\tilde{\psi}||_{L^2(\partial B)}). \tag{2.34}$$

Note that $\mathbf{S}_B^0$ is invertible, and since $|\frac{\tilde{\mu}+\mu}{2(\tilde{\mu}-\mu)}| > \frac{1}{2}$, the operator $-\frac{(\tilde{\mu}+\mu)}{2(\tilde{\mu}-\mu)}I + (\mathbf{K}_B^0)^*$ is invertible as well (see [**10**]). Thus one can see that $\mathcal{T}_0$ is also invertible. In fact, one can readily check that the solution is explicit.

LEMMA 2.1. *For $(\mathbf{f}, \mathbf{g}) \in H^1(\partial B)^3 \times L^2(\partial B)^3$ the solution $(\tilde{\varphi}, \tilde{\psi}) = \mathcal{T}_0^{-1}(\mathbf{f}, \mathbf{g})$ is given by*

$$\tilde{\varphi} = \tilde{\psi} + (\mathbf{S}_B^0)^{-1}[\mathbf{f}], \tag{2.35}$$

$$\tilde{\psi} = \frac{1}{\tilde{\mu} - \mu}\Big(- \frac{(\tilde{\mu} + \mu)}{2(\tilde{\mu} - \mu)}I + (\mathbf{K}_B^0)^*\Big)^{-1} \left[-\tilde{\mu}(-\frac{1}{2}I + (\mathbf{K}_B^0)^*)(\mathbf{S}_B^0)^{-1}[\mathbf{f}] + \mathbf{g}\right]. \tag{2.36}$$

In view of (2.33) and (2.34), one can see that there is $\epsilon_0 > 0$ such that $\mathcal{T}$ is invertible as long as $\epsilon\omega \leq \epsilon_0$. Moreover $\mathcal{T}^{-1}$ takes the form

$$\mathcal{T}^{-1} = \mathcal{T}_0^{-1} + E, \tag{2.37}$$

where the operator E satisfies

$$\|E(\mathbf{f},\mathbf{g})\|_{L^2(\partial B)\times L^2(\partial B)} \leq C\epsilon\omega(\|\mathbf{f}\|_{H^1(\partial B)} + \|\mathbf{g}\|_{L^2(\partial B)}), \tag{2.38}$$

for some constant C independent of ϵ and ω.

Suppose that $\epsilon\omega \leq \epsilon_0 < 1$. Let $(\widetilde{\varphi}^\omega, \widetilde{\psi}^\omega)$ be the solution to (2.29). Then by (2.37) we have

$$(\widetilde{\varphi}^\omega, \widetilde{\psi}^\omega) = \mathcal{T}_0^{-1}(\mathbf{A},\mathbf{B}) + E(\mathbf{A},\mathbf{B}).$$

In view of (2.30) we have

$$\|\mathbf{A}\|_{H^1(\partial B)} \leq C\epsilon(\omega^2+1). \tag{2.39}$$

On the other hand, according to (2.31), $\mathbf{B}$ can be written as

$$\mathbf{B}(\tilde{x}) = (\tilde{\mu}-\mu)\widehat{\nabla}\hat{\mathbf{U}}_0(z,\omega)\mathbf{N}(\tilde{x}) + \mathbf{B}_1(\tilde{x}),$$

where $\mathbf{B}_1$ satisfies

$$\|\mathbf{B}_1\|_{L^2(\partial B)} \leq C\epsilon(\omega^2+1). \tag{2.40}$$

Therefore, we have

$$(\widetilde{\varphi}^\omega, \widetilde{\psi}^\omega) = (\tilde{\mu}-\mu)\mathcal{T}_0^{-1}\left(0, \widehat{\nabla}\hat{\mathbf{U}}_0(z,\omega)\mathbf{N}\right) + \mathcal{T}_0^{-1}(\mathbf{A},\mathbf{B}_1) + E(\mathbf{A},\mathbf{B}). \tag{2.41}$$

Because of (2.38), (2.39), and (2.40), the last two terms in the above equation are error terms satisfying

$$\|\mathcal{T}_0^{-1}(\mathbf{A},\mathbf{B}_1) + E(\mathbf{A},\mathbf{B})\|_{L^2(\partial B)\times L^2(\partial B)} \leq C\epsilon(\omega^2+1).$$

We also need to derive asymptotic expansions for $\frac{\partial\widetilde{\varphi}^\omega}{\partial\omega}$ and $\frac{\partial\widetilde{\psi}^\omega}{\partial\omega}$. By differentiating both sides of (2.29) with respect to ω, we obtain

$$\begin{aligned}\mathbf{S}_B^{\frac{\epsilon\omega}{\sqrt{\tilde{\mu}}}}\Big[\frac{\partial\widetilde{\varphi}^\omega}{\partial\omega}\Big](\tilde{x}) - \mathbf{S}_B^{\frac{\epsilon\omega}{\sqrt{\mu}}}\Big[\frac{\partial\widetilde{\psi}^\omega}{\partial\omega}\Big](\tilde{x}) &= \frac{\partial\mathbf{A}(\tilde{x})}{\partial\omega} - \int_{\partial B}\frac{\partial}{\partial\omega}\mathbf{\Gamma}^{\frac{\epsilon\omega}{\sqrt{\tilde{\mu}}}}(\tilde{x}-\tilde{y})\tilde{\varphi}^\omega(\tilde{y})d\sigma(\tilde{y}) \\ &\quad + \int_{\partial B}\frac{\partial}{\partial\omega}\mathbf{\Gamma}^{\frac{\epsilon\omega}{\sqrt{\mu}}}(\tilde{x}-\tilde{y})\tilde{\psi}^\omega(\tilde{y})d\sigma(\tilde{y})\end{aligned} \tag{2.42}$$

and

$$\begin{aligned}&\tilde{\mu}\frac{\partial}{\partial n}\mathbf{S}_B^{\frac{\epsilon\omega}{\sqrt{\tilde{\mu}}}}\Big[\frac{\partial\widetilde{\varphi}^\omega}{\partial\omega}\Big]\Big|_-(\tilde{x}) - \mu\frac{\partial}{\partial n}\mathbf{S}_B^{\frac{\epsilon\omega}{\sqrt{\mu}}}\Big[\frac{\partial\widetilde{\psi}^\omega}{\partial\omega}\Big]\Big|_+(\tilde{x}) = \frac{\partial\mathbf{B}(\tilde{x})}{\partial\omega} \\ &- \frac{\partial}{\partial n}\int_{\partial B}\frac{\partial}{\partial\omega}\mathbf{\Gamma}^{\frac{\epsilon\omega}{\sqrt{\tilde{\mu}}}}(\tilde{x}-\tilde{y})\tilde{\varphi}^\omega(\tilde{y})d\sigma(\tilde{y}) + \frac{\partial}{\partial n}\int_{\partial B}\frac{\partial}{\partial\omega}\mathbf{\Gamma}^{\frac{\epsilon\omega}{\sqrt{\mu}}}(\tilde{x}-\tilde{y})\tilde{\psi}^\omega(\tilde{y})d\sigma(\tilde{y})\end{aligned} \tag{2.43}$$

on ∂B.

Straightforward computations using (2.10) and (2.30) show that the right-hand side of the equality in (2.42) is of order $\epsilon(\omega+1)$ in the $H^1(\partial B)$-norm. We can also show using (2.31) that $\frac{\partial G_1}{\partial\omega}$ is also of order $\epsilon(\omega+1)$ in the $L^2(\partial B)$-norm. Thus, using the same argument as before, we readily obtain

$$(\frac{\partial\widetilde{\varphi}^\omega}{\partial\omega}, \frac{\partial\widetilde{\psi}^\omega}{\partial\omega}) = (\tilde{\mu}-\mu)\mathcal{T}_0^{-1}\left(0, \widehat{\nabla}(\frac{\partial\hat{\mathbf{U}}_0}{\partial\omega})(z,\omega)\mathbf{N}\right) + O(\epsilon(\omega+1)), \tag{2.44}$$

where the equality holds in $L^2(\partial B)^3 \times L^2(\partial B)^3$.

In view of (2.41) and (2.44), applying Lemma 2.1 (with $\mathbf{f} = 0$) yields the following result.

PROPOSITION 2.2. *Let $(\widetilde{\varphi}^\omega, \widetilde{\psi}^\omega)$ be the solution to (2.29). There exists $\epsilon_0 > 0$ such that if $\epsilon\omega < \epsilon_0$, then the following asymptotic expansions hold:*

$$\widetilde{\varphi}^\omega = \left(\frac{-(\tilde{\mu}+\mu)}{2(\tilde{\mu}-\mu)} I + (\mathbf{K}_B^0)^*\right)^{-1} [\widehat{\nabla}\hat{\mathbf{U}}_0(z,\omega)\mathbf{N}] + O(\epsilon(\omega^2+1)), \tag{2.45}$$

$$\widetilde{\psi}^\omega = \left(\frac{-(\tilde{\mu}+\mu)}{2(\tilde{\mu}-\mu)} I + (\mathbf{K}_B^0)^*\right)^{-1} [\widehat{\nabla}\hat{\mathbf{U}}_0(z,\omega)\mathbf{N}] + O(\epsilon(\omega^2+1)), \tag{2.46}$$

and

$$\frac{\partial\widetilde{\varphi}^\omega}{\partial\omega} = \left(\frac{-(\tilde{\mu}+\mu)}{2(\tilde{\mu}-\mu)} I + (\mathbf{K}_B^0)^*\right)^{-1} [\widehat{\nabla}\frac{\partial}{\partial\omega}\hat{\mathbf{U}}_0(z,\omega)\mathbf{N}] + O(\epsilon(\omega+1)), \tag{2.47}$$

$$\frac{\partial\widetilde{\psi}^\omega}{\partial\omega} = \left(\frac{-(\tilde{\mu}+\mu)}{2(\tilde{\mu}-\mu)} I + (\mathbf{K}_B^0)^*\right)^{-1} [\widehat{\nabla}\frac{\partial}{\partial\omega}\hat{\mathbf{U}}_0(z,\omega)\mathbf{N}] + O(\epsilon(\omega+1)), \tag{2.48}$$

where all the equalities hold in $L^2(\partial B)$.

We are now ready to derive the inner expansion for $\mathbf{w}$. Let Ω be a domain containing D and let $\widetilde{\Omega} = \frac{1}{\epsilon}\Omega - z$. After a change of variables, (2.25) and (2.26) take the forms:

$$\mathbf{w}(\epsilon\tilde{x}+z,\omega) = \begin{cases} \epsilon^2(\dfrac{1}{\mu}-\dfrac{1}{\tilde{\mu}})\displaystyle\int_B \mathbf{\Gamma}^{\frac{\epsilon\omega}{\sqrt{\mu}}}(\tilde{x}-\tilde{y})(\omega^2\hat{\mathbf{U}}_0(\epsilon\tilde{y}+z) - \nabla\hat{q}_0(\epsilon\tilde{y}+z))\,d\tilde{y} \\ \qquad +\epsilon\mathbf{S}_B^{\frac{\epsilon\omega}{\sqrt{\mu}}}[\tilde{\varphi}^\omega](\tilde{x}) \quad \text{in } B, \\ \epsilon\mathbf{S}_B^{\frac{\epsilon\omega}{\sqrt{\tilde{\mu}}}}[\tilde{\psi}^\omega](\tilde{x}) \quad \text{in } \mathbb{R}^3\setminus\overline{B}, \end{cases} \tag{2.49}$$

and

$$p(\epsilon\tilde{x}+z,\omega) = \begin{cases} \epsilon(\dfrac{1}{\mu}-\dfrac{1}{\tilde{\mu}})\displaystyle\int_B \mathbf{F}(\tilde{x}-\tilde{y})\cdot(\omega^2\hat{\mathbf{U}}_0(\epsilon\tilde{y}+z) - \nabla\hat{q}_0(\epsilon\tilde{y}+z))\,d\tilde{y} \\ \qquad +\epsilon\mathcal{Q}_B[\tilde{\varphi}^\omega](\tilde{x}) \quad \text{in } B, \\ \epsilon\mathcal{Q}_B[\tilde{\psi}^\omega](\tilde{x}) \quad \text{in } \mathbb{R}^3\setminus\overline{B}. \end{cases} \tag{2.50}$$

Since

$$\left\|\mathbf{S}_B^{\frac{\epsilon\omega}{\sqrt{\mu}}}[\widetilde{\varphi}^\omega] - \mathbf{S}_B^0[\widetilde{\varphi}^\omega]\right\|_{H^1(\partial B)} \leq C\epsilon\omega\|\widetilde{\varphi}^\omega\|_{L^2(\partial B)},$$

we have

$$\mathbf{w}(\epsilon\tilde{x}+z,\omega) = \begin{cases} \epsilon\mathbf{S}_B^0[\widetilde{\varphi}^\omega](\tilde{x}) + O(\epsilon^2(\omega^2+1)), & \tilde{x}\in B, \\ \epsilon\mathbf{S}_B^0[\widetilde{\psi}^\omega](\tilde{x}) + O(\epsilon^2(\omega+1)), & \tilde{x}\in\widetilde{\Omega}\setminus\overline{B}. \end{cases}$$

It then follows from (2.45) and (2.46) that

$$\mathbf{w}(\epsilon\tilde{x}+z,\omega) = \epsilon\mathbf{S}_B^0\left(-\frac{(\tilde{\mu}+\mu)}{2(\tilde{\mu}-\mu)} I + (\mathbf{K}_B^0)^*\right)^{-1} [\widehat{\nabla}\hat{\mathbf{U}}_0(z,\omega)\mathbf{N}](\tilde{x}) + O(\epsilon^2(\omega^2+1)) \tag{2.51}$$

for $\widetilde{x}\in\widetilde{\Omega}$.

On the other hand, we have

$$\frac{\partial \mathbf{w}}{\partial \omega}(\epsilon\tilde{x}+z,\omega)=\begin{cases}\epsilon \mathbf{S}_B^{\frac{\epsilon\omega}{\sqrt{\mu}}}\left[\dfrac{\partial\widetilde{\varphi}^{\omega}}{\partial\omega}\right](\tilde{x})+O(\epsilon^2(\omega+1)), & \widetilde{x}\in B,\\ \epsilon \mathbf{S}_B^{\frac{\epsilon\omega}{\sqrt{\mu}}}\left[\dfrac{\partial\widetilde{\psi}^{\omega}}{\partial\omega}\right](\tilde{x})+O(\epsilon^2), & \tilde{x}\in\widetilde{\Omega}\setminus\overline{B}.\end{cases}$$

Therefore, from (2.47) and (2.48) we obtain that

(2.52)
$$\frac{\partial \mathbf{w}}{\partial \omega}(\epsilon\tilde{x}+z,\omega)=\epsilon\mathbf{S}_B^0\left(-\frac{(\tilde{\mu}+\mu)}{2(\tilde{\mu}-\mu)}I+(\mathbf{K}_B^0)^*\right)^{-1}[\widehat{\nabla}\frac{\partial}{\partial\omega}\hat{\mathbf{U}}_0(z,\omega)\mathbf{N}](\tilde{x})+O(\epsilon^2(\omega+1))$$

for $\widetilde{x}\in\widetilde{\Omega}$.

Let

$$\mathbf{v}(\tilde{x}):=\mathbf{S}_B^0\left(-\frac{(\tilde{\mu}+\mu)}{2(\tilde{\mu}-\mu)}I+(\mathbf{K}_B^0)^*\right)^{-1}[\widehat{\nabla}\hat{\mathbf{U}}_0(z,\omega)\mathbf{N}](\tilde{x}),$$
$$q(\tilde{x}):=\mathcal{Q}_B\left(-\frac{(\tilde{\mu}+\mu)}{2(\tilde{\mu}-\mu)}I+(\mathbf{K}_B^0)^*\right)^{-1}[\widehat{\nabla}\hat{\mathbf{U}}_0(z,\omega)\mathbf{N}](\tilde{x}).$$

It is easy to check that $(\mathbf{v},q)$ is the solution to

$$\begin{cases}\mu\Delta\mathbf{v}-\nabla q=0 \quad \text{in } \mathbb{R}^3\setminus\overline{B},\\ \tilde{\mu}\Delta\mathbf{v}-\nabla q=0 \quad \text{in } B,\\ \mathbf{v}|_- -\mathbf{v}|_+=0 \quad \text{on } \partial B,\\ (q\mathbf{N}-\tilde{\mu}\dfrac{\partial\mathbf{v}}{\partial\mathbf{N}})\Big|_- -(q\mathbf{N}-\mu\dfrac{\partial\mathbf{v}}{\partial\mathbf{N}})\Big|_+=(\tilde{\mu}-\mu)\widehat{\nabla}\hat{\mathbf{U}}_0(z,\omega)\mathbf{N} \quad \text{on } \partial B,\\ \nabla\cdot\mathbf{v}=0 \quad \text{in } \mathbb{R}^3,\\ \mathbf{v}(\tilde{x})\to 0 \quad \text{as } |\tilde{x}|\to+\infty,\\ q(\tilde{x})\to 0 \quad \text{as } |\tilde{x}|\to+\infty.\end{cases} \tag{2.53}$$

We finally obtain the following theorem from (2.51) and (2.52).

THEOREM 2.3. *Let Ω be a small region containing D and let*

$$\mathbf{R}(x,\omega)=\hat{\mathbf{u}}_0(x,\omega)-\hat{\mathbf{U}}_0(x,\omega)-\epsilon\mathbf{v}\left(\frac{x-z}{\epsilon}\right), \quad x\in\Omega. \tag{2.54}$$

There exists $\epsilon_0>0$ such that if $\epsilon\omega<\epsilon_0$, then

$$\mathbf{R}(x,\omega)=O(\epsilon^2(\omega^2+1)), \quad \nabla_x\mathbf{R}(x,\omega)=O(\epsilon(\omega^2+1)), \quad x\in\Omega. \tag{2.55}$$

Moreover,

$$\frac{\partial\mathbf{R}}{\partial\omega}(x,\omega)=O(\epsilon^2(\omega+1)), \quad \nabla_x\left(\frac{\partial\mathbf{R}}{\partial\omega}\right)(x,\omega)=O(\epsilon(\omega+1)), \quad x\in\Omega. \tag{2.56}$$

Note that the estimates for $\nabla_x\mathbf{R}$ in (2.55) and $\nabla_x(\frac{\partial\mathbf{R}}{\partial\omega})$ in (2.56) can be derived using (2.49).

We now derive the outer expansion of $\mathbf{u}_0$. To this end, let us first recall the notion of the viscous moment tensor (VMT) from [**10**]. Let $(\mathbf{v}_{k\ell},p)$, for $k,\ell=1,2,3$,

be the solution to

$$
\begin{cases}
\mu\Delta\mathbf{v}_{k\ell} - \nabla p = 0 \quad \text{in } \mathbb{R}^3 \setminus \overline{B}, \\
\tilde{\mu}\Delta\mathbf{v}_{k\ell} - \nabla p = 0 \quad \text{in } B, \\
\mathbf{v}_{k\ell}|_- - \mathbf{v}_{k\ell}|_+ = 0 \quad \text{on } \partial B, \\
(p\mathbf{N} - \tilde{\mu}\dfrac{\partial \mathbf{v}_{k\ell}}{\partial \mathbf{N}})\Big|_- - (p\mathbf{N} - \mu\dfrac{\partial \mathbf{v}_{k\ell}}{\partial \mathbf{N}})\Big|_+ = 0 \quad \text{on } \partial B, \\
\nabla \cdot \mathbf{v}_{k\ell} = 0 \quad \text{in } \mathbb{R}^3, \\
\mathbf{v}_{k\ell}(\tilde{x}) - \tilde{x}_k \mathbf{e}_\ell + \dfrac{\delta_{k\ell}}{3}\displaystyle\sum_{j=1}^{3} \tilde{x}_j \mathbf{e}_j = O(|\tilde{x}|^{-2}) \quad \text{as } |\tilde{x}| \to +\infty, \\
p(\tilde{x}) = O(|\tilde{x}|^{-3}) \quad \text{as } |\tilde{x}| \to +\infty.
\end{cases} \tag{2.57}
$$

Here $(\mathbf{e}_1, \mathbf{e}_2, \mathbf{e}_3)$ is the standard basis of $\mathbb{R}^3$.

DEFINITION 2.4. *The VMT* $V(\tilde{\mu}, \mu, B) = (V_{ijk\ell})_{i,j,k,\ell=1,2,3}$ *is defined by*

$$
V_{ijk\ell}(\tilde{\mu}, \mu, B) := (\tilde{\mu} - \mu) \int_B \nabla \mathbf{v}_{k\ell}(\tilde{x}) : \widehat{\nabla}(\tilde{x}_i \mathbf{e}_j)\, d\tilde{x}, \tag{2.58}
$$

where : *denotes the contraction of two matrices, i.e.,* $A : B = \sum_{ij=1}^{3} a_{ij} b_{ij}$.

Since $(\hat{\mathbf{u}}_0 - \hat{\mathbf{U}}_0, \hat{p}_0 - \hat{q}_0)$ satisfies

$$
\begin{cases}
(\Delta + \dfrac{\omega^2}{\mu})(\hat{\mathbf{u}}_0 - \hat{\mathbf{U}}_0) - \dfrac{1}{\mu}\nabla(\hat{p}_0 - \hat{q}_0) = 0 \quad \text{in } \mathbb{R}^3 \setminus \overline{D}, \\
(\Delta + \dfrac{\omega^2}{\mu})(\hat{\mathbf{u}}_0 - \hat{\mathbf{U}}_0) - \dfrac{1}{\mu}\nabla(\hat{p}_0 - \hat{q}_0) = \omega^2 \left(\dfrac{1}{\mu} - \dfrac{1}{\tilde{\mu}}\right)\hat{\mathbf{u}}_0 - \left(\dfrac{1}{\mu} - \dfrac{1}{\tilde{\mu}}\right)\nabla \hat{p}_0 \quad \text{in } D, \\
(\hat{\mathbf{u}}_0 - \hat{\mathbf{U}}_0)\big|_+ - (\hat{\mathbf{u}}_0 - \hat{\mathbf{U}}_0)\big|_- = 0 \quad \text{on } \partial D, \\
-\dfrac{1}{\mu}(\hat{p}_0 - \hat{q}_0)\big|_+ \mathbf{N} + \dfrac{\partial}{\partial \mathbf{N}}(\hat{\mathbf{u}}_0 - \hat{\mathbf{U}}_0)\big|_+ \\
\quad = -\dfrac{1}{\mu}(\hat{p}_0 - \hat{q}_0)\big|_- \mathbf{N} + \dfrac{\partial}{\partial \mathbf{N}}(\hat{\mathbf{u}}_0 - \hat{\mathbf{U}}_0)\big|_- + \dfrac{\tilde{\mu} - \mu}{\mu}\dfrac{\partial \hat{\mathbf{u}}_0}{\partial \mathbf{N}}\Big|_- \quad \text{on } \partial D, \\
\nabla \cdot (\hat{\mathbf{u}}_0 - \hat{\mathbf{U}}_0) = 0 \quad \text{in } \mathbb{R}^3,
\end{cases} \tag{2.59}
$$

together with the radiation condition, the integration of the first equation in (2.59) against the Green function $\mathbf{\Gamma}^{\frac{\omega}{\sqrt{\mu}}}(x, y)$ over $y \in \mathbb{R}^3 \setminus \overline{D}$ and the divergence theorem give us the following representation formula:

$$
\begin{aligned}
\hat{\mathbf{u}}_0(x) = \hat{\mathbf{U}}_0(x) &+ (\frac{\tilde{\mu}}{\mu} - 1)\int_{\partial D} \mathbf{\Gamma}^{\frac{\omega}{\sqrt{\mu}}}(x, y)\frac{\partial \hat{\mathbf{u}}_0}{\partial \mathbf{N}}\Big|_-(y) d\sigma(y) \\
&- (\frac{1}{\mu} - \frac{1}{\tilde{\mu}})\int_D \mathbf{\Gamma}^{\frac{\omega}{\sqrt{\mu}}}(x, y)\nabla \hat{p}_0(y)\, dy + \omega^2(\frac{1}{\mu} - \frac{1}{\tilde{\mu}})\int_D \mathbf{\Gamma}^{\frac{\omega}{\sqrt{\mu}}}(x, y)\hat{\mathbf{u}}_0(y)\, dy.
\end{aligned} \tag{2.60}
$$

It follows from the inner expansion in Theorem 2.3 that, for $y \in \partial D$,

$$
\frac{\partial \hat{\mathbf{u}}_0}{\partial \mathbf{N}}(y) = \frac{\partial \hat{\mathbf{U}}_0}{\partial \mathbf{N}}(y) + \frac{\partial \mathbf{v}}{\partial \mathbf{N}}\left(\frac{y - z}{\epsilon}\right) + O(\epsilon) \tag{2.61}
$$

and, for $x \in D$,

(2.62)
$$\nabla \hat{p}_0(x) = \tilde{\mu}\triangle \hat{\mathbf{u}}_0 + \omega^2 \hat{\mathbf{u}}_0 = \frac{\tilde{\mu}}{\epsilon}(\triangle \mathbf{v})\left(\frac{x-z}{\epsilon}\right) + O(1) = \frac{1}{\epsilon}(\nabla q)\left(\frac{x-z}{\epsilon}\right) + O(1).$$

Since

$$\tilde{\mu}\int_{\partial D} \frac{\partial \hat{\mathbf{u}}_0}{\partial \mathbf{N}}\bigg|_-(y)\, d\sigma(y) - \int_D \nabla \hat{p}_0(y)\, dy = -\omega^2 \int_D \hat{\mathbf{u}}_0(y)\, dy,$$

we obtain that for x far away from z, the following outer expansion holds:

$$\hat{\mathbf{u}}_0(x) \approx \hat{\mathbf{U}}_0(x) - \epsilon^3 \sum_{i,j,\ell=1}^{3} \partial_i \Gamma_{\ell j}^{\frac{\omega}{\sqrt{\mu}}}(x,z)\bigg[(\frac{\tilde{\mu}}{\mu}-1)\int_{\partial B}\left(\frac{\partial \hat{\mathbf{U}}_0}{\partial \mathbf{N}}(z) + \frac{\partial \mathbf{v}}{\partial \mathbf{N}}\bigg|_-(\xi)\right)_j \xi_i\, d\sigma(\xi)$$
$$(\frac{1}{\mu}-\frac{1}{\tilde{\mu}})\int_B \partial_j q(\xi)\xi_i\, d\xi\bigg]\mathbf{e}_\ell,$$

where $\partial_i \Gamma_{\ell j}^{\frac{\omega}{\sqrt{\mu}}}(x,z)$ is the differentiation with respect to the x variable and $\left(\frac{\partial \mathbf{v}}{\partial \mathbf{N}}\right)_j$ is the j-th component of $\frac{\partial \mathbf{v}}{\partial \mathbf{N}}$, which we may further simplify as follows

(2.63)
$$(\hat{\mathbf{u}}_0 - \hat{\mathbf{U}}_0)(x)$$
$$\approx -\epsilon^3(\frac{\tilde{\mu}}{\mu}-1)\sum_{i,j,\ell=1}^{3}\left[\partial_i \Gamma_{\ell j}^{\frac{\omega}{\sqrt{\mu}}}(x,z)\int_B \partial_j \mathbf{v}_i(\xi) + \partial_i \mathbf{v}_j(\xi) + \partial_j \hat{\mathbf{U}}_{0i}(z) + \partial_i \hat{\mathbf{U}}_{0j}(z)\, d\xi\right]\mathbf{e}_\ell.$$

Here $\mathbf{v}_j$ denotes the j-th component of $\mathbf{v}$.

Since

$$\mathbf{v}(\xi) = \sum_{p,q=1}^{3} \partial_q \hat{\mathbf{U}}_0(z)_p \mathbf{v}_{pq}(\xi) - \nabla \hat{\mathbf{U}}_0(z)\xi, \tag{2.64}$$

we have

(2.65)
$$(\hat{\mathbf{u}}_0 - \hat{\mathbf{U}}_0)(x)$$
$$\approx -\epsilon^3(\frac{\tilde{\mu}}{\mu}-1)\sum_{i,j,\ell,p,q=1}^{3}\left[\partial_i \Gamma_{\ell j}^{\frac{\omega}{\sqrt{\mu}}}(x,z)\partial_q \hat{\mathbf{U}}_0(z)_p \int_B \partial_j (\mathbf{v}_{kl})_i(\xi) + \partial_i (\mathbf{v}_{kl})_j(\xi)\, d\xi\right]\mathbf{e}_\ell.$$

We have the following theorem for the outer expansion.

THEOREM 2.5. *Let Ω' be a compact region away from D, namely dist$(\Omega', D) \geq C > 0$ for some constant C, and let*

$$\mathbf{R}(x,\omega) = \hat{\mathbf{u}}_0(x,\omega) - \hat{\mathbf{U}}_0(x,\omega) + \frac{\epsilon^3}{\mu}\sum_{i,j,p,q,\ell=1}^{3} V_{ijkl}\partial_i \Gamma_{\ell j}^{\frac{\omega}{\sqrt{\mu}}}(x,z)\partial_q \hat{\mathbf{U}}_0(z)_p \mathbf{e}_\ell. \tag{2.66}$$

There exists $\epsilon_0 > 0$ such that if $\epsilon\omega < \epsilon_0$, then

$$\mathbf{R}(x,\omega) = O(\epsilon^4(\omega^3+1)), \quad x \in \Omega'. \tag{2.67}$$

Moreover,

$$\frac{\partial \mathbf{R}}{\partial \omega}(x,\omega) = O(\epsilon^4(\omega^2+1)), \quad x \in \Omega'. \tag{2.68}$$

2.3. Far- and near-field asymptotic formulas in the transient regime

Recall that the inverse Fourier transform, $\mathbf{U}_0$, of $\hat{\mathbf{U}}_0$ satisfies

$$\begin{cases} (\partial_t^2 - \mu\Delta)\mathbf{U}_0(x,t) - \nabla F = \delta_{x=\bar{y}}\delta_{t=0}\mathbf{a} \quad \text{in } \mathbb{R}^3 \times \mathbb{R}, \\ \nabla \cdot \mathbf{U}_0 = 0 \quad \text{in } \mathbb{R}^3 \times \mathbb{R}, \\ \mathbf{U}_0(x,t) = 0 \quad \text{for} \quad x \in \mathbb{R}^3 \quad \text{and } t \ll 0. \end{cases}$$

For $\rho > 0$, we define the operator P_ρ on tempered distributions by

$$P_\rho[\psi](t) = \int_{|\omega|\le\rho} e^{-\sqrt{-1}\omega t}\hat{\psi}(\omega)\, d\omega, \tag{2.69}$$

where $\hat{\psi}$ denotes the Fourier transform of ψ. The operator P_ρ truncates the high-frequency component of ψ.

One can easily show that $P_\rho[\mathbf{U}_0]$ satisfies

$$\begin{aligned} &(\partial_t^2 - \Delta)P_\rho[\mathbf{U}_0](x,t) - \nabla P_\rho[F](x-y) = \delta_{x=\bar{y}}\psi_\rho(t)\mathbf{a} \quad \text{in } \mathbb{R}^3 \times \mathbb{R}, \\ &\nabla \cdot P_\rho[\mathbf{U}_0] = 0 \quad \text{in } \mathbb{R}^3 \times \mathbb{R}, \end{aligned} \tag{2.70}$$

where

$$\psi_\rho(t) := \frac{2\sin\rho t}{t} = \int_{|\omega|\le\rho} e^{-\sqrt{-1}\omega t} d\omega.$$

The purpose of this section is to derive and asymptotic expansions for $P_\rho[\mathbf{u}_0 - \mathbf{U}_0](x,t)$. For doing so, we observe that

$$P_\rho[\mathbf{u}_0](x,t) = \int_{|\omega|\le\rho} e^{-\sqrt{-1}\omega t}\hat{\mathbf{u}}_0(x,\omega) d\omega, \tag{2.71}$$

where $\hat{\mathbf{u}}_0$ is the solution to (2.19). Therefore, according to Theorem 2.3, we have

$$P_\rho[\mathbf{u}_0 - \mathbf{U}_0](x,t) - \epsilon \sum_{p,q=1}^{3} \partial_q P_\rho[\mathbf{U}_0](z,t)_p[\mathbf{v}_{pq}(x) - x_p\mathbf{e}_q] = \int_{|\omega|\le\rho} e^{-\sqrt{-1}\omega t}\mathbf{R}(x,\omega) d\omega.$$

Suppose that $|t| \ge c_0$ for some positive number c_0 (c_0 is of order the distance between $\bar{y}$ and z). Then, integrating by parts gives

$$\begin{aligned} \left| \int_{|\omega|\le\rho} e^{-\sqrt{-1}\omega t}\mathbf{R}(x,\omega) d\omega \right| &= \left| \frac{1}{t} \int_{|\omega|\le\rho} \frac{d}{d\omega} e^{-\sqrt{-1}\omega t}\mathbf{R}(x,\omega) d\omega \right| \\ &\le \frac{1}{|t|} \left(|\mathbf{R}(x,\rho)| + |\mathbf{R}(x,-\rho)| \right) + \int_{|\omega|\le\rho} \left| \frac{\partial}{\partial\omega}\mathbf{R}(x,\omega) \right| d\omega \\ &\le C\epsilon^2\rho^2. \end{aligned}$$

Since

$$\epsilon \sum_{p,q=1}^{3} \partial_q P_\rho[\mathbf{U}_0](z,t)_p[\mathbf{v}_{pq}(x) - x_p\mathbf{e}_q] = O(\epsilon\rho),$$

we arrive at the following theorem.

THEOREM 2.6. *Suppose that $\rho = O(\epsilon^{-\alpha})$ for some $\alpha < 1$. Then*

$$P_\rho[\mathbf{u}_0 - \mathbf{U}_0](x,t) = \epsilon \sum_{p,q=1}^{3} \partial_q P_\rho[\mathbf{U}_0](z,t)_p[\mathbf{v}_{pq}(x) - x_p\mathbf{e}_q] + O(\epsilon^{2(1-\alpha)}).$$

We now derive a far-field asymptotic expansion for $P_\rho[\mathbf{u}_0-\mathbf{U}_0]$. Let $\mathbf{G}_\infty(x,y,t)$ be the inverse Fourier transform of $\mathbf{\Gamma}^{\frac{\omega}{\sqrt{\mu}}}(x,y)$. Note that $\mathbf{G}_\infty$ is the limit of $\mathbf{G}$ given by (2.5) as $\sqrt{\lambda+2\mu}\to+\infty$. It then follows that

$$
\begin{aligned}
P_\rho[\mathbf{G}_\infty](x,y,t) &= \int_{|\omega|\le\rho} e^{-\sqrt{-1}\omega t}\mathbf{\Gamma}^{\frac{\omega}{\sqrt{\mu}}}(x,y)d\omega \\
&= \frac{1}{4\pi}\frac{3\gamma_i\gamma_j-\delta_{ij}}{r^3}\left[\phi_\rho(t)-\phi_\rho(t-\frac{r}{\sqrt{\mu}})\right]-\frac{1}{4\pi\mu}\frac{\gamma_i\gamma_j-\delta_{ij}}{r}\psi_\rho(t-\frac{r}{\sqrt{\mu}}),
\end{aligned}
\tag{2.72}
$$

where $\phi_\rho(t):=\int_0^t\psi_\rho(s)ds$.

From Theorem 2.5, we get

$$
\begin{aligned}
&\int_{|\omega|\le\rho} e^{-\sqrt{-1}\omega t}(\hat{\mathbf{u}}_0(x,\omega)-\hat{\mathbf{U}}_0(x,\omega))\,d\omega \\
&= -\frac{\epsilon^3}{\mu}\int_{|\omega|\le\rho} e^{-\sqrt{-1}\omega t}\left(\sum_{i,j,p,q,\ell=1}^{3} V_{ijpq}\partial_i\Gamma_{\ell j}^{\frac{\omega}{\sqrt{\mu}}}(x,z)\partial_q\hat{\mathbf{U}}_0(z)_p\mathbf{e}_\ell\right)d\omega \\
&\quad+\int_{|\omega|\le\rho} e^{-\sqrt{-1}\omega t}\mathbf{R}(x,\omega)\,d\omega,
\end{aligned}
$$

where the remainder is estimated by

$$
\int_{|\omega|\le\rho} e^{-\sqrt{-1}\omega t}\mathbf{R}(x,\omega)\,d\omega = O(\epsilon^{4(1-\frac{3}{4}\alpha)}).
$$

Since

$$
\begin{aligned}
&\int_{|\omega|\le\rho} e^{-\sqrt{-1}\omega t}\left(\sum_{i,j,p,q,\ell=1}^{3} V_{ijpq}\partial_i\Gamma_{\ell j}^{\frac{\omega}{\sqrt{\mu}}}(x,z)\partial_q\hat{\mathbf{U}}_0(z)_p\mathbf{e}_\ell\right)d\omega \\
&= \mu^{-1}\int_{|\omega|\le\rho} e^{-\sqrt{-1}\omega t}\left(\sum_{i,j,p,q,k,\ell=1}^{3} V_{ijpq}\partial_i\Gamma_{\ell j}^{\frac{\omega}{\sqrt{\mu}}}(x,z)\partial_q\Gamma_{pk}^{\frac{\omega}{\sqrt{\mu}}}(z,\bar{y})a_k\mathbf{e}_\ell\right)d\omega \\
&= \mu^{-1}\int_{\mathbb{R}}\left(\sum_{i,j,p,q,k,\ell=1}^{3} V_{ijpq}\partial_i P_\rho[\mathbf{G}_\infty]_{\ell j}(x,z,t-\tau)\partial_q P_\rho[\mathbf{G}_\infty]_{pk}(z,\bar{y},\tau)a_k\mathbf{e}_\ell\right)d\tau,
\end{aligned}
$$

the following theorem holds.

THEOREM 2.7. *Let* $\hat{\mathbf{U}}_0(x,\omega):=\frac{1}{\mu}\mathbf{\Gamma}^{\frac{\omega}{\sqrt{\mu}}}(x-\bar{y})\mathbf{a}$. *Suppose that* $\rho=O(\epsilon^{-\alpha})$ *for some* $\alpha<1$. *Then for* $|x-z|\ge C>0$, *the following far-field expansion holds*

(2.73)

$$
\begin{aligned}
&P_\rho[\mathbf{u}_0-\mathbf{U}_0](x,t) \\
&= -\frac{\epsilon^3}{\mu^2}\int_{\mathbb{R}}\left(\sum_{i,j,p,q,k,\ell=1}^{3} V_{ijpq}\partial_i P_\rho[\mathbf{G}_\infty]_{\ell j}(x,z,t-\tau)\partial_q P_\rho[\mathbf{G}_\infty]_{pk}(z,\bar{y},\tau)a_k\mathbf{e}_\ell\right)d\tau \\
&\quad+O(\epsilon^{4(1-\frac{3}{4}\alpha)}).
\end{aligned}
$$

Note that if we plug (2.72) in the far-field formula (2.73) then we can see that, unlike the acoustic case investigated in [8], the perturbation $P_\rho[\mathbf{u}_0-\mathbf{U}_0](x,t)$ can be seen not only as a polarized wave emitted from the anomaly but it contains,

because of the term $(1/r^3)\phi_\rho(t)$ in (2.72), a near-field like term which does not propagate.

2.4. Asymptotic imaging

2.4.1. Far-field imaging: time-reversal. We present a time-reversal technique for detecting the location z of the anomaly from measurements of the perturbations at x away from the location z. As in the acoustic case, the main idea is to take advantage of the reversibility of the elastic wave equation in a non-viscous medium in order to back-propagate signals to the sources that emitted them [**28, 57**].

Let S be a sphere englobing the anomaly D. Consider, for simplicity, the harmonic regime, we get

$$\int_S \left[\frac{\partial \overline{\mathbf{\Gamma}^{\frac{\omega}{\sqrt{\mu}}}}}{\partial n}(x,z)\mathbf{\Gamma}^{\frac{\omega}{\sqrt{\mu}}}(x,y) - \overline{\mathbf{\Gamma}^{\frac{\omega}{\sqrt{\mu}}}}(x,z)\frac{\partial \mathbf{\Gamma}^{\frac{\omega}{\sqrt{\mu}}}}{\partial n}(x,y)\right] d\sigma(x) = 2\sqrt{-1}\Im m\mathbf{\Gamma}^{\frac{\omega}{\sqrt{\mu}}}(y,z),$$

for $y \in \Omega$, and therefore, for $\mathbf{w}(x) := \hat{\mathbf{u}}_0(x,\omega) - \hat{\mathbf{U}}_0(x,\omega)$, it follows that

$$\begin{aligned}\int_S \left[\frac{\partial \overline{\mathbf{w}}}{\partial n}(x,\omega)\mathbf{\Gamma}^{\frac{\omega}{\sqrt{\mu}}}(x,z) - \overline{\mathbf{w}}(x,\omega)\frac{\partial \mathbf{\Gamma}^{\frac{\omega}{\sqrt{\mu}}}}{\partial n}(x,z)\right] d\sigma(x) \\ = 2\sqrt{-1}\frac{\epsilon^3}{\mu}\nabla\hat{\mathbf{U}}_0(z,\omega)V(\tilde{\mu},\mu,B)\nabla_z\Im m\mathbf{\Gamma}^{\frac{\omega}{\sqrt{\mu}}}(y,z) + O(\epsilon^4\omega^3),\end{aligned}$$

if $\omega > 1$.

This shows that the anti-derivative of time-reversal perturbation focuses on the location of the anomaly with an anisotropic focal spot. Because of the structure of the Green function $\mathbf{\Gamma}^{\frac{\omega}{\sqrt{\mu}}}(y,z)$, time-reversing the perturbation gives birth to a near-field like effect. Moreover, the resolution limit depends on the direction. It is, unlike the acoustic case, anisotropic. These interesting findings were experimentally observed and first reported in [**43**]. Our asymptotic formula (2.73) clearly explains them.

2.4.2. Near-field imaging: optimization approach. Set Ω to be a window containing the anomaly D. As in Chapter 1, Theorem 2.6 suggests to reconstruct the shape and the shear modulus of the elastic inclusion D by minimizing the following functional:

$$\int_{T-\Delta T}^{T+\Delta T} ||P_\rho[\mathbf{u}_0 - \mathbf{U}_0](x,t) - \epsilon\sum_{p,q=1}^{3}\partial_q P_\rho[\mathbf{U}_0](z,t)_p[\mathbf{v}_{pq}(x) - x_p\mathbf{e}_q]||^2_{L^2(\Omega)},$$

where $T = |\bar{y} - z|/\sqrt{\mu}$ is the arrival time and ΔT is a window time. One can add a total variation regularization term.

The choice of the space and time window sizes are critical as observed in [**9**] for the time-harmonic regime. If they are too large, then noisy images are obtained. If they are too small, then resolution is poor. The optimal window sizes are related to the signal-to-noise ratio of the recorded near-field measurements. They express the trade-off between resolution and stability.

2.5. Concluding remarks

In this chapter we have rigorously establish asymptotic expansions of near- and far-field measurements of the transient elastic wave induced by a small elastic anomaly. We have proved that, after truncation of the high-frequency component, the perturbation due to the anomaly can be seen not only as a polarized wave emitted from the anomaly but it contains unlike the acoustic case a near-field like term which does not propagate. We have also shown that time-reversing this perturbation gives birth to a near-field like effect. Moreover, the resolution limit is anisotropic. We have then explained the experimental findings reported in [**43**].

In this chapter we have only considered a purely quasi-incompressible elasticity model. In Chapter 4, we will consider the problem of reconstructing a small anomaly in a viscoelastic medium from wavefield measurements. The Voigt model his a common model to describe the viscoelastic properties of tissues. Catheline *et al.* [**42**] have shown that this model is well adapted to describe the viscoelastic response of tissues to low-frequency excitations. Expressing the ideal elastic field without any viscous effect in terms of the measured field in a viscous medium, we will generalize the methods described here to recover the viscoelastic and geometric properties of an anomaly from wavefield measurements.

CHAPTER 3

Transient imaging with limited-view data

Abstract. We consider for the wave equation the inverse problem of identifying locations of point sources and dipoles from limited-view data. Using as weights particular background solutions constructed by the geometrical control method, we recover Kirchhoff-, back-propagation-, MUSIC-, and arrival time-type algorithms by appropriately averaging limited-view data. We show that if one can construct accurately the geometric control, then one can perform imaging with the same resolution using limited-view as using full-view data.

3.1. Introduction

In Chapter 1, we have investigated the imaging of small anomalies using transient wave boundary measurements; see also the recent works [**5, 7**]. Different approaches for locating them and reconstructing some information about their sizes and physical parameters have been designed. The detection algorithms make use of complete boundary measurements. They are of Kirchhoff-, back-propagation, MUSIC-, and arrival time-types. The resolution of those algorithms in the time-harmonic domain is finite. It is essentially of order one-half the wavelength. See, for instance, [**3**].

In this work, we extend those algorithms to the case with limited-view measurements. For simplicity, we model here the small anomalies as point sources or dipoles. We refer the reader to Chapter 1 and [**5, 7**] for rigorous derivations of these approximate models and their higher-order corrections. It is worth mentioning that in order to model a small anomaly as a point source or a dipole, one has to truncate the high-frequency component of the transient wave reflected by the anomaly.

By using the geometrical control method [**29**], we show how to recover all the classical algorithms that have been used to image point sources and dipole locations. Our main finding in this chapter is that if one can construct accurately the geometric control then one can perform imaging with the same resolution using partial data as using complete data. Our algorithms apply equally well to the case of many source points or dipole locations and are robust with respect to perturbations of the boundary. This is quite important in real experiments since one does not necessarily know the non-accessible part of the boundary with good accuracy.

The chapter is organized as follows. In Section 3.2 we provide a key identity based on the averaging of the limited-view data, using weights constructed by the geometrical control method. Section 3.3 is devoted to developing, for different choices of weights, Kirchhoff-, back-propagation-, MUSIC-, and arrival time-type algorithms for transient imaging with limited-view data. In Section 3.4 we discuss potential applications of the method in emerging biomedical imaging. In Section 3.5

we present results of numerical experiments and comparisons among the proposed algorithms.

3.2. Geometric control

The basic model to be considered in this chapter is the following wave equation:

$$\frac{\partial^2 p}{\partial t^2}(x,t) - c^2 \Delta p(x,t) = 0, \quad x \in \Omega, \quad t \in]0,T[, \tag{3.1}$$

for some final observation time T, with the Dirichlet boundary conditions

$$p(x,t) = 0 \quad \text{on } \partial\Omega\times]0,T[, \tag{3.2}$$

the initial conditions

$$p(x,t)|_{t=0} = 0 \quad \text{in } \Omega, \tag{3.3}$$

and

$$\partial_t p(x,t)|_{t=0} = \delta_{x=z} \quad \text{or} \quad \partial_t p(x,t)|_{t=0} = m_0 \cdot \nabla \delta_{x=z} \quad \text{in } \Omega. \tag{3.4}$$

Here c is the acoustic speed in Ω which we assume to be constant, and m_0 is a constant nonzero vector. We suppose that T is large enough so that

$$T > \frac{\operatorname{diam}(\Omega)}{c}. \tag{3.5}$$

The purpose of this chapter is to design efficient algorithms for reconstructing the location z from boundary measurements of $\frac{\partial p}{\partial \nu}$ on $\Gamma\times]0,T[$, where $\Gamma \subset \partial\Omega$.

Suppose that T and Γ are such that they geometrically control Ω, which roughly means that every geometrical optic ray, starting at any point $x \in \Omega$, at time $t = 0$, hits Γ before time T at a nondiffractive point; see [**29, 78**]. Let $\beta \in \mathcal{C}_0^\infty(\Omega)$ be a cutoff function such that $\beta(x) \equiv 1$ in a sub-domain Ω' of Ω, which contains the source point z.

For a given function w which will be specified later, we construct by the geometrical control method a function $v(x,t)$ satisfying

$$\frac{\partial^2 v}{\partial t^2} - c^2 \Delta v = 0 \quad \text{in } \Omega\times]0,T[, \tag{3.6}$$

with the initial condition

$$v(x,0) = c^2 \beta(x) w(x), \quad \partial_t v(x,0) = 0, \tag{3.7}$$

the boundary condition $v = 0$ on $\partial\Omega \setminus \overline{\Gamma}$, and the final conditions

$$v|_{t=T} = \frac{\partial v}{\partial t}\Big|_{t=T} = 0 \quad \text{in } \Omega. \tag{3.8}$$

Let

$$g_w(x,t) := v(x,t) \quad \text{on } \Gamma\times]0,T[. \tag{3.9}$$

Multiplying (3.1) by v and integrating over $\Omega \times [0,T]$ lead to the following key identity of this chapter:

$$\int_0^T \int_\Gamma \frac{\partial p}{\partial \nu}(x,t) g_w(x,t)\, d\sigma(x)\, dt = w(z) \quad \text{or} \quad - m_0 \cdot \nabla w(z). \tag{3.10}$$

Note that the probe function constructed in [**5**] corresponds to one of the following choices for w in Ω:

$$w(x) := \frac{\delta\left(\tau - \frac{|x-y|}{c}\right)}{4\pi|x-y|} \quad \text{in three dimensions} \tag{3.11}$$

or

$$w(x) := \delta\left(\tau - \frac{1}{c}\theta \cdot x\right) \quad \text{in two dimensions,} \tag{3.12}$$

where θ is a unit vector.

The reader is referred, for instance, to [**25, 106, 68**] for numerical investigations of the geometrical control method.

3.3. Imaging algorithms

In this section, we only consider the initial condition $\partial_t p(x,t)|_{t=0} = \delta_{x=z}$ in Ω. One can treat the case of the initial data $\partial_t p(x,t)|_{t=0} = m_0 \cdot \nabla \delta_{x=z}$ in the exactly same way. Using the functions v constructed by the geometrical control method with different choices of initial data w, one recovers several classical algorithms for imaging point sources. For simplicity, we only consider a single point source, but the derived algorithms are efficient for locating multiple sources as well. The reader is referred to [**48**] for a review on source localization methods.

3.3.1. Kirchhoff algorithm. Let $y \in \mathbb{R}^d \setminus \overline{\Omega}, d = 2, 3$, and $\omega \in \mathbb{R}$. Set

$$w(x) = e^{\sqrt{-1}\omega|x-y|}, \quad x \in \Omega.$$

Then, for a given search point z^S in Ω, we have from (3.10)

$$\begin{aligned}\int_{\mathbb{R}} e^{-\sqrt{-1}\omega|z^S-y|} \int_0^T \int_\Gamma \frac{\partial p}{\partial \nu}(x,t) g_w(x,t)\, d\sigma(x)\, dt\, d\omega &= \int_{\mathbb{R}} e^{-\sqrt{-1}\omega(|z^S-y|-|z-y|)}\, d\omega \\ &= \delta_{|z^S-y|-|z-y|=0},\end{aligned}$$

where δ is the Dirac mass. Taking a (virtual) planar array of receivers y outside Ω yields then a Kirchhoff-type algorithm for finding z.

In fact, let $\omega_k, k = 1, \ldots, K$, be a set of frequencies and let $y_1, \ldots, y_N$, be a set of virtual receivers. To find the location z one maximizes over z^S the following imaging functional:

$$\mathcal{I}_{\mathrm{KI}}(z^S) := \frac{1}{K} \Re e \sum_{\omega_k} \sum_{y_n} e^{-\sqrt{-1}\omega|z^S-y_n|} \int_0^T \int_\Gamma \frac{\partial p}{\partial \nu}(x,t) g_{w_{k,n}}(x,t)\, d\sigma(x)\, dt,$$

where $w_{k,n}(x) = e^{\sqrt{-1}\omega_k|x-y_n|}$.

3.3.2. Back-propagation algorithm. If one takes w to be a plane wave:

$$w(x) = e^{\sqrt{-1}\omega\theta\cdot x}, \quad \theta \in S^{d-1},$$

where S^{d-1} is the unit sphere in $\mathbb{R}^d$, then one computes for a given search point $z^S \in \Omega$,

$$\int_{S^{d-1}} e^{-\sqrt{-1}\omega\theta\cdot z^S} \int_0^T \int_\Gamma \frac{\partial p}{\partial \nu}(x,t) g_w(x,t)\, d\sigma(x)\, dt\, d\sigma(\theta) = \int_{S^{d-1}} e^{\sqrt{-1}\omega\theta\cdot(z-z^S)}\, d\sigma(\theta).$$

But

$$\int_{S^{d-1}} e^{\sqrt{-1}\omega\theta\cdot(z-z^S)}\,d\sigma(\theta) = \begin{cases} j_0(\omega|z-z^S|) & \text{for } d=3,\\ J_0(\omega|z-z^S|) & \text{for } d=2,\end{cases}$$

where j_0 is the spherical Bessel function of order zero and J_0 is the Bessel function of the first kind and of order zero.

This is a back-propagation algorithm. Let $\theta_1,\dots,\theta_N$, be a discretization of the unit sphere S^{d-1}. One plots at each point z^S in the search domain the following imaging functional:

$$\mathcal{I}_{\rm BP}(z^S) := \frac{1}{N}\Re e\sum_{\theta_n} e^{-\sqrt{-1}\omega\theta_n\cdot z^S}\int_0^T\int_\Gamma \frac{\partial p}{\partial\nu}(x,t)g_{w_n}(x,t)\,d\sigma(x)\,dt,$$

where $w_n(x) = e^{\sqrt{-1}\omega\theta_n\cdot x}$. The resulting plot will have a large peak at z. Note that the higher the frequency ω is, the better is the resolution. However, high frequency oscillations cause numerical instabilities. There is a trade-off between resolution and stability.

3.3.3. MUSIC algorithm. Take

$$w(x) = e^{\sqrt{-1}\omega(\theta+\theta')\cdot x},\quad \theta,\theta'\in S^{d-1}.$$

It follows from (3.10) that

$$\int_0^T\int_\Gamma \frac{\partial p}{\partial\nu}(x,t)g_w(x,t)\,d\sigma(x)\,dt = e^{\sqrt{-1}\omega(\theta+\theta')\cdot z}.$$

Therefore, one can design a MUSIC-type algorithm for locating z. For doing so, let $\theta_1,\dots,\theta_N$ be N unit vectors in $\mathbb{R}^d$. Define the matrix $A=(A_{nn'})_{n,n'=1}^N$ by

$$A_{nn'} := \int_0^T\int_\Gamma \frac{\partial p}{\partial\nu}(x,t)g_{w_{n,n'}}(x,t)\,d\sigma(x)\,dt,$$

with

$$w_{n,n'}(x) = e^{\sqrt{-1}\omega(\theta_n+\theta_{n'})\cdot x}.$$

Let P be the orthogonal projection onto the range of A. Given any point z^S in the search domain form the vector

$$h(z^S) := (e^{\sqrt{-1}\omega\theta_1\cdot z^S},\dots,e^{\sqrt{-1}\omega\theta_N\cdot z^S})^T,$$

where T denotes the transpose. Then plot the MUSIC imaging functional:

$$\mathcal{I}_{\rm MU}(z^S) := \frac{1}{||(I-P)h(z^S)||}.$$

The resulting plot will have a large peak at z. Again, the higher the frequency ω is, the better is the resolution.

3.3.4. Arrival time and time-delay of arrival algorithms. Taking w to be a distance function,

$$w(x) = |y-x|,$$

to a virtual receiver y on a planar array outside Ω yields arrival-time and time-delay of arrival algorithms. In fact, we have

$$\int_0^T\int_\Gamma \frac{\partial p}{\partial\nu}(x,t)g_w(x,t)\,d\sigma(x)\,dt = |y-z|.$$

Let $y_1, \dots, y_N$ be N receivers and compute

$$r_n := \int_0^T \int_\Gamma \frac{\partial p}{\partial \nu}(x,t) g_{w_n}(x,t)\, d\sigma(x)\, dt,$$

with $w_n(x) = |y_n - x|$. Then, the point z can be found as the intersection of spheres of centers y_n and radii r_n.

Using time-of-arrival differences instead of arrival times would improve the robustness of the algorithm. Introduce the time-of-arrival difference, $t_{n,n'}$, between the receiver y_n and $y_{n'}$ as follows:

$$t_{n,n'} := \int_0^T \int_\Gamma \frac{\partial p}{\partial \nu}(x,t)(g_{w_n} - g_{w_{n'}})(x,t)\, d\sigma(x)\, dt.$$

At least $N = 4$ sources are required to locate z. The location z can be found as the intersection of three sets of hyperboloids. See, for instance, [**40, 104, 96, 47, 66, 32, 48**].

3.4. Applications to emerging biomedical imaging

In this section we show how to apply the designed algorithms to emerging biomedical imaging. Of particular interest are radiation force imaging, magneto-acoustic current imaging, and photo-acoustic imaging.

3.4.1. Radiation force imaging. As it has been said Chapter 1, in radiation force imaging, one generates vibrations inside the organ, and acquires a spatio-temporal sequence of the propagation of the induced transient wave to estimate the location and the viscoelastic parameters of a small anomaly inside the medium.

Let z be the location of the anomaly. Let Ω be a large ball englobing the anomaly. In the far-field, the problem, roughly speaking, reduces to finding the location of the anomaly from measurements of the pressure p on $\partial\Omega\times]0,T[$, that is, the solution to (3.1) with the initial conditions

$$p(x,t)|_{t=0} = 0 \quad \text{and} \quad \partial_t p(x,t)|_{t=0} = m_0 \cdot \nabla \delta_{x=z} \quad \text{in } \Omega. \tag{3.13}$$

A time-reversal technique can be designed to locate the anomaly. Suppose that one is able to measure p and its normal derivative at any point x on $\partial\Omega$. If both p and its normal derivative on $\partial\Omega$ are time-reversed and emitted from $\partial\Omega$, then the time-reversed wave travels back to the location z of the anomaly. See Chapter 1.

Suppose now that the measurements of p and its normal derivative are only done on the part Γ of $\partial\Omega$. Note first that

$$\frac{\partial p}{\partial \nu}|_{\partial\Omega\times]0,T[} = \Lambda_{\mathrm{DtN}}[p|_{\partial\Omega\times]0,T[}],$$

where Λ_{DtN} is the Dirichlet-to-Neumann operator for the wave equation in $\mathbb{R}^3 \setminus \Omega$. For any function v satisfying (3.6), (3.7), and (3.8), integrating by parts yields

$$\int_0^T \int_{\partial\Omega} p(x,t)(\Lambda^*_{\mathrm{DtN}}[v] + \frac{\partial v}{\partial \nu})(x,t)\, d\sigma(x)\, dt = m_0 \cdot \nabla w(z),$$

where Λ^*_{DtN} denotes the adjoint of Λ_{DtN}. Next, constructing by the geometrical control method, g_w such that v satisfies (3.6), (3.7), and (3.8), together with the boundary condition

$$\Lambda^*_{\mathrm{DtN}}[v] + \frac{\partial v}{\partial \nu} = \begin{cases} 0 & \text{on } \partial\Omega \setminus \overline{\Gamma} \times]0,T[\\ g_w & \text{on } \Gamma\times]0,T[, \end{cases}$$

one obtains

$$\int_0^T \int_\Gamma p(x,t) g_w(x,t)\, d\sigma(x)\, dt = m_0 \cdot \nabla w(z).$$

Making similar choices for w to those in the previous section provide different algorithms for locating the anomaly.

3.4.2. Magneto-acoustic current imaging. In magneto-acoustic current imaging, one detects a pressure signal created in the presence of a magnetic field by electrically active tissues [**70, 90, 91**]. In the presence of an externally applied magnetic field, biological action currents, arising from active nerve or muscle fibers, experience a Lorentz force. The resulting pressure or tissue displacement contains information about the action current distribution.

Let $z \in \Omega$ be the location of an electric dipole, which represents an active nerve or muscle fiber, with strength c. The wave equation governing the induced pressure distribution p is (3.1), with the boundary condition (3.2), the initial conditions (3.3), and

$$\partial_t p(x,t)|_{t=0} = \delta_{x=z} \quad \text{in } \Omega. \tag{3.14}$$

The algorithms constructed in the previous section apply immediately to finding z from partial boundary measurements of the normal derivative of p.

3.4.3. Photo-acoustic imaging. The photo-acoustic effect refers to the generation of acoustic waves by the absorption of optical energy [**105, 56**]. In photo-acoustic imaging, energy absorption causes thermo-elastic expansion of the tissue, which in turn leads to propagation of a pressure wave. This signal is measured by transducers distributed on the boundary of the organ, which is in turn used for imaging optical properties of the organ. Mathematically, the pressure p satisfies (3.1) with the boundary condition (3.2) and the initial conditions

$$p(x,t)|_{t=0} = a\delta_{x=z} \quad \text{in } \Omega, \tag{3.15}$$

and

$$\partial_t p(x,t)|_{t=0} = 0 \quad \text{in } \Omega. \tag{3.16}$$

Here a is the absorbed energy.

Construct by the geometrical control method a function $v(x,t)$ satisfying (3.6), the initial condition (3.7), the boundary condition $v = 0$ on $\partial\Omega \setminus \overline{\Gamma}$, and the final conditions (3.8). Choosing w as in Section 3.4 yields different detection algorithms.

3.5. Numerical illustrations

To test the geometrical control imaging approach, we implemented numerical simulations of both the forward problem, the wave equation (3.1)-(3.4), and the inverse problem where we compute the geometrical control function (3.6)-(3.9) and implement the inversion algorithms of Section 3.3.

To simulate the wave equation, we used a standard P1-finite elements discretization in space and a finite difference scheme in time. For time-cost considerations, we settled with an explicit (leap-frog) scheme along with the use of mass lumping (row-sum technique).

The method we present here has been implemented and tested on various types of two-dimensional meshes. We will present results obtained on three different sets of meshes (see Figure 3.1 and Table 3.1):

Set name	Coarse mesh			Fine mesh		
	# of nodes	# of elements	h	# of nodes	# of elements	$2h$
squareReg0	36	50	0.2	121	200	0.1
squareReg2	441	800	0.05	1681	3200	0.025
circle	270	490	0.0672	1029	1960	0.0336

TABLE 3.1. Geometries and meshes.

- squareReg0 and squareReg2 are regular meshes of the unit square $[-0.5\ 0.5]^2$.
- circle are unstructured meshes of the unit disc.

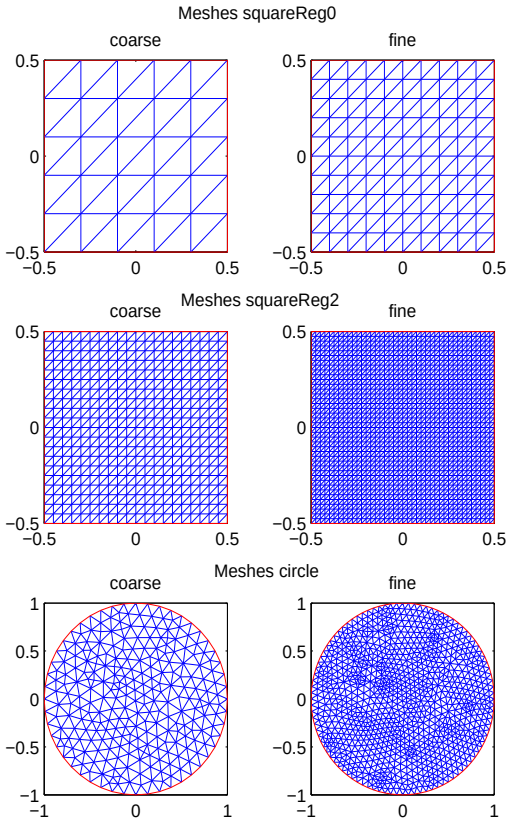

FIGURE 3.1. The coarse and fine meshes used on the square and circular geometries.

For computation of imaging functionals of Kirchhoff-, back-propagation-, and MUSIC-types, one has to be very careful with the spatial frequency ω. One has to make sure that the function $w(x;\omega)$ is accurately represented on the meshes we use. This imposes strict limitations on the range of frequencies that can be used.

Finally, the considered initial conditions for the simulated measurements are $p(x,0) = 0$ and $\frac{\partial p}{\partial t}(x,0) = \delta_h(x_0)$, where δ_h is a Gaussian approximation of the Dirac distribution and $x_0 = [0.21 \ \ -0.17]$ (see Figure 3.2).

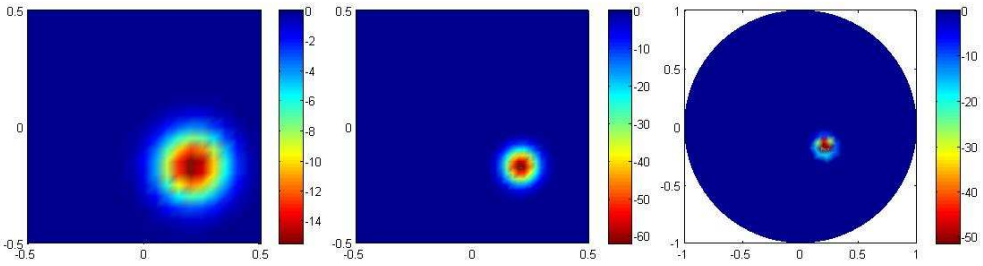

FIGURE 3.2. Initial time derivative, for the three geometries, used for the simulated measures.

To illustrate the performance of our approach with regards to limiting the view, we applied the algorithm to both a full and a partial view setting.

For the square medium, we assumed measurements were taken only on two adjacent edges - this corresponds to the theoretical (and practical) limit that still ensures geometric controllability. For the circular medium, we assumed measurements between angles $\frac{\pi}{4}$ and $\frac{3\pi}{2}$, as shown in Figure 3.4.

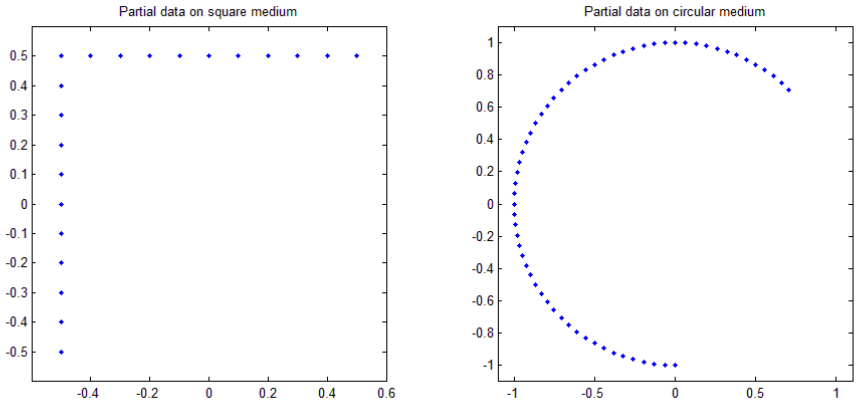

FIGURE 3.3. Limited-view observation boundaries for square and disc.

Before presenting the numerical results, we describe the numerical method used for computing the geometrical control, which is based on the Hilbert Uniqueness Method (HUM) of Lions.

3.5.1. Geometrical control: HUM using conjugate gradient iteration on a bi-grid mesh. The solution g_w of (3.6)-(3.9) has been shown to be unique provided that T and the control boundary Γ geometrically control Ω [**29**]. A systematic and constructive method for computing such a control is given by the Hilbert Uniqueness Method (HUM) of Lions [**79**]. A detailed study of the algorithm can be found in [**59**], [**25**], and [**106**]. The method applies a conjugate gradient algorithm as follows:

- Let $e_0, e_1 \in \mathrm{H}_0^1(\Omega) \times \mathrm{L}^2(\Omega)$, where $\mathrm{H}_0^1(\Omega)$ is the standard Sobolev space with zero boundary values;
- Solve forwards on $(0,T)$ the wave equation

$$\left\{\begin{array}{l} \dfrac{\partial^2\phi}{\partial t^2}(x,t) - c^2\Delta\phi(x,t) = 0, \\ \phi(x,t) = 0 \qquad \text{on } \partial\Omega, \\ \phi(x,0) = e_0(x), \qquad \dfrac{\partial\phi}{\partial t}(x,0) = e_1(x); \end{array}\right. \tag{3.17}$$

- Solve backwards the wave equation

$$\left\{\begin{array}{l} \dfrac{\partial^2\psi}{\partial t^2}(x,t) - c^2\Delta\psi(x,t) = 0, \\ \psi(x,t) = \left\{\begin{array}{ll} 0 & \text{on } \partial\Omega\backslash\bar{\Gamma}, \\ \frac{\partial\phi}{\partial\nu}(x,t) & \text{on } \Gamma, \end{array}\right. \\ \psi(x,T) = 0, \qquad \dfrac{\partial\psi}{\partial t}(x,T) = 0; \end{array}\right. \tag{3.18}$$

- Set

$$\Lambda(e_0,e_1) = \left\{\frac{\partial\psi}{\partial t}(x,0), -\psi(x,0)\right\}; \tag{3.19}$$

- The solution v of (3.6)-(3.8) can be identified with ψ when

$$\Lambda(e_0,e_1) = \left\{0, -c^2\beta(x)w(x)\right\}$$

and $g_w(x,t) = \psi(x,t)$ on Γ.

Remark 3.1. *In the case where the initial condition is a pressure field (e.g., photo-acoustics)* $p(x,0) = p_0(x)$, $\frac{\partial p}{\partial t}(x,0) = 0$, *we need to have* $v(x,0) = 0$, $\frac{\partial v}{\partial t}(x,0) = c^2\beta(x)w(x)$. *This can be easily obtained by solving :* $\Lambda(e_0,e_1) = \left\{c^2\beta(x)w(x), 0\right\}$.

To proceed, we used a conjugate gradient algorithm on a discretized version Λ_h of the operator defined in (3.19), where we solve the wave equation using the finite-element finite-difference discretization described previously. To deal with unwanted effects linked with high spatial frequencies, we used a bi-grid method of Glowinski [**59**] based on a fine mesh with discretization length h and a coarse mesh with length $2h$. The wave equation is solved on the fine mesh and the residuals of Λ_h are computed after projection onto the coarse mesh.

Let us define I_h^{2h} and I_{2h}^h to be the projectors from the fine mesh to the coarse mesh and vice versa. The conjugate gradient algorithm is now as follows:

- Let e_0^0, e_1^0 be given initial guesses on the coarse mesh;
- Solve numerically (3.17) forwards with initial conditions $I_{2h}^h e_0^0$, $I_{2h}^h e_1^0$ and solve (3.18) backwards, both on the fine grid;

- Compute the initial residuals $g^0 = \{g_0^0, g_1^0\}$ on the coarse grid as follows:

$$\begin{cases} -\Delta g_0^0 = I_h^{2h} \dfrac{\psi^1 - \psi^{-1}}{2\Delta t} - I_h^{2h} u_1 & \text{in } \Omega, \\ g_0^0 = 0 & \text{on } \partial\Omega, \end{cases}$$

  and

$$g_1^0 = \psi^0 - I_h^{2h} u_0;$$

- If the norm of the residuals

$$\|\{g_0^0, g_1^0\}\|_h^2 = \int_{\mathcal{T}_h} |g_1^0|^2 + |\nabla g_0^0|^2$$

  is small enough, we have our solution, else we set the first search direction $w^0 = g^0$ and start the conjugate gradient;
- Suppose we know $e^k = \{e_0^k, e_1^k\}$, $g^k = \{g_0^k, g_1^k\}$ and $w^k = \{w_0^k, w_1^k\}$;
- Solve numerically (3.17) forwards with initial conditions $I_{2h}^h w_0^k$, $I_{2h}^h w_1^k$ and solve (3.18) backwards both on the fine grid;
- Compute the remaining residuals $\xi^k = \{\xi_0^k, \xi_1^k\}$ on the coarse grid as follows:

$$\begin{cases} -\Delta_h \xi_0^k = I_h^{2h} \dfrac{\psi^1 - \psi^{-1}}{2\Delta t}, \\ \xi_0^k = 0 & \text{on } \partial\Omega, \end{cases}$$

  and

$$\xi_1^k = \psi^0;$$

- Calculate the length of the step in the w^k direction

$$\rho^k = \frac{\|g^k\|_h}{\langle \xi^k, w^k \rangle_h},$$

  where $\langle \xi^k, w^k \rangle_h = \displaystyle\int_{\mathcal{T}_h} \nabla \xi_0^k \nabla w_0^k + \xi_1^k w_1^k$;
- Update the quantities

$$e^{k+1} = e^k - \rho^k w^k,$$
$$g^{k+1} = g^k - \rho^k \xi^k;$$

- If $\|g^{k+1}\|_h$ is small, then e^{k+1} is our solution, else compute

$$\gamma^k = \frac{\|g^{k+1}\|_h}{\|g^k\|_h},$$

  and set the new descent direction

$$w^{k+1} = g^{k+1} + \gamma^k w^k.$$

REMARK 3.2 (Remarks on the numerical convergence). *The numerical procedure described in the previous section has been proved to converge in the case of finite difference method on the unit square* [**68**]. *This result can be easily extended in the case of a finite element method on a regular mesh. Convergence results for more general meshes are not available yet. They will be the subject of a future study.*

3.5.2. Reconstruction results. We present here some results obtained by algorithms presented in Section 3.4. For each algorithm we will consider both the full view and the partial view cases.

- **Kirchhoff algorithm.** We limited ourselves to the frequency range : $W = [-\omega_{\max}, \omega_{\max}]$ with a step-size $\Delta\omega = \omega_{\max}/n_\omega$ where $\omega_{\max}$ and n_ω depend on the mesh coarseness.

  For time considerations we chose a reduced array of three virtual receivers
  - $Y = \{[0.6\ \ -0.6],\ [0.6\ 0],\ [0.6\ 0.6]\}$ for the square medium.
  - $Y = \{[1\ \ -1],\ [1\ 0],\ [1\ 1]\}$ for the circular medium.

  We compute and represent the function $\mathcal{I}_{\mathrm{KI}}(z^S)$ for z^S on the fine mesh. The estimated position is at the maximum of $\mathcal{I}_{\mathrm{KI}}(z^S)$. Reconstruction results are given in Figure 3.4.
- **Back-propagation algorithm.** We chose frequencies well represented on the mesh ($\omega = 9$ for squareReg0, $\omega = 30$ for squareReg2 and $\omega = 20$ for circle) and a 30-point discretization of the unit circle for θ.

  We compute and represent the function $\mathcal{I}_{\mathrm{BP}}(z^S)$ for z^S on the fine mesh. The estimated position is at the maximum of $\mathcal{I}_{\mathrm{BP}}(z^S)$. Results are given in Figure 3.5.
- **Arrival-time algorithm.** We considered minimal arrays of two virtual receivers $Y = \{[0\ 0.6]; [0.6\ 0]\}$ for the square medium. For each receiver we computed the value of $r_k = d(x_0, y_k)$, where x_0 is the position of the source and y_k the position of the receiver. We represent the circles $\mathcal{C}(y_k, r_k)$ and their intersections. Results are given in Figure 3.6.
- **MUSIC algorithm.** Working with the same parameters, we compute and represent the function $\mathcal{I}_{\mathrm{MU}}(z^S)$ for z^S on the fine mesh. The estimated position is at the maximum of $\mathcal{I}_{\mathrm{MU}}(z^S)$. Reconstruction results are given in Figure 3.7.

In Table 3.2 we give the estimations x_{est} of the source location $x_0 = [0.21 - 0.17]$ for each algorithm, and the error $d(x_0, x_{\mathrm{est}})$. For comparison, we give $h_{\min}$, the smallest distance between 2 points in the fine mesh.

3.5.3. Case of multiple sources. Except for the arrival-time algorithm, all the methods presented in this chapter are well-suited for identifying several point-like sources. To illustrate this, we simulated measurements on squareReg2 with three sources located at $[0.21\ \ -0.17]$, $[-0.22\ \ -0.3]$ and $[0.05\ 0.27]$.

- We applied the Kirchhoff imaging algorithm with a different set of virtual receivers:

  $$Y = \{[0.6\ 0],\ [0.6\ 0.6],\ [0\ 0.6],\ [-0.6\ 0.6],\ [-0.6\ 0]\}\,.$$

  The reason for taking more virtual receivers is that Kirchhoff works on intersecting circles centered at the receivers and passing through the sources. Too few receivers can generate false positives. Results are given in Figure 3.10.
- We ran the back-propagation and MUSIC algorithms with exactly the same parameters as previously. Results are given in Figures 3.11 and 3.12 respectively.

Algorithm	Mesh	View	x_{est}	$h_{\min}$	$d(x_0, x_{\text{est}})$
Kirchhoff	squareReg0	Full	[0.2 -0.15]	0.1	0.0224
		Partial	[0.2 -0.15]		0.0224
	squareReg2	Full	[0.2 -0.175]	0.025	0.0112
		Partial	[0.2 -0.175]		0.0112
	circle	Full	[0.1949 -0.1619]	0.0336	0.0171
		Partial	[0.1949 -0.1619]		0.0171
Back-propagation	squareReg0	Full	[0.2 -0.15]	0.1	0.0224
		Partial	[0.2 -0.15]		0.0224
	squareReg2	Full	[0.2125 -0.175]	0.025	0.0056
		Partial	[0.2125 -0.175]		0.0056
	circle	Full	[0.1949 -0.1619]	0.0336	0.0171
		Partial	[0.1949 -0.1619]		0.0171
Arrival time	squareReg0	Full	[0.1877 -0.1433]	0.1	0.0348
		Partial	[0.1882 -0.1314]		0.0444
	squareReg2	Full	[0.2050 -0.1768]	0.025	0.0085
		Partial	[0.2048 -0.1774]		0.009
	circle	Full	[0.1802 -0.2196]	0.0336	0.0579
		Partial	[0.1790 -0.2119]		0.0522
MUSIC	squareReg0	Full	[0.15 -0.2]	0.1	0.0671
		Partial	[0.15 -0.2]		0.0671
	squareReg2	Full	[0.175 -0.1625]	0.025	0.0358
		Partial	[0.175 -0.175]		0.0354
	circle	Full	[0.2804 -0.139]	0.0336	0.0769
		Partial	[0.2416 -0.0974]		0.0792

TABLE 3.2. Numerical results for localization of the source at $x_0 = [0.21, -0.17]$ using four algorithms and three geometries.

3.5.4. Boundary perturbation. In real experiments, one does not necessarily know the uncontrolled part of the boundary with good accuracy. A major concern for real applications of the method is thus its robustness with respect to perturbations of the boundary.

We tested our algorithms by perturbing the boundary nodes outwards

$$x_{i,\text{perturbed}} = x_i + \epsilon U n_{x_i},$$

where ϵ is an amplitude factor, U is a uniform random variable in [0 1] and n_{x_i} is the outward normal at the point x_i. We simulated measurements on the perturbed mesh, which is then supposed unknown since we computed the geometric control on the unperturbed mesh.

To illustrate the results, we used squareReg2 with three levels of perturbation, $\epsilon = 0.01$, 0.025 and 0.05 (see Figure 3.5.4) and the same initial condition as before, that is a Dirac approximation located at $[0.21 \ -0.17]$.

We give the results, with the three perturbations, for the Kirchhoff (Figure 3.13), the back-propagation (Figure 3.14) and the arrival-time (Figure 3.15) algorithms. Modifying the mesh as we did generates smaller elements and thus changes the CFL condition for the wave-equation solver. Computation time becomes too

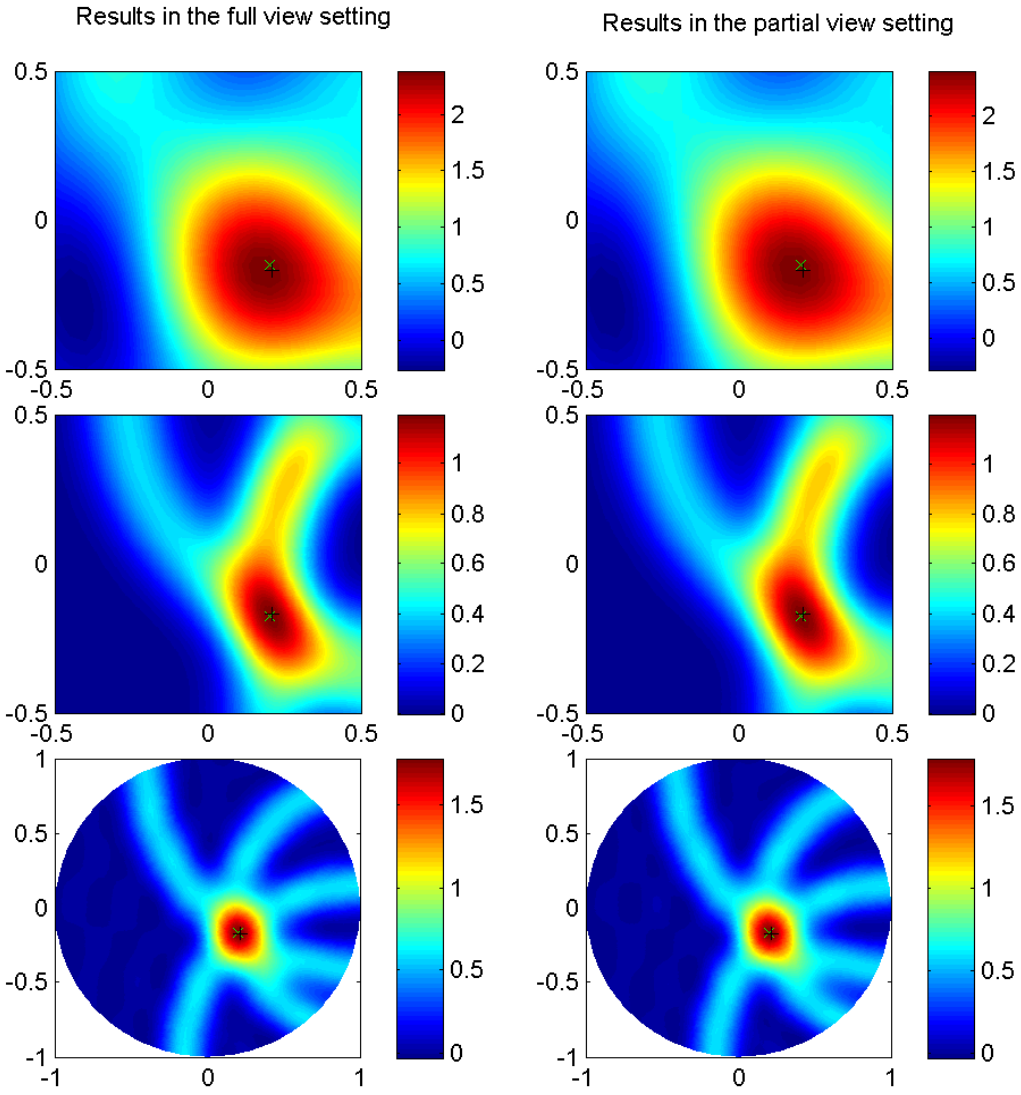

FIGURE 3.4. Kirchhoff results for the geometries of Table 3.1 - from top to bottom: squareReg0, squareReg2, circle. The (black/white) x denotes the (numerical/theoretical) center of the source.

expensive for the MUSIC algorithm. For this reason we do not present MUSIC results here.

As expected the estimation of the source position deteriorates as we increase the boundary uncertainty. The errors are summarized in Table 3.3.

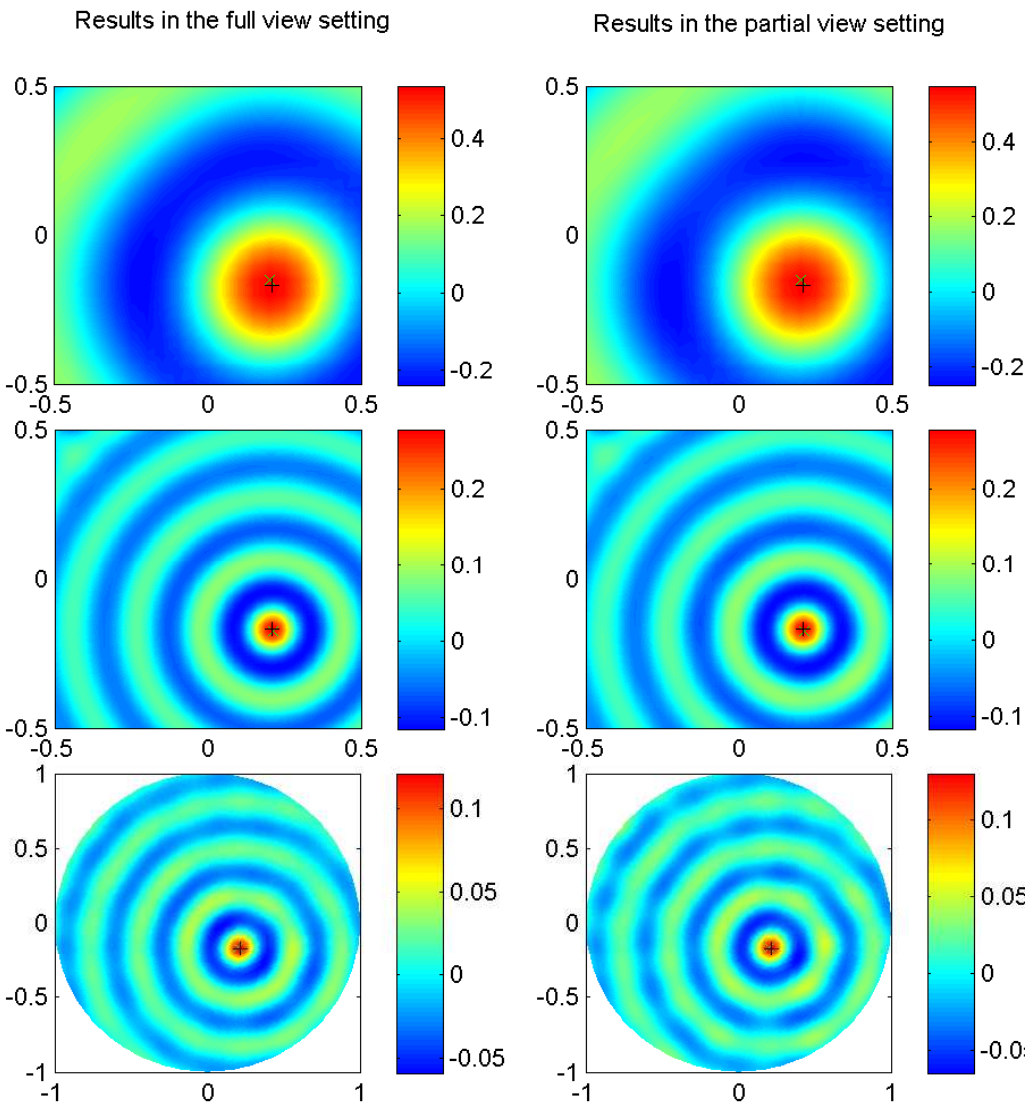

FIGURE 3.5. Back-propagation results for the geometries of Table 3.1 - from top to bottom: squareReg0, squareReg2, circle. The (black/white) x denotes the (numerical/theoretical) center of the source.

3.6. Concluding remarks

In this chapter we have constructed Kirchhoff-, back-propagation-, MUSIC-, and arrival time-type algorithms for imaging point sources and dipoles from limited-view data. Our approach is based on averaging of the limited-view data, using

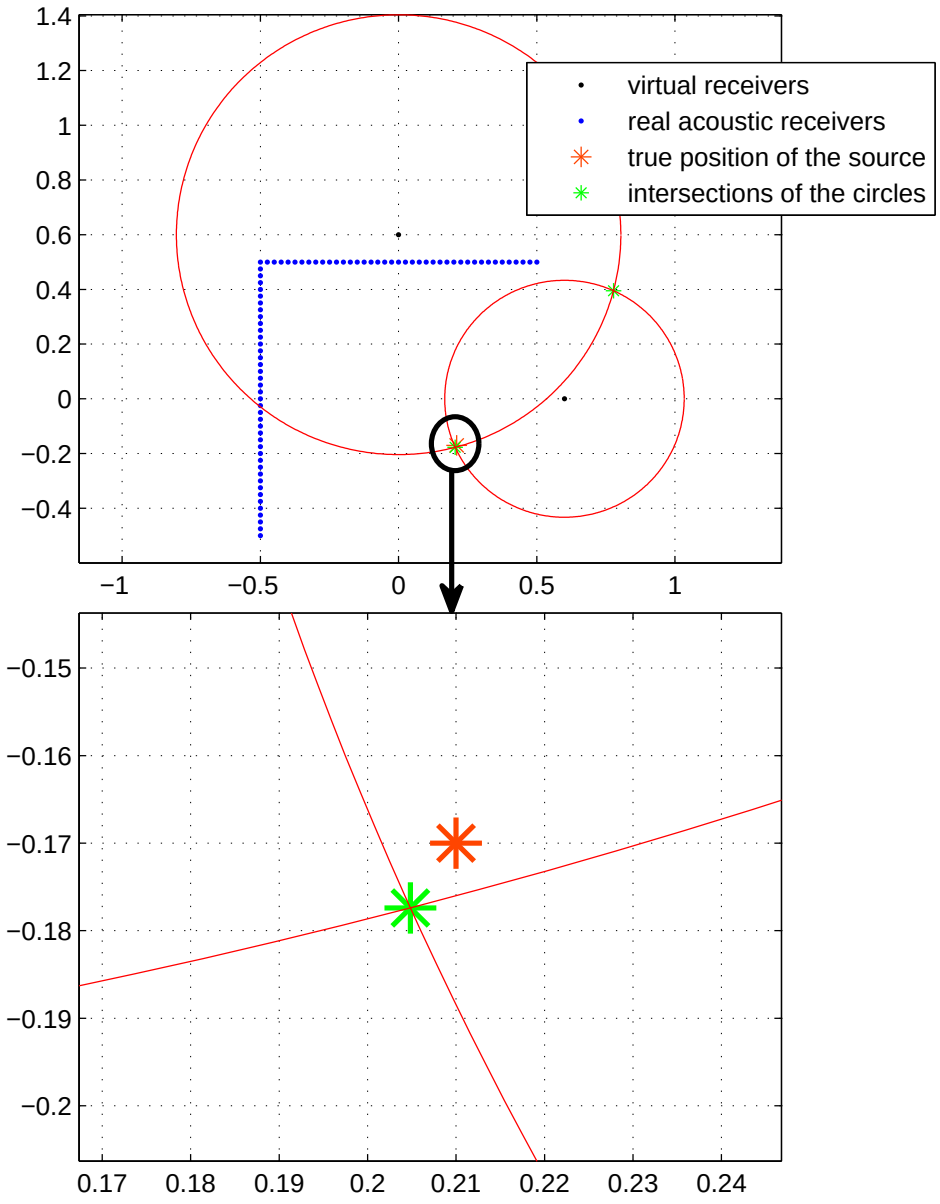

FIGURE 3.6. Example of arrival time results for squareReg2 geometry.

weights constructed by the geometrical control method. It is quite robust with respect to perturbations of the non-accessible part of the boundary. We have shown that if one can construct accurately the geometric control then one can perform imaging with the same resolution using partial data as using complete data.

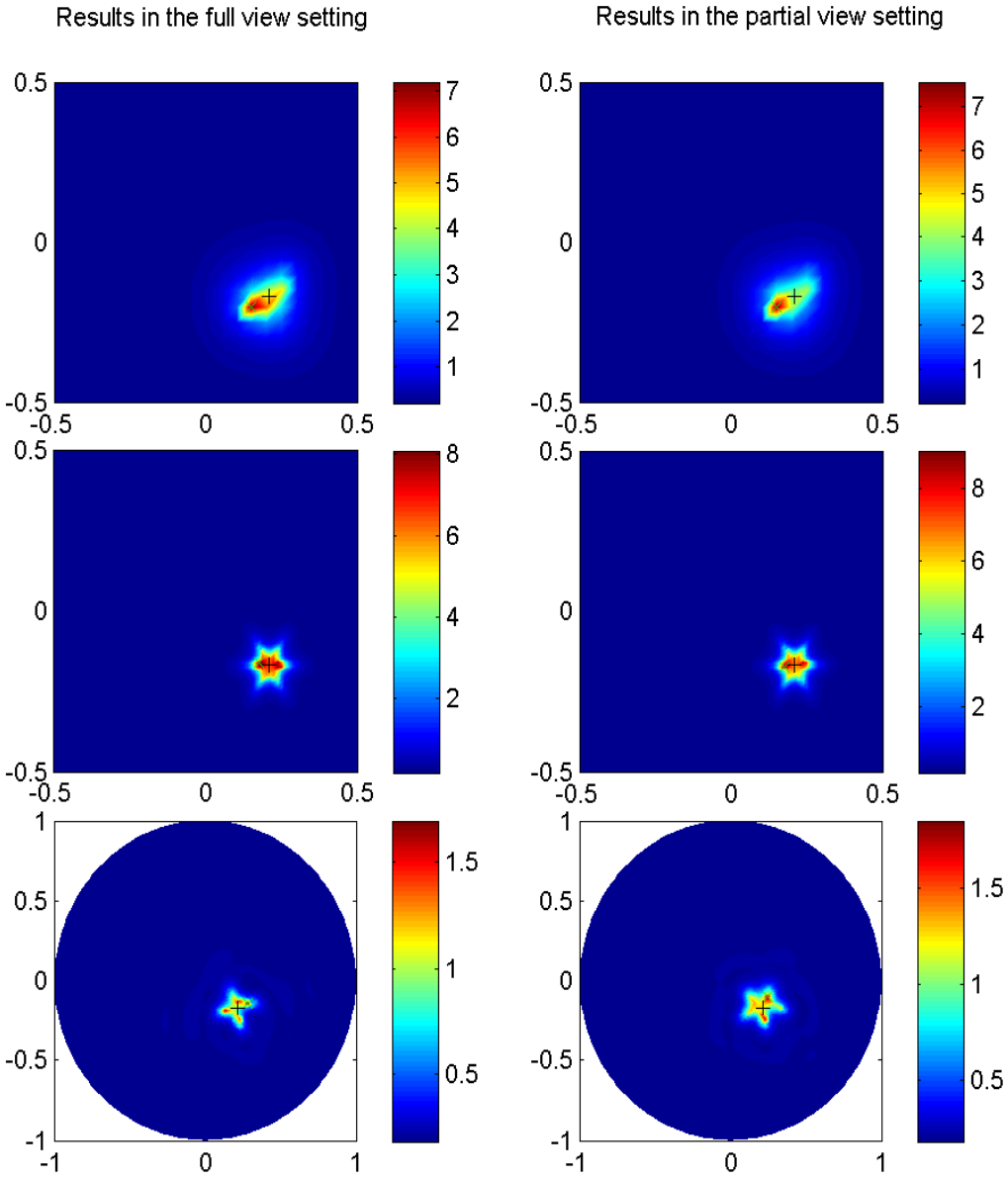

FIGURE 3.7. MUSIC results for the geometries of Table 3.1 - from top to bottom: sqReg0, sqReg2, circle. The (black/white) x denotes the (numerical/theoretical) center of the source.

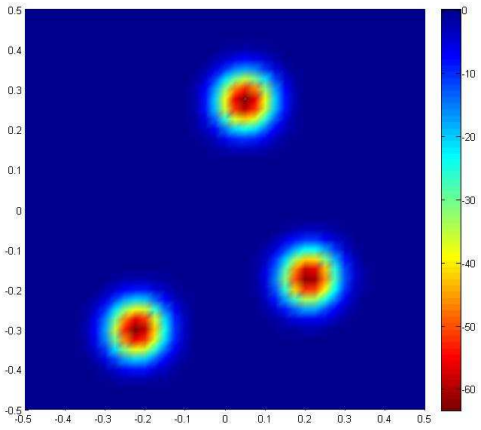

FIGURE 3.8. Initial time derivative for the case of multiple sources.

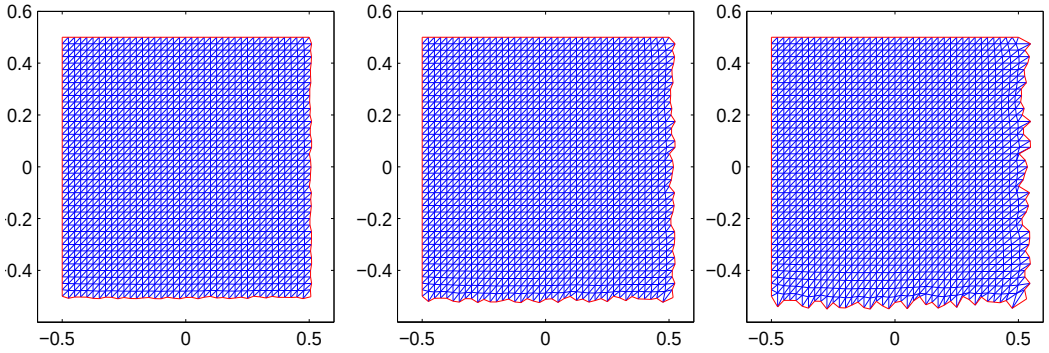

FIGURE 3.9. Perturbation of the mesh for $\epsilon = 0.01$, 0.025 and 0.05.

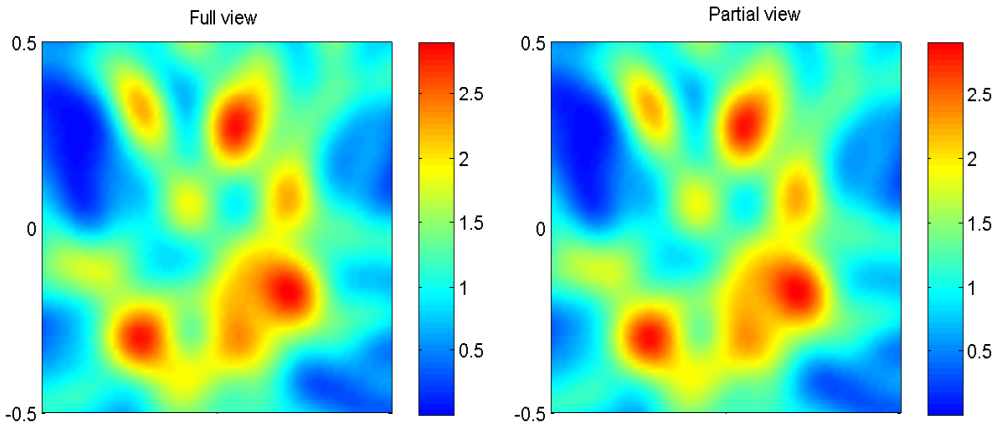

FIGURE 3.10. Kirchhoff results for the geometry sqReg2 with several inclusions.

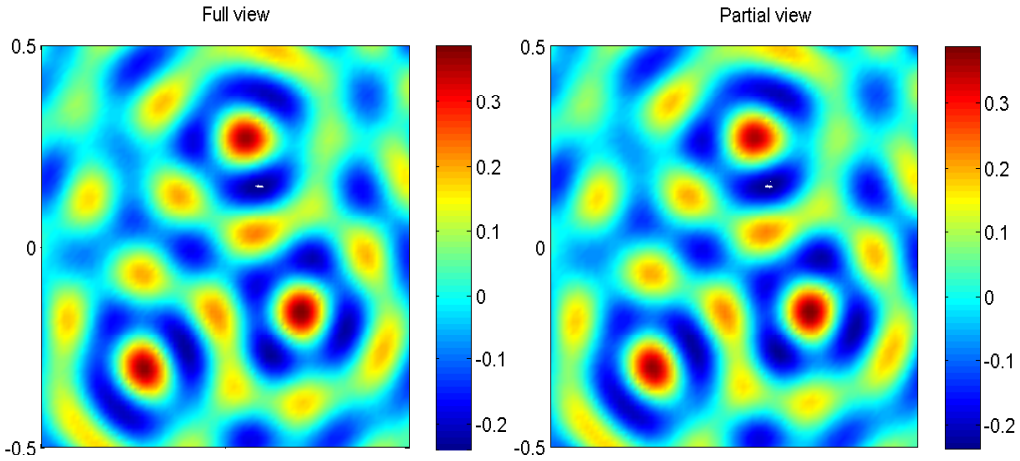

FIGURE 3.11. Back-propagation results for the geometry sqReg2 with several inclusions.

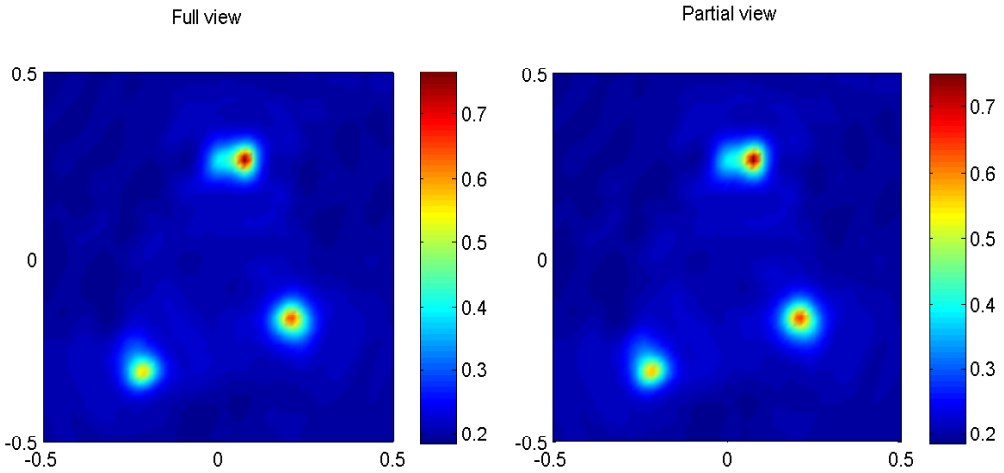

FIGURE 3.12. MUSIC results for the geometry sqReg2 with several inclusions.

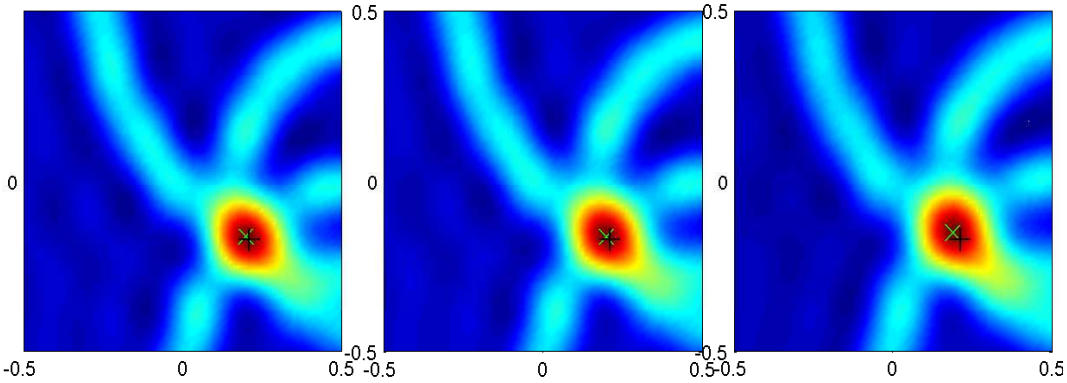

FIGURE 3.13. Kirchhoff results for the geometry sqReg2 with perturbed boundary (from left-to-right,$\epsilon = 0.01$, 0.025 and 0.05). The (black/white) x denotes the (numerical/theoretical) center of the source.

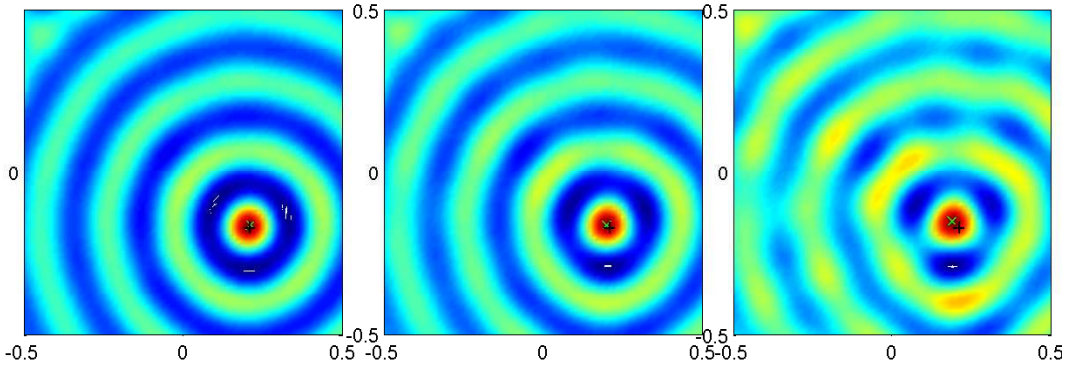

FIGURE 3.14. Back-propagation results for the geometry sqReg2 with perturbed boundary (from left-to-right, $\epsilon = 0.01$, 0.025 and 0.05). The (black/white) x denotes the (numerical/theoretical) center of the source.

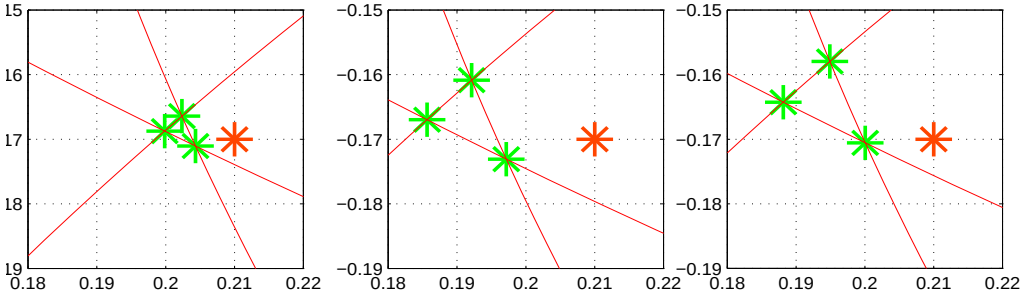

FIGURE 3.15. Arrival-time results for the geometry sqReg2 with perturbed boundary (from left-to-right, $\epsilon = 0.01$, 0.025 and 0.05)

Algorithm	Perturbation amplitude ϵ	x_{est}	$d(x_0, x_{\text{est}})$
Kirchhoff	0.01	[0.2 -0.1625]	0.0125
	0.025	[0.2 -0.1625]	0.0125
	0.05	[0.1875 -0.15]	0.03
Back-propagation	0.01	[0.2125 -0.1625]	0.0079
	0.025	[0.2 -0.1625]	0.0125
	0.05	[0.1875 -0.15]	0.03
Arrival time	0.01	[0.2022 -0.1687]	0.0079
	0.025	[0.1917 -0.167]	0.0186
	0.05	[0.1944 -0.1643]	0.0166

TABLE 3.3. Numerical results for localization of the source at $x_0 = [0.21 \ -0.17]$ using sqReg2 geometry with boundary perturbations.

CHAPTER 4

Imaging in visco-elastic media obeying a frequency power-law

Abstract. In this chapter we consider the problem of reconstructing a small anomaly in a viscoelastic medium from wavefield measurements. We choose Szabo's model [**95**] to describe the viscoelastic properties of the medium. Expressing the ideal elastic field without any viscous effect in terms of the measured field in a viscous medium, we generalize the imaging procedures in Chapter 2 to detect an anomaly in a visco-elastic medium from wavefield measurements.

4.1. Introduction

In Chapter 2 we have considered anomaly imaging in a purely quasi-incompressible elastic medium. In this chapter, we consider the problem of reconstructing a small anomaly in a viscoelastic medium from wavefield measurements. The Voigt model is a common model to describe the viscoelastic properties of tissues. Catheline *et al.* [**42**] have shown that this model is well adapted to describe the viscoelastic response of tissues to low-frequency excitations. We choose a more general model derived by Szabo [**95**] that describes observed power-law behavior of many viscoelastic materials. It is based on a time-domain statement of causality. It reduces to the Voigt model for the specific case of quadratic frequency loss. Expressing the ideal elastic field without any viscous effect in terms of the measured field in a viscous medium, we generalize the methods described in Chapter 2 to recover the viscoelastic and geometric properties of an anomaly from wavefield measurements.

The chapter is organized as follows. In Section 4.2 we introduce a general viscoelastic wave equation. Section 4.3 is devoted to the derivation of the Green function in a viscoelastic medium. In Section 4.4 we present anomaly imaging procedures in visco-elastic media.

4.2. General visco-elastic wave equation

When a wave travels through a biological medium, its amplitude decreases with time due to attenuation. The attenuation coefficient for biological tissue may be approximated by a power-law over a wide range of frequencies. Measured attenuation coefficients of soft tissue typically have linear or greater than linear dependence on frequency [**95**].

In an ideal medium, *i.e.*, without attenuation, Hooke's law expresses the following relationship between stress and strain tensors:

$$\mathcal{T} = \mathcal{C} : \mathcal{S}, \tag{4.1}$$

where $\mathcal{T}$, $\mathcal{C}$ and $\mathcal{S}$ are respectively the stress, the stiffness and the strain tensor of orders $2, 4$ and 2 and : represents the tensorial product.

Consider a dissipative medium. Suppose that the medium is homogeneous and isotropic. We write

$$\mathcal{C} = [\mathcal{C}_{ijkl}] = [\lambda\delta_{ij}\delta_{kl} + \mu(\delta_{ik}\delta_{jl} + \delta_{il}\delta_{jk})], \tag{4.2}$$

$$\eta = [\eta_{ijkl}] = [\eta_s\delta_{ij}\delta_{kl} + \eta_p(\delta_{ik}\delta_{jl} + \delta_{il}\delta_{jk})], \tag{4.3}$$

where δ is the Kronecker delta function, μ, λ are the Lamé parameters, and η_s, η_p are the shear and bulk viscosities, respectively. Here we have adopted the generalized summation convention over the repeated index.

Throughout this chapter we suppose that

$$\eta_p, \eta_s << 1. \tag{4.4}$$

For a medium obeying a power-law attenuation model and under the smallness condition (4.4), a generalized Hooke's law reads [**95**]

$$\mathcal{T}(x,t) = \mathcal{C} : \mathcal{S}(x,t) + \eta : \mathcal{M}(\mathcal{S})(x,t) \tag{4.5}$$

where the convolution operator $\mathcal{M}$ is given by

$$\mathcal{M}(\mathcal{S}) = \begin{cases} -(-1)^{y/2}\frac{\partial^{y-1}\mathcal{S}}{\partial t^{y-1}} & \text{y is an even integer,} \\ \frac{2}{\pi}(y-1)!(-1)^{(y+1)/2}\frac{H(t)}{t^y} * \mathcal{S} & \text{y is an odd integer,} \\ -\frac{2}{\pi}\Gamma(y)\sin(y\pi/2)\frac{H(t)}{|t|^y} * \mathcal{S} & \text{y is a non integer.} \end{cases} \tag{4.6}$$

Here $H(t)$ is the Heaviside function and Γ denotes the gamma function.

Note that for the common case, $y = 2$, the generalized Hooke's law (4.5) reduces to the Voigt model,

$$\mathcal{T} = \mathcal{C} : \mathcal{S} + \eta : \frac{\partial \mathcal{S}}{\partial t}. \tag{4.7}$$

Taking the divergence of (4.5) we get

$$\nabla \cdot \mathcal{T} = \left(\bar{\lambda} + \bar{\mu}\right)\nabla(\nabla \cdot \mathbf{u}) + \bar{\mu}\Delta\mathbf{u},$$

where

$$\bar{\lambda} = \lambda + \eta_p\mathcal{M}(\cdot) \quad \text{and} \quad \bar{\mu} = \mu + \eta_s\mathcal{M}(\cdot).$$

Next, considering the equation of motion for the system, *i.e.*,

$$\rho\frac{\partial^2\mathbf{u}}{\partial t^2} - \mathbf{F} = \nabla \cdot \mathcal{T}, \tag{4.8}$$

with ρ being the constant density and $\mathbf{F}$ the applied force and using the expression for $\nabla \cdot \mathcal{T}$, we obtain the generalized visco-elastic wave equation

$$\rho\frac{\partial^2\mathbf{u}}{\partial t^2} - \mathbf{F} = \left(\bar{\lambda} + \bar{\mu}\right)\nabla(\nabla \cdot \mathbf{u}) + \bar{\mu}\Delta\mathbf{u}. \tag{4.9}$$

4.3. Green's function

In this section we find the Green function of the viscoelastic wave equation (4.9). For doing so, we first need a Helmholtz decomposition.

4.3.1. Helmholtz decomposition. The following lemma holds.

LEMMA 4.1. *If the displacement field* $\mathbf{u}(t,x)$ *satisfies (4.9) and if the body force* $\mathbf{F} = \nabla\varphi_f + \nabla\times\psi_f$ *then there exist potentials* φ_u *and* ψ_u *such that*

- $\mathbf{u} = \nabla\varphi_u + \nabla\times\psi_u$; $\nabla\cdot\psi_u = 0$;
- $\frac{\partial^2\varphi_u}{\partial t^2} = \frac{\varphi_f}{\rho} + c_p^2\Delta\varphi_u + \nu_p\mathcal{M}(\Delta\varphi_u) \approx \frac{\varphi_f}{\rho} - \frac{\nu_p\mathcal{M}(\varphi_f)}{\rho c_p^2} + c_p^2\Delta\varphi_u + \frac{\nu_p}{c_p^2}\mathcal{M}(\partial_t^2\varphi_u)$;
- $\frac{\partial^2\psi_u}{\partial t^2} = \frac{\psi_f}{\rho} + c_s^2\Delta\psi_u + \nu_s\mathcal{M}(\Delta\psi_u) \approx \frac{\psi_f}{\rho} - \frac{\nu_s\mathcal{M}(\psi_f)}{\rho c_s^2} + c_s^2\Delta\psi_u + \frac{\nu_s}{c_s^2}\mathcal{M}(\partial_t^2\psi_u)$,

with

$$c_p^2 = \frac{\lambda+2\mu}{\rho},\ c_s^2 = \frac{\mu}{\rho},\ \nu_p = \frac{\eta_p+2\eta_s}{\rho}, \quad \textit{and} \quad \nu_s = \frac{\eta_s}{\rho}.$$

Let

$$K_m(\omega) = \omega\sqrt{(1-\frac{\nu_m}{c_m^2}\hat{\mathcal{M}}(\omega))}, \quad m = s,p, \tag{4.10}$$

where the multiplication operator $\hat{\mathcal{M}}(\omega)$ is the Fourier transform of the convolution operator $\mathcal{M}$.

Supposing that φ_u and ψ_u are causal implies the causality of the inverse Fourier transforms of $K_m(\omega), m = s,p$. Applying the Kramers-Krönig relations, it follows that

$$-\Im m K_m(\omega) = \mathcal{H}\Big[\Re e K_m(\omega)\Big] \quad \text{and} \quad \Re e K_m(\omega) = \mathcal{H}\Big[\Im m K_m(\omega)\Big], \quad m = p,s, \tag{4.11}$$

where $\mathcal{H}$ is the Hilbert transform. Note that $\mathcal{H}^2 = -I$. The convolution operator $\mathcal{M}$ given by (4.6) is based on the constraint that causality imposes on (4.5). Under the smallness assumption (4.4), the expressions in (4.6) can be found from the Kramers-Krönig relations (4.11). One drawback of (4.11) is that the attenuation, $\Im m K_m(\omega)$, must be known at all frequencies to determine the dispersion, $\Re e K_m(\omega)$. However, bounds on the dispersion can be obtained from measurements of the attenuation over a finite frequency range [**85**].

4.3.2. Solution of (4.9) with a concentrated force. Let u_{ij} denote the i-th component of the solution $\mathbf{u}_j$ of the elastic wave equation related to a force $\mathbf{F}$ concentrated in the x_j-direction. Let $j = 1$ for simplicity and suppose that

$$\mathbf{F} = T(t)\delta(x-\xi)\mathbf{e}_1 = T(t)\delta(x-\xi)(1,0,0), \tag{4.12}$$

where ξ is the source point and $(\mathbf{e}_1,\mathbf{e}_2,\mathbf{e}_3)$ is an orthonormal basis of $\mathbb{R}^3$. The corresponding Helmholtz decomposition of the force $\mathbf{F}$ can be written as

$$\begin{cases} \mathbf{F} = \nabla\varphi_f + \nabla\times\psi_f, \\ \varphi_f = -\frac{T(t)}{4\pi}\frac{\partial}{\partial x_1}\left(\frac{1}{r}\right), \\ \psi_f = \frac{T(t)}{4\pi}\left(0, \frac{\partial}{\partial x_3}\left(\frac{1}{r}\right), -\frac{\partial}{\partial x_2}\left(\frac{1}{r}\right)\right), \end{cases} \tag{4.13}$$

where $r = |x-\xi|$ [**88**].

Consider the Helmholtz decomposition for $\mathbf{u}_1$ as

$$\mathbf{u}_1 = \nabla\varphi_1 + \nabla\times\psi_1, \tag{4.14}$$

where φ_1 and ψ_1 are respectively the solutions of the equations

$$\Delta\varphi_1 - \frac{1}{c_p^2}\frac{\partial^2\varphi_1}{\partial t^2} + \frac{\nu_p}{c_p^4}\mathcal{M}(\partial_t^2\varphi_1) = \frac{\varphi_f}{c_p^2\rho} - \frac{\nu_p\mathcal{M}(\varphi_f)}{\rho c_p^4}, \tag{4.15}$$

$$\Delta\psi_1 - \frac{1}{c_s^2}\frac{\partial^2\psi_1}{\partial t^2} + \frac{\nu_s}{c_s^4}\mathcal{M}(\partial_t^2\psi_1) = \frac{\psi_f}{c_s^2\rho} - \frac{\nu_s\mathcal{M}(\psi_f)}{\rho c_s^4}. \tag{4.16}$$

Taking the Fourier transform of (4.14),(4.15) and (4.16) with respect to t we get

$$\hat{\mathbf{u}}_1 = \nabla\hat{\varphi}_1 + \nabla\times\hat{\psi}_1 \tag{4.17}$$

$$\Delta\hat{\varphi}_1 + \frac{K_p^2(\omega)}{c_p^2}\hat{\varphi}_1 = \frac{\hat{\varphi}_f}{\rho c_p^2} - \frac{\nu_p\hat{\mathcal{M}}(\omega)\hat{\varphi}_f}{\rho c_p^4}, \tag{4.18}$$

$$\Delta\hat{\psi}_1 + \frac{K_s^2(\omega)}{c_s^2}\hat{\psi}_1 = \frac{\hat{\psi}_f}{\rho c_s^2} - \frac{\nu_s\hat{\mathcal{M}}(\omega)\hat{\psi}_f}{\rho c_s^4}, \tag{4.19}$$

with $K_m(\omega), m = p, s$, given by (4.10).

It is well known that the Green functions of the Helmholtz equations (4.18) and (4.19) are

$$\hat{g}^m(r,\omega) = \frac{e^{\sqrt{-1}\frac{K_m(\omega)}{c_m}r}}{4\pi r}, \quad m = s, p.$$

Therefore, following [**88**], we get the following expression for $\hat{\varphi}_1$:

$$\hat{\varphi}_1(x,\omega;\xi) = -\frac{1}{\rho c_p^2}(1 - \frac{\nu_p\hat{\mathcal{M}}(\omega)}{c_p^2})\frac{\hat{T}(\omega)}{4\pi\rho}\frac{\partial}{\partial x_1}\left(\frac{1}{r}\right)\int_0^{r/c_p}\zeta e^{\sqrt{-1}K_p(\omega)\zeta}\,d\zeta. \tag{4.20}$$

In the same way, the vector $\hat{\psi}_1$ is given by

$$\hat{\psi}_1(x,\omega;\xi) = \frac{1}{\rho c_s^2}(1-\frac{\nu_s\hat{\mathcal{M}}(\omega)}{c_s^2})\frac{\hat{T}(\omega)}{4\pi\rho}\left(0, \frac{\partial}{\partial x_3}\left(\frac{1}{r}\right), -\frac{\partial}{\partial x_2}\left(\frac{1}{r}\right)\right)\int_0^{r/c_s}\zeta e^{\sqrt{-1}K_s(\omega)\zeta}\,d\zeta. \tag{4.21}$$

Introduce the following notation:

$$I_m(x,\omega) = A_m\int_0^{r/c_m}\zeta e^{\sqrt{-1}K_m(\omega)\zeta}\,d\zeta \tag{4.22}$$

$$E_m(x,\omega) = A_m e^{\sqrt{-1}K_m(\omega)\frac{r}{c_m}}, \tag{4.23}$$

$$A_m(\omega) = (1 - \frac{\nu_m\hat{\mathcal{M}}(\omega)}{c_m^2}), \quad m = p, s. \tag{4.24}$$

We obtain, after a lengthy but simple calculation, that $\hat{u}_{i1}$ is given by

$$\hat{u}_{i1} = \frac{\hat{T}(\omega)}{4\pi\rho}\frac{\partial^2}{\partial x_i x_1}\left(\frac{1}{r}\right)[I_s(r,\omega) - I_p(r,\omega)] + \frac{\hat{T}(\omega)}{4\pi\rho c_p^2 r}\frac{\partial r}{\partial x_i}\frac{\partial r}{\partial x_1}E_p(r,\omega)$$

$$+\frac{\hat{T}(\omega)}{4\pi\rho c_s^2 r}\left(\delta_{i1} - \frac{\partial r}{\partial x_i}\frac{\partial r}{\partial x_1}\right)E_s(r,\omega),$$

and therefore, it follows that the solution u_{ij} for an arbitrary j is

$$\hat{u}_{ij} = \frac{\hat{T}(\omega)}{4\pi\rho}(3\gamma_i\gamma_j - \delta_{ij})\frac{1}{r^3}[I_s(r,\omega) - I_p(r,\omega)] + \frac{\hat{T}(\omega)}{4\pi\rho c_p^2}\gamma_i\gamma_j\frac{1}{r}E_p(r,\omega)$$

$$+\frac{\hat{T}(\omega)}{4\pi\rho c_s^2}(\delta_{ij} - \gamma_i\gamma_j)\frac{1}{r}E_s(r,\omega),$$

where $\gamma_i = (x_i - \xi_i)/r$.

4.3.3. Green's function. If we substitute $T(t) = \delta(t)$, where delta is the Dirac mass, then the function $u_{ij} = G_{ij}$ is the i-th component of the Green function related to the force concentrated in the x_j-direction. In this case we have $\hat{T}(\omega) = 1$. Thus we have the following expression for $\hat{G}_{ij}$:

$$\hat{G}_{ij} = \tfrac{1}{4\pi\rho}\left(3\gamma_i\gamma_j - \delta_{ij}\right)\tfrac{1}{r^3}\left[I_s(r,\omega) - I_p(r,\omega)\right] + \tfrac{1}{4\pi\rho c_p^2}\gamma_i\gamma_j\tfrac{1}{r}E_p(r,\omega)$$

$$+\tfrac{1}{4\pi\rho c_s^2}\left(\delta_{ij} - \gamma_i\gamma_j\right)\tfrac{1}{r}E_s(r,\omega),$$

which implies that

$$\hat{G}_{ij}(r,\omega;\xi) = \hat{g}_{ij}^p(r,\omega) + \hat{g}_{ij}^s(r,\omega) + \hat{g}_{ij}^{ps}(r,\omega), \tag{4.25}$$

where

$$\hat{g}_{ij}^{ps}(r,\omega) = \frac{1}{4\pi\rho}\left(3\gamma_i\gamma_j - \delta_{ij}\right)\frac{1}{r^3}\left[I_s(r,\omega) - I_p(r,\omega)\right], \tag{4.26}$$

$$\hat{g}_{ij}^{p}(r,\omega) = \frac{A_p(\omega)}{\rho c_p^2}\gamma_i\gamma_j\hat{g}^p(r,\omega), \tag{4.27}$$

and

$$\hat{g}_{ij}^{s}(r,\omega) = \frac{A_s(\omega)}{\rho c_s^2}\left(\delta_{ij} - \gamma_i\gamma_j\right)\hat{g}^s(r,\omega). \tag{4.28}$$

Let $G(r,t;\xi) = (G_{ij}(r,t;\xi))$ denote the transient Green function of (4.9) associated with the source point ξ. Let $G^m(r,t;\xi)$ and $W_m(r,t)$ be the inverse Fourier transforms of $A_m(\omega)\hat{g}^m(r,\omega)$ and $I_m(r,\omega), m = p, s$, respectively. Then, from (4.25-4.28), we have

$$G_{ij}(r,t;\xi) = \tfrac{1}{\rho c_p^2}\gamma_i\gamma_j G^p(r,t;\xi) + \tfrac{1}{\rho c_s^2}\left(\delta_{ij} - \gamma_i\gamma_j\right)G^s(r,t;\xi)$$

$$+\tfrac{1}{4\pi\rho}\left(3\gamma_i\gamma_j - \delta_{ij}\right)\tfrac{1}{r^3}\left[W_s(r,t) - W_p(r,t)\right].$$

Note that by a change of variables,

$$W_m(r,t) = \frac{4\pi}{c_m^2}\int_0^r \zeta^2 G^m(\zeta,t;\xi)d\zeta.$$

4.4. Imaging procedure

Consider the limiting case $\lambda \to +\infty$. The Green function for a quasi-incompressible visco-elastic medium is given by

$$G_{ij}(r,t;\xi) = \tfrac{1}{\rho c_s^2}\left(\delta_{ij} - \gamma_i\gamma_j\right)G^s(r,t;\xi)$$

$$+\tfrac{1}{16\pi^2\rho c_s^2}\left(3\gamma_i\gamma_j - \delta_{ij}\right)\tfrac{1}{r^3}\int_0^r \zeta^2 G^s(\zeta,t;\xi)d\zeta.$$

To generalize the detection algorithms presented in Chapter 2 to the visco-elastic case we shall express the ideal Green function without any viscous effect in terms of the Green function in a viscous medium. From

$$G^s(r,t;\xi) = \frac{1}{\sqrt{2\pi}}\int_{\mathbb{R}} e^{-\sqrt{-1}\omega t}A_s(\omega)g^s(r,\omega)\,d\omega,$$

it follows that

$$G^s(r,t;\xi) = \frac{1}{\sqrt{2\pi}} \int_{\mathbb{R}} A_s(\omega) \frac{e^{\sqrt{-1}(-\omega t + \frac{K_s(\omega)}{c_s} r)}}{4\pi r}\, d\omega.$$

4.4.1. Approximation of the Green function. Introduce the operator

$$L\phi(t) = \frac{1}{2\pi} \int_{\mathbb{R}} \int_0^{+\infty} A_s(\omega)\phi(\tau) e^{\sqrt{-1}K_s(\omega)\tau} e^{-\sqrt{-1}\omega t}\, d\tau\, d\omega,$$

for a causal function ϕ. We have

$$G^s(r,t;\xi) = L(\frac{\delta(\tau - r/c_s)}{4\pi r}),$$

and therefore,

$$L^* G^s(r,t;\xi) = L^* L(\frac{\delta(\tau - r/c_s)}{4\pi r}),$$

where L^* is the $L^2(0,+\infty)$-adjoint of L.

Consider for simplicity the Voigt model. Then, $\hat{\mathcal{M}}(\omega) = -\sqrt{-1}\omega$ and hence,

$$K_s(\omega) = \omega \sqrt{1 + \frac{\sqrt{-1}\nu_s}{c_s^2}\omega} \approx \omega + \frac{\sqrt{-1}\nu_s}{2c_s^2}\omega^2,$$

under the smallness assumption (4.4). The operator L can then be approximated by

$$\tilde{L}\phi(t) = \frac{1}{2\pi} \int_{\mathbb{R}} \int_0^{+\infty} A_s(\omega)\phi(\tau) e^{-\frac{\nu_s}{2c_s^2}\omega^2\tau} e^{\sqrt{-1}\omega(\tau - t)}\, d\tau\, d\omega.$$

Since

$$\int_{\mathbb{R}} e^{-\frac{\nu_s}{2c_s^2}\omega^2\tau} e^{\sqrt{-1}\omega(\tau-t)}\, d\omega = \frac{\sqrt{2\pi}c_s}{\sqrt{\nu_s\tau}} e^{-\frac{c_s^2(\tau-t)^2}{2\nu_s\tau}},$$

and

$$\sqrt{-1}\int_{\mathbb{R}} \omega e^{-\frac{\nu_s}{2c_s^2}\omega^2\tau} e^{\sqrt{-1}\omega(\tau-t)}\, d\omega = -\frac{\sqrt{2\pi}c_s}{\sqrt{\nu_s\tau}} \frac{\partial}{\partial t} e^{-\frac{c_s^2(\tau-t)^2}{2\nu_s\tau}},$$

it follows that

$$\tilde{L}\phi(t) = \int_0^{+\infty} \frac{t}{\tau}\phi(\tau) \frac{c_s}{\sqrt{2\pi\nu_s\tau}} e^{-\frac{c_s^2(\tau-t)^2}{2\nu_s\tau}}\, d\tau. \tag{4.29}$$

Analogously,

$$\tilde{L}^*\phi(t) = \int_0^{+\infty} \frac{\tau}{t}\phi(\tau) \frac{c_s}{\sqrt{2\pi\nu_s t}} e^{-\frac{c_s^2(\tau-t)^2}{2\nu_s t}}\, d\tau. \tag{4.30}$$

Since the phase in (4.30) is quadratic and ν_s is small then by the stationary phase theorem 4.2, we can prove that

$$\tilde{L}^*\phi \approx \phi + \frac{\nu_s}{2c_s^2}\partial_{tt}(t\phi), \quad \tilde{L}\phi \approx \phi + \frac{\nu_s}{2c_s^2} t\partial_{tt}\phi,$$

and

$$\tilde{L}^*\tilde{L}\phi \approx \phi + \frac{\nu_s}{c_s^2}\partial_t(t\partial_t\phi), \tag{4.31}$$

and therefore,

$$(L^*\tilde{L})^{-1}\phi \approx \phi - \frac{\nu_s}{c_s^2}\partial_t(t\partial_t\phi). \tag{4.32}$$

4.4.2. Reconstruction methods. From the previous section, it follows that the ideal Green function, $\delta(\tau - r/c_s)/(4\pi r)$, can be approximately reconstructed from the viscous Green function, $G^s(r,t;\xi)$, by either solving the ODE

$$\phi + \frac{\nu_s}{c_s^2}\partial_t(t\partial_t\phi) = L^*G^s(r,t;\xi),$$

with $\phi = 0, t \ll 0$ or just making the approximation

$$\delta(\tau - r/c_s)/(4\pi r) \approx L^*G^s(r,t;\xi) - \frac{\nu_s}{c_s^2}\partial_t(t\partial_t L^*G^s(r,t;\xi)).$$

Once the ideal Green function is reconstructed, one can find its source ξ using the algorithms in Chapter 2. One can also find the shear modulus of the anomaly using the ideal near-field measurements which can be reconstructed from the near-field measurements in the viscous medium.

4.5. Numerical illustrations

For the following illustrations, we take $\rho = 1000$, $c_s = 1$, $c_p = 40$, $r = 0.015$ and $\nu_p = 0$.

Figure 1 : We plot, for differents values of y and $\nu_s$the function

$$t \to \frac{1}{\rho c_p^2}\left(G^p(r,t;\xi) + G^s(r,t;\xi)\right) + \frac{1}{4\pi\rho r^3}\left[W_s(r,t) - W_p(r,t)\right].$$

Figure 2 : We plot, for differents values of y and ν_s at $t = 0.015$ the function

$$(x,y) \to \frac{1}{\rho c_p^2}\left((x/r)^2 G^p(r,t;\xi) + (1-(x/r)^2)G^s(r,t;\xi)\right) + \frac{1}{4\pi\rho r^3}(3(x/r)^2 - 1)\left[W_s(r,t) - W_p(r,t)\right].$$

Figure 3 : For $\phi(t) = exp(-50 * (t-1).^2)''$, an L^∞-error between $L\phi$ and $\phi + \frac{\nu_s}{2c_s^2}t\phi''$ is ploted : we observe an error of two, as expected by stationary phase theorem.

4.6. Concluding remarks

In this chapter we have computed the Green function in a visco-elastic medium obeying a frequency power-law. For the Voigt model, which corresponds to a quadratic frequency loss, we have used the stationary phase theorem to reconstruct the ideal Green function from the visco-elastic one by solving an ODE. Once the ideal Green function is reconstructed, one can find its source ξ using the algorithms in Chapter 2. For more general power-law media, one can recover the ideal Green function from the visco-elastic one by inverting a fractional derivative operator.

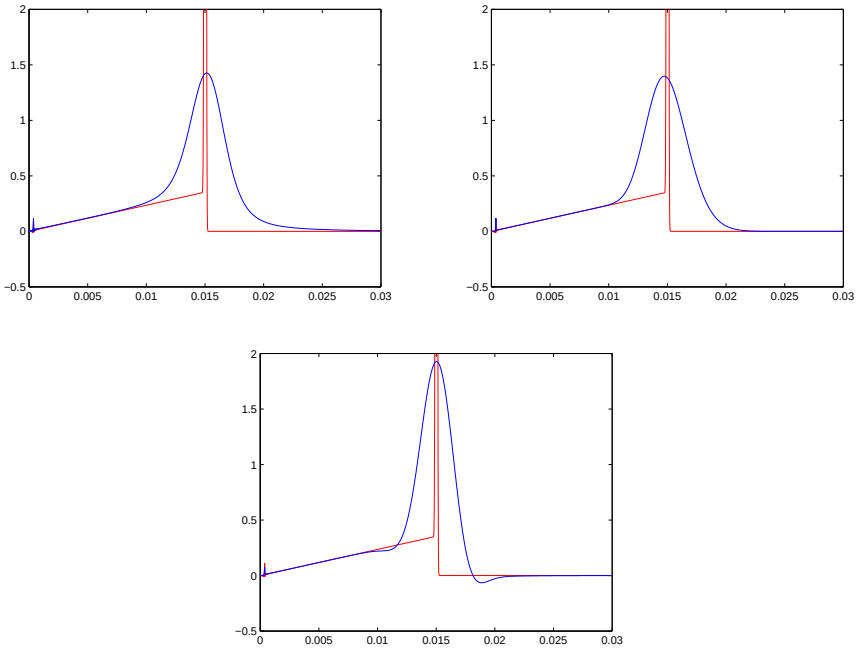

FIGURE 4.1. Temporal response to a spatiotemporal delta function using a purely elastic Green's function (red line) and a viscous Green's function (blue line) : Left, $y = 1.5$, $\nu_s = 4$; Center, $y = 2$, $\nu_s = 0.2$; Right, $y = 2.5$, $\nu_s = 0.002$. □

Appendix A: Proof of the approximation formula

The proof of formula (4.31) is based on the following theorem (see [**65**, Theorem 7.7.1]).

THEOREM 4.2. **(Stationary Phase)** *Let $K \subset [0,\infty)$ be a compact set, X an open neighborhoud of K and k a positive integer. If $\psi \in C_0^{2k}(K)$, $f \in C^{3k+1}(X)$ and $Im(f) \geq 0$ in X, $Im(f(t_0)) = 0$, $f'(t_0) = 0$, $f''(t_0) \neq 0$, $f' \neq 0$ in $K \setminus \{t_0\}$ then for $\epsilon > 0$*

$$\left| \int_K \psi(t) e^{if(t)/\epsilon} dx - e^{if(t_0)/\epsilon} \left(\lambda f''(t_0)/2\pi i\right)^{-1/2} \sum_{j<k} \epsilon^j L_j \psi \right| \leq C\epsilon^k \sum_{\alpha \leq 2k} \sup |\psi^{(\alpha)}(x)|.$$

Here C is bounded when f stays in a bounded set in $C^{3k+1}(X)$ and $|t - t_0|/|f'(t)|$ has a uniform bound. With,

$$g_{t_0}(t) = f(t) - f(t_0) - \frac{1}{2} f''(t_0)(t - t_0)^2,$$

which vanishes up to third order at t_0, we have

$$L_j \psi = \sum_{\nu - \mu = j} \sum_{2\nu \geq 3\mu} i^{-j} \frac{2^{-\nu}}{\nu! \mu!} (-1)^\nu f''(t_0)^{-\nu} (g_{t_0}^\mu \psi)^{(2\nu)}(t_0). \ \square$$

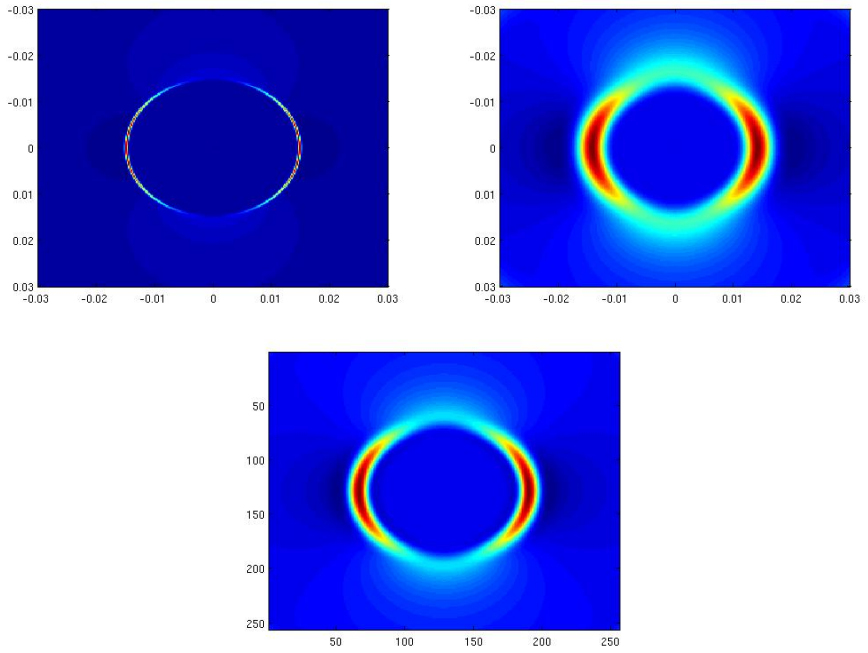

FIGURE 4.2. $2D$ spatial response to a spatiotemporal delta function at $t = 0.015$ with a purely elastic Green's function, a viscous Green's function with $y = 2$, $\nu_s = 0.2$ and $y = 2.5$, $\nu_s = 0.002$. □

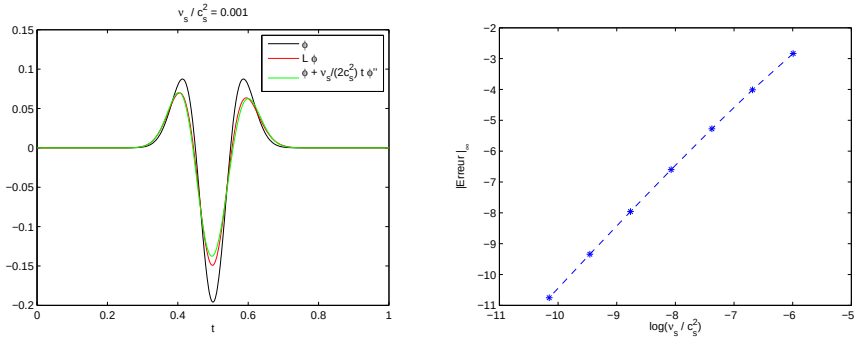

FIGURE 4.3. Approximation of L via stationary phase theorem : Left, comparison between $L\phi$ and $\phi + \frac{\nu_s}{c_s^2} t\phi''$ where $\frac{\nu_s}{c_s^2} = 0.0001$ and ϕ is a mexican hat, Right, error $\frac{\nu_s}{c_s^2} \to \|L\phi - \phi + \frac{\nu_s}{c_s^2}\|_\infty$ in logarithmic scale. □

Note that L_1 can be expressed as the sum $L_1\psi = L_1^1\psi + L_1^2\psi + L_1^3\psi$, where L_1^j is respectively associate to the pair $(\nu_j, \mu_j) = (1,0), (2,1), (3,2)$ and is identified to

$$\begin{cases} L_1^1\psi &= \frac{-1}{2i} f''(t_0)^{-1}\psi^{(2)}(t_0), \\ L_1^2\psi &= \frac{1}{2^2 2! i} f''(t_0)^{-2}(g_{t_0} u)^{(4)}(t_0) = \frac{1}{8i} f''(t_0)^{-2}\left(g_{t_0}^{(4)}(t_0)\psi(t_0) + 4g_{t_0}^{(3)}(t_0)\psi'(t_0)\right), \\ L_1^3\psi &= \frac{-1}{2^3 2! 3! i} f''(t_0)^{-3}(g_{t_0}^2\psi)^{(6)}(t_0) = \frac{-1}{2^3 2! 3! i} f''(t_0)^{-3}(g_{t_0}^2)^{(6)}(t_0)\psi(t_0). \end{cases}$$

Now we turn to the proof of formula (4.31). Let us first consider the case of operator L^*. We have

$$\tilde{L}^*\phi(t) = \int_0^{+\infty} \frac{\tau}{t}\phi(\tau)\frac{c_s}{\sqrt{2\pi\nu_s t}} e^{-\frac{c_s^2(\tau-t)^2}{2\nu_s t}} d\tau = \frac{1}{t\sqrt{\epsilon}}\left(\int_0^{+\infty} \psi(\tau) e^{if(\tau)/\epsilon}\right),$$

with, $f(\tau) = i\pi(\tau-t)^2$, $\epsilon = \frac{2\pi\nu_s t}{c_s^2}$ and $\psi(\tau) = \tau\phi(\tau)$. Remark that the phase f satisfies at $\tau = t$, $f(t) = 0$, $f'(t) = 0$, $f''(t) = 2i\pi \neq 0$. Moreover, we have

$$\begin{cases} e^{if(t)/\epsilon}\left(\epsilon^{-1}f''(t)/2i\pi\right)^{-1/2} = \sqrt{\epsilon} \\ g_t(\tau) = f(\tau) - f(t) - \frac{1}{2}f''(t)(\tau-t)^2 = 0 \\ L_1\psi(t) = L_1^1\psi(t) = \frac{-1}{2i}f''(t)^{-1}\psi^{''}(t) = \frac{1}{4\pi}(t\phi)''. \end{cases}$$

Thus, Theorem 4.2 implies that

$$\left|\tilde{L}^*\phi(t) - \left(\phi(t) + \frac{\nu_s}{2c_s^2}(t\phi)''\right)\right| \leq \frac{C}{t}\epsilon^{3/2}\sum_{\alpha\leq 4}\sup|(t\phi)^{(\alpha)}|.$$

The case of the operator $\tilde{L}$ is very similar. Note that

$$\tilde{L}\phi(t) = \int_0^{+\infty} \frac{t}{\tau}\phi(\tau)\frac{c_s}{\sqrt{2\pi\nu_s\tau}} e^{-\frac{c_s^2(\tau-t)^2}{2\nu_s\tau}} d\tau = \frac{t}{\sqrt{\epsilon}}\left(\int_0^{+\infty} \psi(\tau) e^{if(\tau)/\epsilon}\right),$$

with $f(\tau) = i\pi\frac{(\tau-t)^2}{\tau}$, $\epsilon = \frac{\nu_s}{2\pi c_s^2}$ and $\psi(\tau) = \phi(\tau)\tau^{-\frac{3}{2}}$. It follows that

$$f'(\tau) = i\pi\left(1 - \frac{t^2}{\tau^2}\right), \quad f''(\tau) = 2i\pi\frac{t^2}{\tau^3}, \quad f''(t) = 2i\pi\frac{1}{t},$$

and the function $g_t(\tau)$ equals to

$$g_t(\tau) = i\pi\frac{(\tau-t)^2}{\tau} - i\pi\frac{(\tau-t)^2}{t} = i\pi\frac{(t-\tau)^3}{\tau t}.$$

We deduce that

$$\begin{cases} (g_t\psi)^{(4)}(t) &= \left(g_t^{(4)}(t)\psi(t) + 4g_t^{(3)}(t)\psi'(t)\right) = i\pi\left(\frac{24}{t^3}\psi(t) - \frac{24}{t^2}\psi'(t)\right) \\ (g_t^2\psi)^{(6)}(t) &= (g_t^2)^{(6)}(t)\psi(t) = -\pi^2\frac{6!}{t^4}\psi(t), \end{cases}$$

and then,

$$\begin{cases} L_1^1\psi = \frac{-1}{i}\left(\frac{1}{2}(f''(t))^{-1}\psi''(t)\right) = \frac{1}{4\pi}t\left(\frac{\tilde{\phi}}{\sqrt{t}}\right)'' = \frac{1}{4\pi}\left(\sqrt{t}\tilde{\phi}''(t) - \frac{\tilde{\phi}'(t)}{\sqrt{t}} + \frac{3}{4}\frac{\tilde{\phi}}{t^{3/2}}\right) \\ L_1^2\psi = \frac{1}{8i}f''(t)^{-2}\left(g_t^{(4)}(s)\psi(s) + 4g_t^{(3)}(t)\psi'(t)\right) = \frac{1}{4\pi}\left(3\left(\frac{\tilde{\phi}(t)}{\sqrt{t}}\right)' - 3\frac{\tilde{\phi}(t)}{t^{3/2}}\right) = \frac{1}{4\pi}\left(3\frac{\tilde{\phi}'(t)}{\sqrt{t}} - \frac{9}{2}\frac{\tilde{\phi}(t)}{t^{3/2}}\right) \\ L_1^3\psi = \frac{-1}{2^3 2!3!i}f''(t)^{-3}(g_t^2)^{(6)}(t)\psi(s) = \frac{1}{4\pi}\left(\frac{15}{4}\frac{\tilde{\phi}(t)}{t^{3/2}}\right), \end{cases}$$

where $\tilde{\phi}(\tau) = \phi(\tau)/\tau$. Then, we have

$$\begin{aligned} L^1\psi &= L_1^1\psi + L_1^2\psi + L_1^3\psi \\ &= \frac{1}{4\pi}\left(\sqrt{t}\tilde{\phi}''(t) + (3-1)\frac{\tilde{\phi}'(t)}{\sqrt{t}} + \left(\frac{3}{4} - \frac{9}{2} + \frac{15}{4}\right)\frac{\tilde{\phi}(t)}{t^{3/2}}\right) = \frac{1}{4\pi\sqrt{t}}\left(t\tilde{\phi}(t)\right)'' = \frac{1}{4\pi\sqrt{t}}\phi''(t), \end{aligned}$$

and again Theorem 4.2 shows that

$$\left|\tilde{L}\phi(t) - \left(\phi(t) + \frac{\nu_s}{2c_s^2}t\phi''(t)\right)\right| \leq Ct\epsilon^{3/2}\sum_{\alpha\leq 4}\sup|\psi^{(\alpha)}(t)|.$$

Bibliography

[1] K. Aki and P.G. Richards, *Quantitative Seismology: Theory and Methods*, Vol. 1, W. H. Freeman and Company, San Francisco, California, 1980.

[2] H. Ammari, An inverse initial boundary value problem for the wave equation in the presence of imperfections of small volume, SIAM J. Control Optim., 41 (2002), 1194–1211.

[3] H. Ammari, *An Introduction to Mathematics of Emerging Biomedical Imaging*, Mathématiques et Applications, Vol. 62, Springer-Verlag, Berlin, 2008.

[4] H. Ammari, M. Asch, L. Guadarrama Bustos, V. Jugnon, and H. Kang, Transient wave imaging with limited-view data, SIAM. J. Imag. Sci., submitted.

[5] H. Ammari, E. Bossy, V. Jugnon, and H. Kang, Mathematical modelling in photo-acoustic imaging of small absorbers, SIAM Rev., to appear.

[6] H. Ammari, E. Bretin, V. Jugnon, H. Kang, and A. Wahab, Photo-acoustic imaging in dissipative media, in preparation.

[7] H. Ammari, Y. Capdeboscq, H. Kang, and A. Kozhemyak, Mathematical models and reconstruction methods in magneto-acoustic imaging, Euro. J. Appl. Math., 20 (2009), 303–317.

[8] H. Ammari, P. Garapon, L. Guadarrama Bustos, and H. Kang, Transient anomaly imaging by the acoustic radiation force, J. Differ. Equat., to appear.

[9] H. Ammari, P. Garapon, and F. Jouve, Separation of scales in an elastic inverse problem, J. Comput. Math. (special issue) 28 (2010), 354–370.

[10] H. Ammari, P. Garapon, H. Kang, and H. Lee, A Method of Biological Tissues Elasticity Reconstruction Using Magnetic Resonance Elastography Measurements, Quart. Appl. Math., 66 (2008), 139–175.

[11] H. Ammari, L. Guadarrama Bustos, H. Kang, and H. Lee, Transient elasticity imaging and time reversal, Proc. Royal Soc. Edinburgh: Sect. A, submitted.

[12] H. Ammari, E. Iakovleva, and D. Lesselier, Two numerical methods for recovering small inclusions from the scattering amplitude at a fixed frequency, SIAM J. Sci. Comput., 27 (2005), 130–158.

[13] H. Ammari and H. Kang, High-order terms in the asymptotic expansions of the steady-state voltage potentials in the presence of inhomogeneities of small diameter, SIAM J. Math. Anal., 34 (2003), 1152–1166.

[14] H. Ammari and H. Kang, *Reconstruction of Small Inhomogeneities from Boundary Measurements*, Lecture Notes in Mathematics, Volume 1846, Springer-Verlag, Berlin, 2004.

[15] H. Ammari and H. Kang, Boundary layer techniques for solving the Helmholtz equation in the presence of small inhomogeneities, J. Math. Anal. Appl., 296 (2004), 190–208.

[16] H. Ammari and H. Kang, Reconstruction of elastic inclusions of small volume via dynamic measurements, Appl. Math. Opt., 54 (2006), 223–235.

[17] H. Ammari and H. Kang, *Polarization and Moment Tensors: with Applications to Inverse Problems and Effective Medium Theory*, Applied Mathematical Sciences Series, Vol. 162, Springer-Verlag, New York, 2007.

[18] H. Ammari and H. Kang, Properties of the generalized polarization tensors, SIAM Mult. Model. Simul., 1 (2003), 335–348.

[19] H. Ammari, H. Kang, E. Kim, K. Louati, and M. Vogelius, A MUSIC-type algorithm for detecting internal corrosion from electrostatic boundary measurements, Numer. Math., 108 (2008), 501–528.

[20] H. Ammari, H. Kang, H. Lee, and W.K. Park, Asymptotic imaging of perfectly conducting cracks, SIAM J. Sci. Comput., to appear.

[21] H. Ammari, H. Kang, G. Nakamura, and K. Tanuma, Complete asymptotic expansions of solutions of the system of elastostatics in the presence of an inclusion of small diameter and detection of an inclusion, J. Elasticity, 67 (2002), 97–129.

[22] H. Ammari and A. Khelifi, Electromagnetic scattering by small dielectric inhomogeneities, J. Math. Pures Appl., 82 (2003), 749–842.

[23] H. Ammari, M. Vogelius and D. Volkov, Asymptotic formulas for perturbations in the electromagnetic fields due to the presence of inhomogeneities of small diameter II. The full Maxwell equations, J. Math. Pures Appl., 80 (2001), 769–814.

[24] P.M. Anselone, *Collectively Compact Operator Approximation Theory and Applications to Integral Equations,* Prentice-Hall, Englewood Cliffs, NJ, 1971.

[25] M. Asch and G. Lebeau, Geometrical aspects of exact boundary controllability for the wave equation–a numerical study, ESAIM Control Optim. Calc. Var., 3 (1998), 163–212.

[26] G. Bao, S. Hou, and P. Li, Recent studies on inverse medium scattering problems, Lecture Notes in Comput. Sci. Eng., Vol. 59, 165–186, 2007.

[27] P.E. Barbone and J.C. Bamber, Quantitative elasticity imaging: what can and cannot be inferred from strain images, Phys. Med. Biol., 47 (2002), 2147–2164.

[28] C. Bardos and M. Fink, Mathematical foundations of the time reversal mirror, Asymptot. Anal., 29 (2002), 157–182.

[29] C. Bardos, G. Lebeau, and J. Rauch, Sharp sufficient conditions for the observation, control, and stabilization of waves from the boundary, SIAM J. Control Optim., 30 (1992), 1024-1065.

[30] G.K. Batchelor and J.T. Green, The determination of the bulk stress is suspension of spherical particles to order c^2, J. Fluid. Mech. 56 (1972), 401-427.

[31] M.I. Belishev, Recent progress in the boundary control method, Inverse Problems, 23 (2007), R1-R67.

[32] J. Benesty, J. Chen, and Y. Huang, Time-delay estimation via linear interpolation and cross correlation, IEEE Trans. Speech Audio Process., 12 (2004), 509–519.

[33] J. Bercoff, M. Tanter, and M. Fink, Supersonic shear imaging: a new technique for soft tissue elasticity mapping, IEEE Trans. Ultrasonics, Ferro., Freq. Control, 51 (2004), 396–409.

[34] J. Bercoff, M. Tanter, M. Muller, and M. Fink, The role of viscosity in the impulse diffraction field of elastic waves induced by the acoustic radiation force, IEEE Trans. Ultrasonics, Ferro., Freq. Control, 51 (2004), 1523–1536.

[35] A.C. Birch and A.G. Kosovichev, Travel time sensitivity kernels, Solar Phys., 192 (2000), 193–201.

[36] L. Borcea, G.C. Papanicolaou, C. Tsogka, and J.G. Berrymann, Imaging and time reversal in random media, Inverse Problems, 18 (2002), 1247–1279.

[37] E. Bretin, L. Guadarrama Bustos, and A. Wahab, Visco-elastic anomaly imaging, in preparation.

[38] Y. Capdeboscq and H. Kang, Improved Hashin-Shtrikman bounds for elastic moment tensors and an application, preprint 2007.

[39] Y. Capdeboscq and M.S. Vogelius, Optimal asymptotic estimates for the volume of internal inhomogeneities in terms of multiple boundary measurements, Math. Model. Num. Anal., 37 (2003), 227–240.

[40] G.C. Carter, Special Issue on Time-Delay Estimation, IEEE Trans. Acoust., Speech, Sig. Process., vol. ASSP-29, June 1981.

[41] D. Cassereau and M. Fink, Time-reversal of ultrasonic fields. III. Theory of the closedtime-reversal cavity, IEEE Trans. Ultrasonics, Ferroelectrics and Frequency Control 39 (1992), 579–592.

[42] S. Catheline, J-L Gennisson, G. Delon, R. Sinkus, M. Fink, S. Abouelkaram, and J. Culioli, Mesurement of viscoelastic properties of solid using transient elastography: An inverse problem approach, J. Acoust. Soc. Amer., 116 (2004), 3734–3741.

[43] S. Catheline, N. Benech, J. Brum, and C. Negreira, Time-reversal of elastic waves in soft solids, Phys. Rev. Lett., 100 (2008), 064301.

[44] D.H. Chambers and J.G. Berryman, Analysis of the time-reversal operator for a small spherical scatterer in an electromagnetic field, IEEE Trans. Antennas and Propagation, 52 (2004), 1729–1738.

[45] D.H. Chambers and J.G. Berryman, Time-reversal analysis for scatterer characterization, Phys. Rev. Lett., 92 (2004), 023902.

[46] Y.T. Chan and K.C. Ho, A simple and efficient estimator for hyperbolic location, IEEE Trans. Sig. Process., 42 (1994), 1905–1915.
[47] T.F. Chan and X.-C. Tai, Level set and total variation regularization for elliptic inverse problems with discontinuous coefficients, J. Comput. Phys., 193 (2003), 40–66.
[48] J.C. Chen, K. Yao, and R.E. Hudson, Source localization and beamforming, IEEE Sig. Process. Magazine, March 2002, 30–39.
[49] A. Costa, Viscosity of high crystal content melts: dependence on solid fraction, Geophys. Research lett., 20 (2005), DOI:10.1029.
[50] T. Deffieux, J.L. Genisson, A. Nordez, M. Tanter, and M. Fink, Ultrafast Imaging of in vivo muscle contraction using ultrasound, Appl. Phys. Lett., vol. 89, nov. 2006.
[51] A.J. Devaney, Time reversal imaging of obscured targets from multistatic data, IEEE Trans. Antennas Propagat., 523 (2005), 1600–1610.
[52] P. Docherty, A brief comparison of some Kirchhoff integral formulas for migration and inversion, GEOPHYSICS, 56 (1991), 1164–1169.
[53] G. Evans, J. Blackledge, and P. Yardley, *Analytic Methods for Partial Differential Equations*, Springer-Verlag, London, 2000.
[54] M. Fink, Time reversed acoustics, Physics Today 50 (1997), 34.
[55] M. Fink, Time-reversal acoustics in *Inverse Problems, Multi-Scale Analysis and Homogenization,* 151–179, edited by H. Ammari and H. Kang, Contemp. Math., Vol. 408, Rhode Island, Providence, 2006.
[56] A.R. Fisher, A.J. Schissler, and J.C. Schotland, Photoacoustic effect of multiply scattered light, Phys. Rev. E, 76 (2007), 036604.
[57] J.P. Fouque, J. Garnier, G. Papanicolaou, and K. Solna, *Wave Propagation and Time Reversal in Randomly Layered Media*, Springer-Verlag, New York, 2007.
[58] F.G. Friedlander, *The Wave Equation on a Curved Space-Time*, Cambridge University Press, Cambridge, 1975.
[59] R. Glowinski, Ensuring well posedness by analogy; Stokes problem and boundary control for the wave equation, J. Comput. Phys., 103 (1992), 189–221.
[60] J.F. Greenleaf, M. Fatemi, and M. Insana, Selected methods for imaging elastic properties of biological tissues, Annu. Rev. Biomed. Eng., 5 (2003), 57–78.
[61] S. Gdoura and L. Guadarrama Bustos, Transient wave imaging of anomalies: a numerical study, in preparation.
[62] D.J. Hansen and M.S. Vogelius, High frequency perturbation formulas for the effect of small inhomogeneities, preprint.
[63] D.J. Hansen, C. Poignard, and M.S. Vogelius, Asymptotically precise norm estimates of scattering from a small circular inhomogeneity, Appl. Anal., 86 (2007), 433–458.
[64] C. Hazard and K. Ramdani, Selective acoustic focusing using time-harmonic reversal mirrors, SIAM J. Appl. Math., 64 (2004), 1057–1076.
[65] L. Hörmander, *The analysis of Linear Partial Differential Operators. I. Distribution Theory and Fourier Analysis*, Classics in Mathematics, Springer-Verlag, Berlin, 2003.
[66] Y. Huang, J. Benesty, G.W. Elko, and R.M. Mersereau, Real-time passive source localization: a practical linear-correction least-squares approach, IEEE Trans. Speech Audio Process., 9 (2001), 943–956.
[67] L. Huwart, F. Peeters, R. Sinkus, L. Annet, N. Salameh, LC. Ter Beek, Y. Horsmans, and BE. Van Beers, Liver fibrosis: non invasive assessment with MR Elastography, NMR Biomed (2006), vol. 19.
[68] L.I. Ignat and E. Zuazua, Convergence of a two-grid algorithm for the control of the wave equation, J. Europ. Math. Soc., 11 (2009), 351–391.
[69] V. Isakov, On uniqueness of recovery of a discontinuous conductivity coefficient, Comm. Pure Appl. Math., 41 (1988), 865–877.
[70] M.R. Islam and B.C. Towe, Bioelectric current image reconstruction from magneto-acoustic measurements, IEEE Trans. Med. Img. 7 (1988), 386–391.
[71] H. Kang, E. Kim, J.-Y. Lee, Identification of elastic inclusions and elastic moment tensors by boundary measurements, Inverse Problems, 19 (2003), 703–724.
[72] H. Kang and G.W. Milton, Solutions to the Pólya-Szegö conjecture and the weak Eshelby conjecture, Arch. Rational Mech. Anal, 188 (2008), 93–116.
[73] F.C. Karal and J. B. Keller, Elastic, Electromagnetic and other waves in a random medium, J. Math. Physics, 5 (1964), 537–547.

[74] A. Katchalov, Y. Kurylev, and M. Lassas, *Inverse Boundary Spectral Problems*, Monographs and Surveys in Pure and Applied Mathematics, Chapman & Hall/CRC, 2001.

[75] J.F. Kelly, R.J. McGough, and M.M. Meerschaert, Analytical time-domain green's functions for power-law media, J. Acous. Soc. Amer., 124 (2008), 2861–2872.

[76] A.G. Kosovichev, T.L. Duvall, and P.H. Scherrer, Time-distance inversion methods and results, Solar Phys., 192 (2000), 159–176.

[77] O.A. Ladyzhenskaya, *The mathematical Theory of Viscous Incompressible Flow*, Second English Edition, Gordon and Breach, New York, 1969.

[78] G. Lebeau, Control of hyperbolic equations, Journées Equat. Dérivées Part., 1992, 1–24.

[79] J.-L. Lions, *Contrôlabilité exacte, Perturbations et Stabilisation de Systèmes Distribués*, Tome 1, Contrôlabilité exacte, Masson, Paris, 1988.

[80] R. Lipton, Inequalities for electric and elastic polarization tensors with applications to random composites, J. Mech. Phys. Solids, 41 (1993), 809–833.

[81] D.R. Luke and A.J. Devaney, Identifying scattering obstacles by the construction of nonscattering waves, SIAM J. Appl. Math., 68 (2007), 271–291.

[82] A. Manduca, T.E. Oliphant, M.A. Dresner, J.L. Mahowald, S.A. Kruse, E. Amromin, J.P. Felmlee, J.F. Greenleaf, and R.L. Ehman, Magnetic resonance elastography: Non-invasive mapping of tissue elasticity, Medical Image Analysis, 5 (2001), 237–254.

[83] M.L. Mansfield, J.F. Douglas, and E.J. Garboczi, Intrinsic viscosity and electrical polarizability of arbitrary shaped objects, Physical Review E, 64 (2001), 061401.

[84] T.D. Mast, A. Nachman, and R.C. Waag, Focusing and imagining using eigenfunctions of the scattering operator, J. Acoust. Soc. Am., 102 (1997), 715–725.

[85] G.W. Milton, D.J. Eyre, and J.V. Mantese, Finite frequency range Kramers-Krönig relations: bounds on the dispersion, Phys. Rev. Lett., 79 (1997), 3062–3075.

[86] R. Muthupillai, D.J. Lomas, P.J. Rossman, J.F. Greenleaf, A. Manduca, and R.L. Ehman, Magnetic resonance elastography by direct visualization of propagating acoustic strain waves, Science, 269 (1995), 1854–1857.

[87] C. Prada and M. Fink, Eigenmodes of the time-reversal operator: A solution to selective focusing in multiple-target media, Wave Motion, 20 (1994), 151-163.

[88] J. Pujol, *Elastic Wave Propagation and Generation in Seismology*, Cambridge University Press, United Kingdom, 2003.

[89] J. de Rosny, G. Lerosey, A. Tourin, and M. Fink, Time reversal of electromagnetic Waves, Lecture Notes in Comput. Sci. Eng., Vol. 59, , 2007.

[90] B.J. Roth and P.J. Basser, A model of the stimulation of a nerve fiber by electromagnetic induction, IEEE Trans. Biomed. Eng., 37 (1990), 588–597.

[91] B.J. Roth, P.J. Basser, and J.P. Jr Wikswo, A theoretical model for magneto-acoustic imaging of bioelectric currents, IEEE Trans. Biomed. Eng., 41 (1994), 723–728.

[92] S.G. Samko, A.A. Kilbas, and O.I. Marichev, *Fractional Integrals and Derivatives: Theory and Applications*, Gordon and Breach Science Publishers, 1987.

[93] A.P. Sarvazyan, O.V. Rudenko, S.C. Swanson, J.B. Fowlkers, and S.V. Emelianovs, Shear wave elasticity imaging: a new ultrasonic technology of medical diagnostics, Ultrasound in Med. & Biol., 24 (1998), 1419-1435.

[94] T.L. Szabo, Time domain wave equations for lossy media obeying a frequency power law, J. Acous. Soc. Amer., 96 (1994), 491–500.

[95] T.L. Szabo and J. Wu, A model for longitudinal and shear wave propagation in viscoelastic media, J. Acous. Soc. Amer., 107 (2000), 2437–2446.

[96] H.C. Schau and A.Z. Robinson, Passive source localization employing intersecting spherical surfaces from time-of-arrival differences, IEEE Trans. Acoust. Speech, Process., 35 (1987), 1223–1225.

[97] R. Sinkus, J. Lorenzen, D. Schrader, M. Lorenzen, M. Dargatz, and D. Holz, High-resolution tensor MR elastography for breast tumour detection, Phys. Med. Biol., 45 (2000), 1649–1664.

[98] R. Sinkus, M. Tanter, S. Catheline, J. Lorenzen, C. Kuhl, E. Sondermann, and M. Fink, Imaging anisotropic and viscous properties of breast tissue by magnetic resonance-elastography, Mag. Res. Med., 53 (2005), 372–387.

[99] R. Sinkus, M. Tanter, T. Xydeas, S. Catheline, J. Bercoff, and M. Fink, Viscoelastic shear properties of in vivo breast lesions measured by MR elastography, Mag. Res. Imag., 23 (2005), 159–165.

[100] E.E.W. Van Houten, K.D. Paulsen, M.I. Miga, F.E. Kennedy, and J.B. Weaver, An Overlapping Subzone Technique for MR-Based Elastic Property Reconstruction, Mag. Reson. Med., 42 (1999), 779–786.

[101] E.E.W. Van Houten, M.M. Doyley, F.E. Kennedy, J.B. Weaver, and K.D. Paulsen, Initial In Vivo Experience with Steady-State Subzone-Based MR Elastography of the Human Breast, J. Magn. Reson. Imag., 17 (2000), 72–85.

[102] G.C. Verchota, Layer potentials and boundary value problems for Laplace's equation in Lipschitz domains. Jour. of Func. Anal., 59 (1984), 572-611.

[103] M. Vogelius and D. Volkov, Asymptotic formulas for perturbations in the electromagnetic fields due to the presence of inhomogeneities, Math. Model. Numer. Anal., 34 (2000), 723–748.

[104] M. Wax and T. Kailath, Optimum localization of multiple sources by passive arrays, IEEE Trans. Acoust. Speech, Process., 31 (1983), 1210–1217.

[105] M. Xu and L.V. Wang, Photoacoustic imaging in biomedicine, Review of Scientific Instruments 77, 041101, 2006.

[106] E. Zuazua, Propagation, observation, and control of waves approximated by finite difference methods, SIAM Rev., 47 (2005), 197–243.

Index